PHOTOVOLTAIC THERMAL HYBRID COLLECTORS

FOR A DISTRICT CCHP SYSTEM:

MODELLING AND OPTIMIZATION

Relatore:

Prof. Andrea Lazzaretto

Prof. Sotirios Karellas

Ph.D. Tryfonas Roumpedakis

Marco Rossi

1197619

Anno Accademico 2019/2020

INDEX

ὡς δὲ ἐκεῖνος ἀσπασάμενος

καὶ προσειπὼν αὐτόν ἠρώτησεν εἴ τινος τυγχάνει δεόμενος,

'μικρὸν' (Διογένης) εἶπεν, 'ἀπὸ τοῦ ἡλίου μετάστηθι'

Πλούταρχος, Ἀλέξανδρος

And when that monarch addressed him with greetings,

and asked if he wanted anything,

'Yes,' (Diogenes) said, 'stand a little out of my sun.'

Plutarch, Alexander

ABSTRACT

This work studied the modelling and the optimization of a system based on the solar hybrid technology for the combined production of heating, cooling and electric power destined to the usage on a district of residential and utility buildings. The loads and the environmental conditions are hourly annual values taken from databases for the cities of Athens in Greece and Vicenza in Italy.

A mixed integer non-linear programming was used to develop the dynamic system. An optimization process is then applied by implementing a minimum finding problem, in which a genetic algorithm was exploited. The objective functions were economic and energetic parameters, i.e. the discounted payback period and the global utilization factor.

The main components are the photovoltaic-thermal hybrid collector, the heat pump, the natural gas heater, the inverter, the thermal storage tanks and the connection with the electricity grid and the gas pipelines. The substitution of the hybrid panel with a common solar separated solution and the introduction of a battery are studied for comparison purposes by applying the same external conditions.

Results show that the hybrid system is economically competitive with a separated solution, even though the global utilization of energy is lower. It is evaluated the dependency of the objective functions on economic parameters and design variables, such as the surface of the panels and the volumes of the thermal storage tanks.

SOMMARIO

Questo lavoro ha sviluppato la modellazione e l'ottimizzazione di un sistema basato sulla tecnologia dei pannelli solari ibridi per la trigenerazione di riscaldamento, raffrescamento ed energia elettrica destinata ad un uso residenziale per un quartiere con edifici residenziali ed esercizi commerciali. I carichi e le condizioni ambientali sono valori orari annuali tratti da banche dati per le città di Atene in Grecia e Vicenza in Italia.

Per sviluppare il modello in modo dinamico è stata adottata una programmazione non lineare e variabili integrali. Viene quindi applicato un processo di ottimizzazione implementando un problema di ricerca del minimo, in cui è stato sfruttato un particolare tipo di algoritmo evolutivo. Le funzioni obiettivo usate sono parametri economici ed energetici, cioè il payback attualizzato e il fattore di utilizzo globale.

I componenti principali del sistema sono il collettore ibrido fotovoltaico-termico, la pompa di calore, la caldaia a gas naturale, l'inverter, i serbatoi di accumulo termico e il collegamento con la rete elettrica e i gasdotti. La sostituzione del pannello ibrido con una comune soluzione solare separata e l'introduzione di una batteria sono state studiate a fini comparativi applicando le stesse condizioni esterne.

I risultati mostrano che il sistema ibrido è economicamente competitivo con una soluzione separata, anche se l'utilizzo globale di energia è inferiore. Inoltre viene valutata la dipendenza delle funzioni obiettivo dai parametri economici e dalle variabili di progetto quali la superficie dei pannelli e i volumi dei serbatoi di accumulo termico.

ACRONYMS AND SYMBOLS

BESS	Battery Energy Storage System
CCHP	Combined Cooling, Heating and Power
CF	Cash Flow
CO_2	Carbon dioxide
CH_4	Methane
CHP	Combined Heat and Power
COP	Coefficient of Performance
DCF	Discounted Cash Flow
DHW	Domestic Hot Water
EER	Energy Efficiency Rating
EU	European Union
GA	Genetic Algorithm
GWP	Global Warming Potential
HP	Heat Pump
IEA	International Energy Agency
IPCC	International Panel of Climate Change
LWT	Leaving Water Temperature
MILP	Mixed-Integer Linear Programming
MINLP	Mixed-Integer Nonlinear Programming

NGH   Natural Gas Heater

NPV   Net Present Value

OECD   Organization for Economic Co-operation and Development

ORC   Organic Rankine Cycle

PB   Payback period

PEC   Primary Energy Consumption

PV   Photovoltaic

PV/T   Photovoltaic Thermal

RES   Renewable Energy System

SEER   Seasonal Energy Efficiency Rating

SCOP   Seasonal Coefficient of Performance

STC   Standard Conditions

TFC   Total Final Consumption

TST   Thermal Storage Tank

Symbols

Q thermal energy

$\dot{Q}$ thermal power

W electric energy

$\dot{W}$ electric power

T temperature

I	current
V	voltage
A	surface
Vol	volume
G	solar irradiance
u_w	wind velocity
r	discount factor
a	thermal performance parameter
p	pressure
$\dot{m}$	mass flow rate
c	price
C	cost
C_{CF}	cash flow
S_{CF}	salvage cash flow

Subscripts

c	cooling
h	heating
u	user
w	hot water
amb	ambient

$comb$ combustion

L loss

COL collector

TOT total

CDF cumulative discounted flow

FC fixed capital

Greek symbols

β tilt angle

δ declination

ε global utilization factor

η efficiency

θ incidence angle

μ heat-power ratio

φ latitude

ω hour angle

1. INTRODUCTION

Energy is one of the major factors that led to an improvement in human health and welfare. This has brought to the condition of a rapid development in terms of number and quality of life (1). Moreover, energy demand has been growing throughout the years: the causes of this increase vary from country to country and lay on multiple aspects (5). However, it has been widely demonstrated that some human activities connected to this growth caused the emission into the atmosphere of gasses that contributed to generate the anthropic greenhouse effect. To this phenomenon is linked the Climate Change: an alteration of Earth climate that is leading to a higher global temperature, according to IPCC (2). One of the most GWP gasses emission sector is the energy production, due to traditional fossil fuelled power plants. For this reason, in the last few decades the market and organizations like OECD and EU are proposing policies for alternative technologies that take advantage of RES (3) (6) (7).

1.1 CCHP systems & PV/T hybrid collectors

Energy consumption is an aspect that lies within every human activity. Considering the three main sectors reported in Figure 1.1 (4) it can be noticed how to the residential and commercial sectors belong a wide slice of final consumption, around one third of the overall. More specifically, a district of domestic and utility users requires three different types of energy: power, heating and cooling. The first is the electricity required, the second can be divided into DHW and space heating, while the third is space cooling. The last two are seasonal needs, in winter and in summer respectively, while the others are required throughout the whole year. Energy plants that have the characteristics to supply all these energy requirements are called trigeneration systems, or CCHP.

Solar irradiance is a widely known RES for both power and heat production. This double generation can be exploited with a single PV/T hybrid collector: a combination of a PV panel and a thermal collector. PV panel efficiency gets lower the higher the cell temperature gets. Reducing this temperature with a heat exchanger not only increases the PV cell efficiency, but also makes available a certain amount of heat for a building use.

Total final consumption (TFC) by sector, World 1990-2017

Industry

Transport

Residential

Commercial and public services

Non-energy use
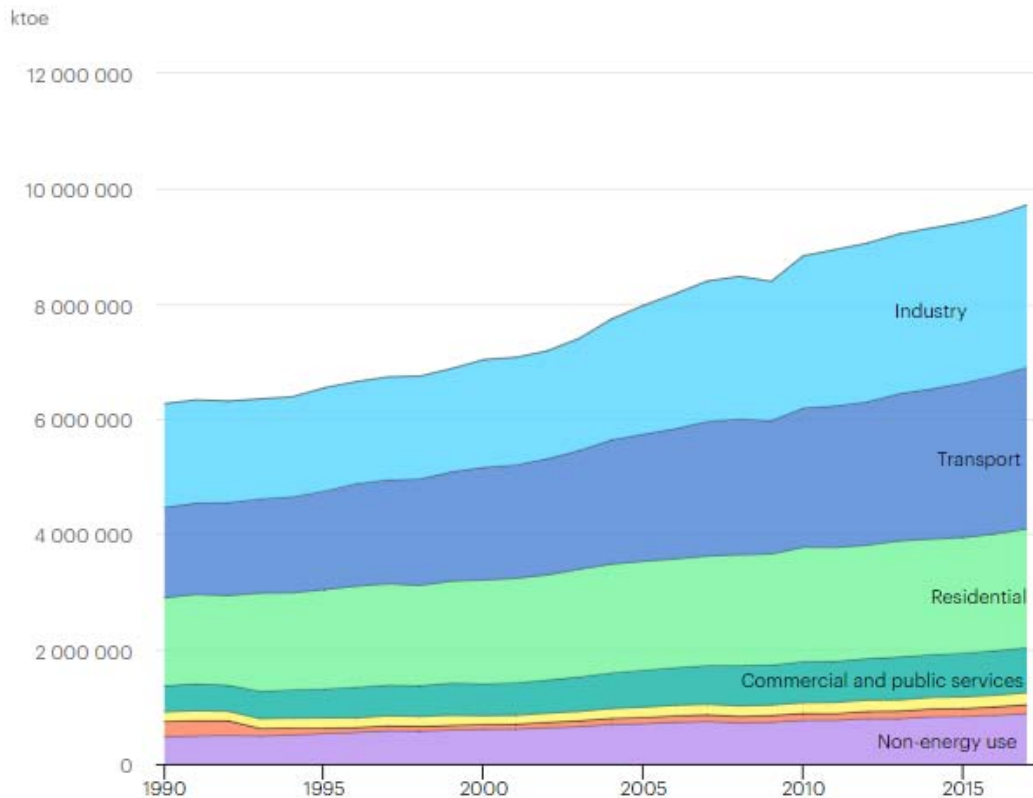
Figure 1.1: TFC by sector in the world from 1990 to 2017 (source: IEA) (4)

1.2   Literature review

Systems based on solar energy, as well as other RES, have the main problem of producing energy when is not required and vice versa. In order to match the demand and production in energy sector a storage is needed. While for fossil fuels the storage is represented by the reservoirs of the material itself, for RES an accumulation mean is required. In literature this theme has been carried on first by (Yokoyama, 1995) (8) where it was proposed an optimal operational planning method for CHP systems with thermal storage: the optimization problem has been formulated as a large-scale MILP one. (Toffolo, 2002) (9) and (Lazzaretto, 2004) (10) works suggest how to perform a multi-objective optimization in order to find solutions that simultaneously satisfy all the objectives, i.e. a search for the set of Pareto optimal solutions with respect to the competing objectives. (Wang, 2019) (11) follows the last one and gives an emphasis on evolutionary algorithms. (Rech, 2019) (12) optimizes a fleet of energy units with MINLP and supplies instructions

to select variables and equations that are required to simulate the dynamic behaviour of each conversion and storage unit in the system.

1.3   Thesis goal

In this work, the best sizing for each component is been searched in order to satisfy a multi-energy district load. The problem has been treated as a multi-objective one, in which the economical, energetic and environmental aspects have been considered. Both the loads and environmental data are taken as determinist input for two different climate conditions: one in Vicenza (Italy) and one in Athens (Greece). Since the model considers real processes, a linearized simplification has not been followed. The problem has been solved with a dynamic method and by leaving as decision variables the area of the PV/T hybrid collectors field and the sizing of the TSTs to optimize the energy production.

Element of originality of this work is the utilization of the PV/T hybrid collector. Not only it allows the trigeneration, but it is also useful to analyse aspects relative to the storages. In the end, it has been evaluated if its characteristics can give a relevant contribute to obtain the objective functions.

2. SOLAR ENERGY CONVERSION

This chapter explains how the single components of the system have been chosen, in accordance with the purposes mentioned in the first chapter. In order to use solar irradiance as an energy source for CCHP systems, an analysis of the main solar energy conversion devices has been proposed to supply all district residential loads. The one chosen for this thesis is a PV/T system, in which the heat produced is used for DHW and the power is needed to satisfy both the electrical and space heating and cooling demand. In fact, connected to the electric circuit, an electrical driven heat pump (HP) has been exploited. Finally, are requested devices that allow to store energy when over produced and to provide it when not enough.

2.1 Solar irradiance to power

Solar irradiance to power conversion is divided into two main processes: the conversion of solar irradiance into electrical power and the conversion of electric power from direct (DC) to alternate current (AC).

The former is a technology that can fit into the categories of photovoltaics (PV) and concentrated solar power (CSP). The latter depends on the type of technology involved in the first part: an inverter is required for static conversion of PV direct current (DC), while at the bottom of an electric generator a power is needed to convert the mechanical energy of a thermodynamic cycle into alternate current (AC) power at grid frequency.

Moreover, a mean to store power has been investigated.

2.1.1 From solar irradiance to electric energy

The exploitation of solar energy can be carried out using two different technologies: Photovoltaic panel (PV) and Concentrated Solar Power (CSP).

The *Photovoltaic panel* technology generates energy by the PV effect. Using a couple of solid-state semiconductors, of which the solar cell is made, it is possible to generate a flow of electrons. The two materials are differentiated by the type of dopant element inserted: for a p-type semiconductor the main dopant shares a vacancy, e.g. boron, while

for a n-type silicon the main dopant shares an electron, e.g. phosphor. The incoming photons of the global solar global irradiance hit the surface of the module and furnishes energy to the solar cell: if this is sufficient to win the energy gap between the valence and conduction bands, a difference of potential is set between these layers and the electrons movement from the positive layer (p) to the negative (n) produces an electric direct current Figure 1 (13) (14) (15). This electricity generated can be stored in a battery or sent to the electricity grid. Many technologies have been studied and explored throughout the years, such as mono- or poly-crystalline silicon, copper indium gallium selenide (CIGS), gallium arsenide (GaAs) and cadmium telluride (CdTe).

The ones that have conquered the vast majority of PV panels market are the silicon-based ones (Figure 2.2 and Figure 2.3) (16). For a single commercial panel, the common sizes stand below the kW (17). This aspect, in addition to its design simplicity, its low maintenance costs, its high power-density (the highest among other renewable technologies) and its modularity makes it optimal for a domestic usage.

On the other hand, PV technology has many disadvantages. Even though the reduction of the production cost of a PV module is an almost accomplished challenge, the efficiency of a typical PV module is very low. This is not only due to its inability to absorb solar radiation from the complete solar spectrum but also because most of the solar radiation is converted into heat losses. Furthermore, high temperatures induce further efficiency decline. In order to alleviate this problem, it is an urgent need to reduce the temperature of the PV system. The simplest and least expensive method to accomplish that is with either natural or forced-air circulation. A more effective but expensive method of cooling is water-heat extraction (36) as in PV/T Systems, which will be subsequently elaborated.
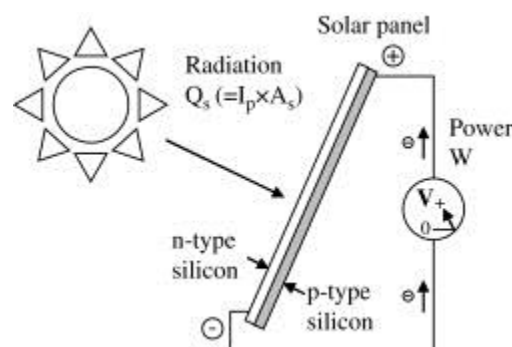
Figure 2.1: Schematic diagram of a solar photovoltaic panel silicon base.

16
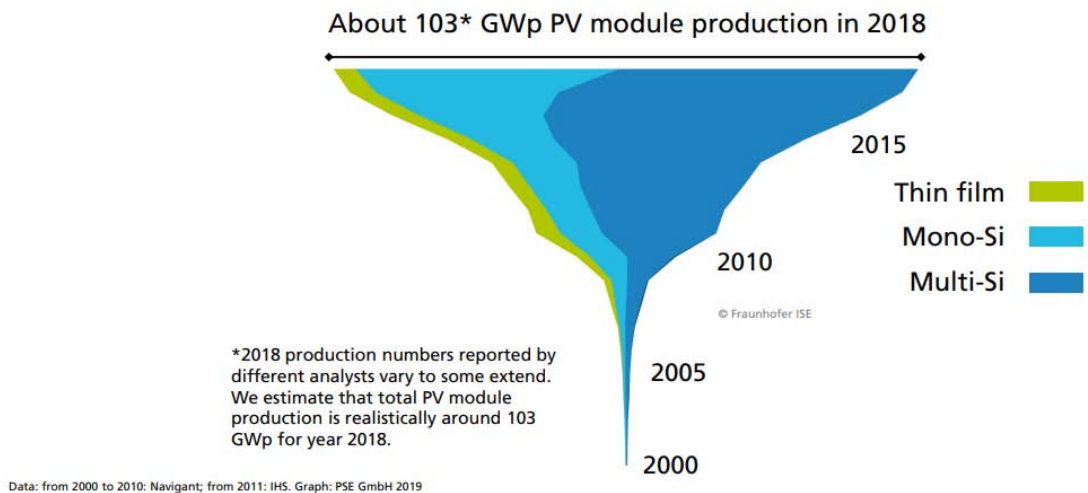
Figure 2.2: Annual PV Production by Technology Worldwide (in GWp)
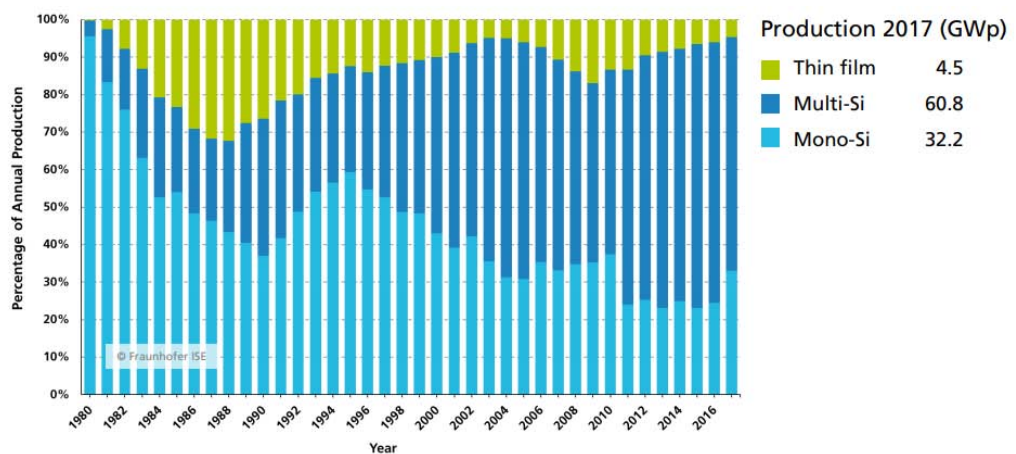
Figure 2.3: PV Production by Technology Percentage of Global Annual Production

The principle of *Concentrated Solar Power* is to take the heat produced by the sole direct solar irradiance and run a thermodynamic cycle with an organic heat vector fluid. A common Rankine cycle is not the best solution because the temperatures reached are way lower than the ones required to have a proper efficiency. Instead, an Organic Rankine Cycle (ORC) can well exploit the lower temperatures (18). An ORC works with a heat vector fluid that exchanges heat with the operative fluid; this then expands inside a turbine; condensates and is pumped again inside the heater (Figure 2.4). The shaft of the turbine is coupled with an electric generator, which provides electric power in AC.
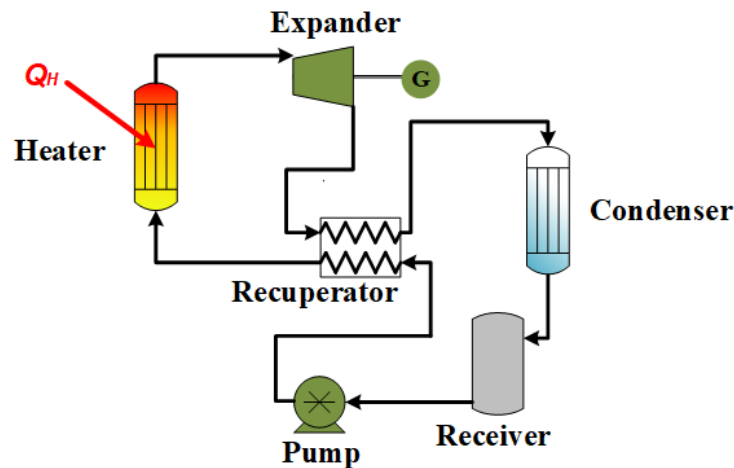
Figure 2.4: Schematic process scheme of a typical ORC configuration

Since energy is generated from heating a fluid using concentrators and mirrors, the main CSP configurations are divided by the type of reflector used (Figure 2.5):

- Parabolic trough collector. This technology is based on the reflection of direct sunlight onto parabolic mirrors towards an absorber pipe containing a Heat Transfer Fluid (HTF) (19).

- Solar power tower. The reflections of hundreds of mirrors, called heliostats, are concentrated into a single point (20). Electricity is generated by a thermo-dynamical cycle.

- Linear Fresnel reflector. It is based on the previous configurations. Unlike the first configuration, the receiver is not located within the mirrors, but in a separate tower (21). A recent design called a compact linear Fresnel reflector employs two parallel receivers in each row, making it more compact than parabolic trough collectors (22).

- Parabolic dish systems. A set of mirrors form a parabolic shape that concentrates sunlight in a focal point. This system can follow the sun in two directions, making it more efficient but also more expensive.

For whichever of these applications, the designed power is much higher than in PV because is possible to reach high temperatures necessary to start a thermodynamic cycle. In order to economically justify the cost of production and the wide area required the CSP optimal size is bigger than 100 MW (23). Therefore, such high power does not adapt well for a domestic user.
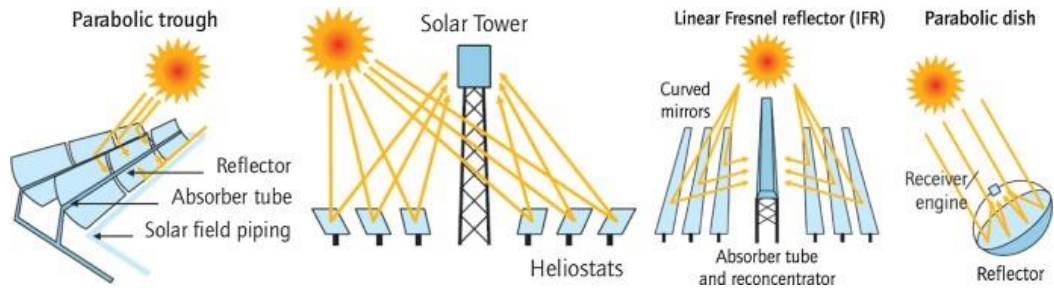
Figure 2.5: Current CSP configurations.

Compared to other energy conversion systems, solar power from PV panels is far quieter to generate and harness, drastically reducing the noise pollution required converting energy to a useful form. Residential size solar energy systems also have very little impact on the surrounding environment, in contrast with other RESs such as wind and hydroelectric power. Solar panels have no moving parts and require very little maintenance beyond regular cleaning. Without moving parts to break and replace, after the initial costs of installing the panels, maintenance and repair costs are very reasonable. The main problem of using solar energy is the cost involved. Solar efficiency and cost vary widely depending on the material and the manufacturing methods they are made from. Even when the cost of the panels is ignored, the cost of the storage units cannot be neglected. Other negative aspects of solar energy usage lay on the fact that is aleatory and its unstable production. In fact, a few cloudy days can have a large effect on the system, and during the night no energy can be collected at all (24).

In a comparison between the two main technologies described, the value of temperature must also be considered. The CSP efficiency increases with higher temperatures reached because the thermodynamic cycle increases its production the wider the difference of temperature between the hot and the cold source. On the other side, the PV works with the photovoltaic effect of a solar cell, in which a higher thermal motion means a higher electrons unstableness and therefore a decreasing efficiency. To increase PV efficiency the removal of heat is a key factor: if a heat exchanger is introduced and is connected to the panel the result not only improves the power production, but also furnish a surplus of heat that can be later used.

2.1.2 PV/T hybrid collector

The technology used to generate energy is the PV/T hybrid collector. This type of PV system has been developed in the effort to increase its efficiency and at the same time to generate heat and power. This could be possible by merging PV modules and solar thermal components. The increasing efficiency is strictly linked to the reduction of cell temperature with the circulation of a working fluid of the thermal subsystem. An unexpected benefit of this decrease of temperature is the extension of PV panel life since is prevented the silicon decay caused by high temperatures. The heat removed can later be used in various applications, including space and water heating, crop drying, industrial process heating and preheating. PV/T systems provide CHP generation in smaller area and with only low added cost compared to the installation of a separated PV and solar thermal system (37). The PV layer may fully or partially cover the thermal absorber.

PV/T systems can be classified in many ways, one useful manner is to divide them into three categories, according to the type of their PV module: flat plate, flexible and concentrated.

Flat plate PV/T systems consist of a flat-plate PV module which produces electricity from solar irradiance and a solar thermal absorber at the back which cools down the PV by extracting the heat in excess. This can be later used for a wide range of applications, such as hot water supply, solar cooling, thermal storage, desalination, space and pool heating. Flat plate systems may be glazed or unglazed. The first system results in higher power production, while the latter in increased heat extraction. Nevertheless, no more than three glass covers are recommended due to very low electrical efficiency (38).

Flexible PV/T operates like flat plate systems in low and medium temperature. Their structure is like that of flat plate systems, but their PV material is often amorphous Silicon (α-Si). Their electrical efficiency is pretty low (5-10%) (39) compared to the equivalent value of flat plate PV/T (6.7-15%) (40) but their thermal efficiencies are equal (22-79%) (40). Flexible PV/T systems can be used for hot water supply, space heating and freshwater production.

Concentrated PV/T systems operate in high temperatures due to their compound parabolic concentrator. Their electrical efficiency is almost equal to that of flat plate collectors (7-

16%) while their thermal efficiency is (39-70%) (41). Concentrated PV/T are ideal for absorption and adsorption refrigeration and dehumidification due to the high temperature of their working fluid as well as for hot water supply, freshwater production and greenhouse drying.

The structures of the above-mentioned three types of PV/T systems dependants on the PV module type are showed in Figure 2.6.

1: Glazing cover; 2: EVA-encapsulate; 3: Solar PV cells; 4: EVA-encapsulate;   1: Thin film PV; 2: Metal roof; 3: Fin sheet; 4: Thermal pipes; 5: Insulation
5: TPT back sheet; 6: Thermal absorber; 7: Thermal insulation

1:TPT
2:EVA
3:PV module
4:square pipe
5:thermal insulation
6:front glazing
7:concentrator
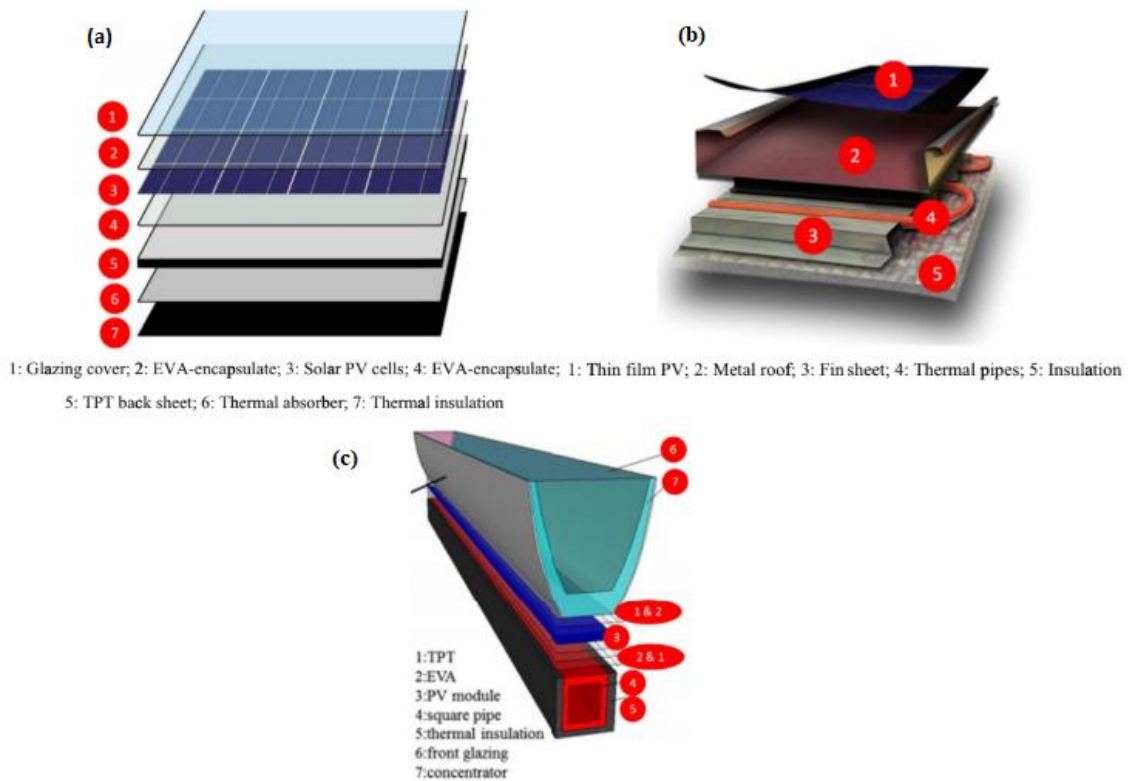
Figure 2.6: Schematic of (a) Flat Plate PV/T (b) Flexible PV/T (c) Concentrated PV/T (42).

Latest studies indicate that different kinds of thermal absorbers are better suited depending on the PV/T module application. The most appropriate type of thermal absorber in PV/T technology is the *sheet-and-tube* structure thanks to its good heat-transfer efficiency and its low cost due to established industry. Nevertheless, it is not exclusively used as it is characterized by complex structure with demanding welding techniques and heavy weight with risk of leakage of the working fluid. Another widely implemented thermal absorber in PVT technology is *rectangular tunnel with or without fins/grooves*. A great range of working fluids, such as water, air, phase change materials, thermal oil and nanofluids, can be used in large scale projects. Their simple structure, low

cost and low weight have led to their great popularity despite their relatively low efficiency. The addition of fins or grooves improves the heat-transfer efficiency as the flow becomes more turbulent (38) (43). These two types of thermal absorbers can be installed in all three types of PV/T modules aforementioned.

Flat plate tube is a common absorber of flat plate PV/T modules as it improves the contact between the thermal and the PV layer. However, its high flow resistance and leakage risk combined with the increased fluid temperature confine its establishment as a prominent thermal absorber. Novel technologies for flat plate and flexible PVT modules include the *micro-channel heat pipe* which is characterized by its high heat transfer performance and reliability (44) but also by its increased thermal resistance and uneven temperature distribution, the *extruded heat exchanger* with its simple and inexpensive construction but its high volume of working fluid, the *roll-bond heat exchanger* which is characterized by its uniform temperature profile, low weight and high efficiency, yet it is not long-term reliable and there is a high risk of corrosion, and the *cotton wick structure* which is inexpensive but inefficient.

The integration of PV/T modules has an impact on their thermal efficiency due to thermal resistance between PV layer and thermal absorber. Different integration methods have been proposed depending on the application. *Direct contact* of the two layers is the simplest solution with no additional thermal resistance, however high freezing risk in cold environments and low heat removal efficiency have led to its limited application. This method can be used in flat plate and flexible PV/T modules. Another method which can be implemented in all PV/T modules is the use of *thermal adhesive*. This technique is simple and cheap, but the formation of narrow air-gap bubbles and the imprecision of the adhesive thickness result in increased heat losses (40). Mechanical fixing of flat plate and concentrated PV/T systems ensures firm combination of the PV and thermal layer. Nevertheless, the existence of air gaps combined with high cost and weight of the equipment decrease the overall efficiency. The most promising integration technique for flat plate PV/T systems is the *EVA based lamination*. This method is cost-effective and secures a firm, low thermal-resistant combination, although careful attention need to be paid during the lamination process in order to avoid geometry deformation (45).

PV/T systems can be also classified according to the type of working fluid of the thermal subsystem: the conventional are air-, water- and bifluid-based PV/T collectors.

In *air-based PV/T collectors*, air is designed to pass through the PV surface with either active or passive mode through various absorber configurations. Single or double pass can be used, where the former is less efficient than the latter (46). Experiments conducted by Jin et al. (47) showed that higher thermal efficiency is obtained with a glazed system while higher electrical efficiency is achieved with an unglazed one.   The main disadvantage of air-based systems is their inability to work efficiently at high temperature due to air low density and heat capacity.

Water-based PV/T collectors achieve higher thermal output compared to air-based, as water has better heat transfer properties than air. Nevertheless, the cost of an additional water heat exchanger should be taken into consideration during the design of the system. Research results indicate that the use of glass covers results in higher thermal and energy output, while an unglazed system provides higher electrical and exergy output (48).

Bifluid based PV/T collectors are designed in order to overcome the limitations of air- and water-based PV/T modules. The two fluids used by researchers are water and air, resulting in higher total efficiency at the expense of higher power consumption and more expensive construction.

Novel PV/T systems proposed are meant to increase electricity production and include the use of nanofluids, heat pipes and phase change materials (PCM). Nanofluids may be used either as heat transfer fluids or as optical filters depending on their properties and characteristics, resulting in significant enhancement on performance parameters of PV/T systems (49) (50). Heat pipes extract heat form the PV back surface for the evaporation process. This heat is then offered as a thermal output to a working fluid via the condensation process and can be used for various applications, such as hot water supply, space heating etc. At last, PCM proposed in literature improve the efficiency of PV/T systems. Nevertheless, careful attention should be paid to their melting temperature and thickness in order to integrate them as well as possible.

Figure 2.7: Comparison of performance parameters of various PV/T systems (53)
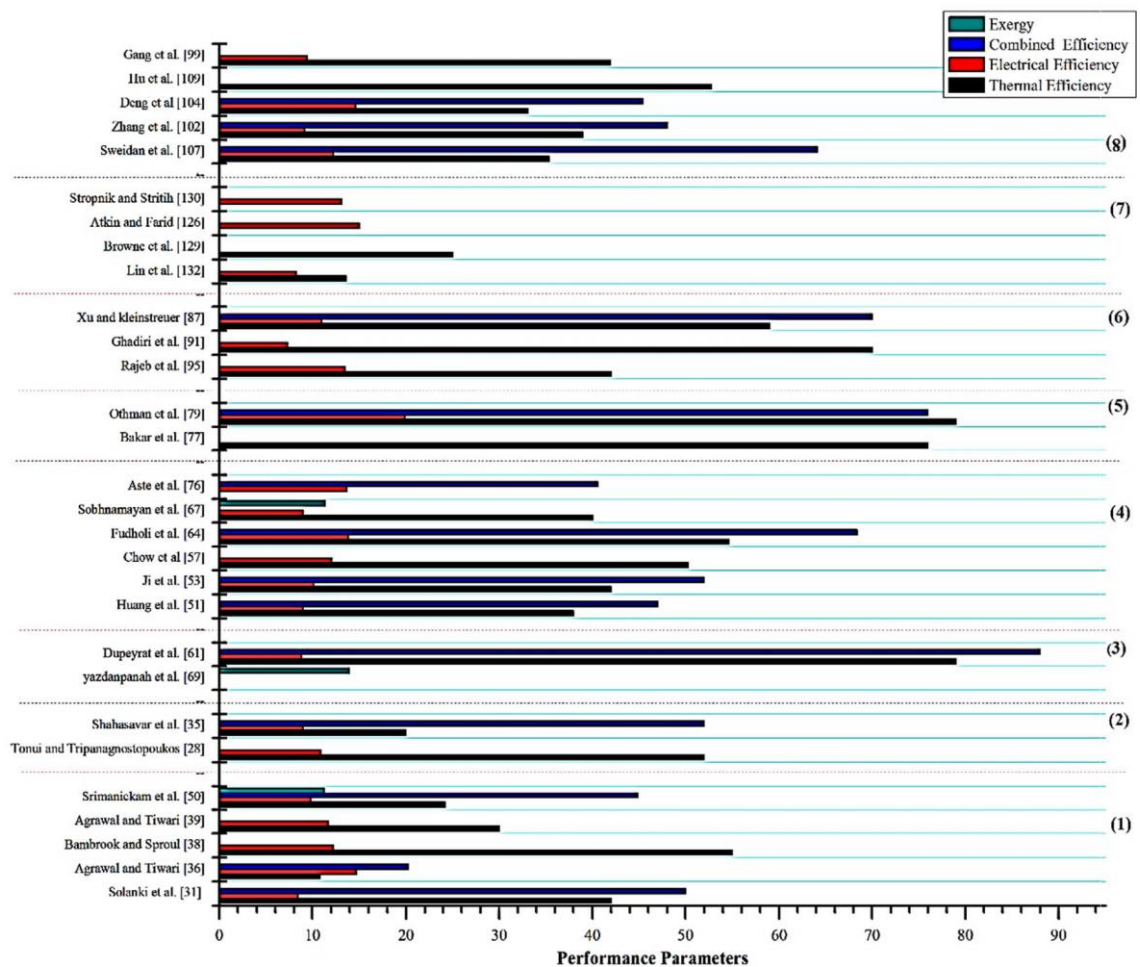
(1) - Air based PV/T (Monocrystalline)   (5) - Bifluid based PV/T (Monocrystalline)

(2) - Air based PV/T (Polycrystalline)   (6) - Nanofluid based PV/T (Monocrystalline)

(3) - Water based PV/T (Monocrystalline)   (7) - PCM based PV/T (Monocrystalline)

(4) - Water based PV/T (Polycrystalline)   (8) - Heatpipe based PV/T (Monocrystalline)

Research work has been extensively carried out in building integrated PV/T hybrid collectors in order to accomplish a more viable and prominent solution for building heat load. Compared to a conventional building integrated PV panel, this solution has an overall efficiency 17-20% higher (54). A great number of working fluids have been studied, such as water, air, heat pipe, PCM, showing promising results as a sustainable technology for heat and electricity production (51) (52). Further analysis stated that the application of hybrid collectors in building has the best potential and higher market for liquid PV/T systems that supply DHW (37). Figure 2.7 shows that the technology that allows the highest combined efficiency is the water-based PV/T monocrystalline system. Moreover, building integrated PV/T hybrid collectors is the only sustainable application

24

of PV/T system found in the literature (53). In order to have less thermal stress and a slightly higher efficiency during the summer, the best way to integrate a PV/T hybrid collector in a building is to extract the heat into the building envelope with a forced air ventilation. However, this solution is more complex, while a natural air ventilation is the least efficient solution: in a yearly evaluation the conventional PV/T collector installed above the envelope (building-added) is still a good compromise (55). Also, a building-added water-based PV/T system is environmentally more efficient than a building-integrated air-based PV/T system (56).

With all the considerations stated so far, the type of PV/T hybrid collector chosen is a flat-plate water-based one and has been implemented as if it was installed above the building envelope.

2.1.3 From DC to AC, power storage and grid connection

Set that the power is provided by a technology based on the PV effect, a consideration must be taken into account. The electricity produced by a PV module is in direct current (DC) while a common user connected to whichever distribution grid requires an alternate current (AC). Moreover, in order to track the maximum power point (MPPT) at which the PV module can extract the highest amount of energy from the available solar irradiance, a power electronic device is needed. A tool that can satisfy both these requests is the power inverter. An example of this component is represented in Figure 2.8.

The power produced when is not absorbed by the load must be stored. The introduction of an electrical battery storage is not convenient if an electrical network is available (26). Since the system is based on two cities located on the mainland of the relative country, this can be easily plugged to the grid. Therefore, the surplus of energy has been sent to the electricity grid. Moreover, the grid connection provides electrical power whenever the one produced from the PV/T panel is not enough or null. However, the introduction of an electrochemical battery storage was considered for a comparison case.
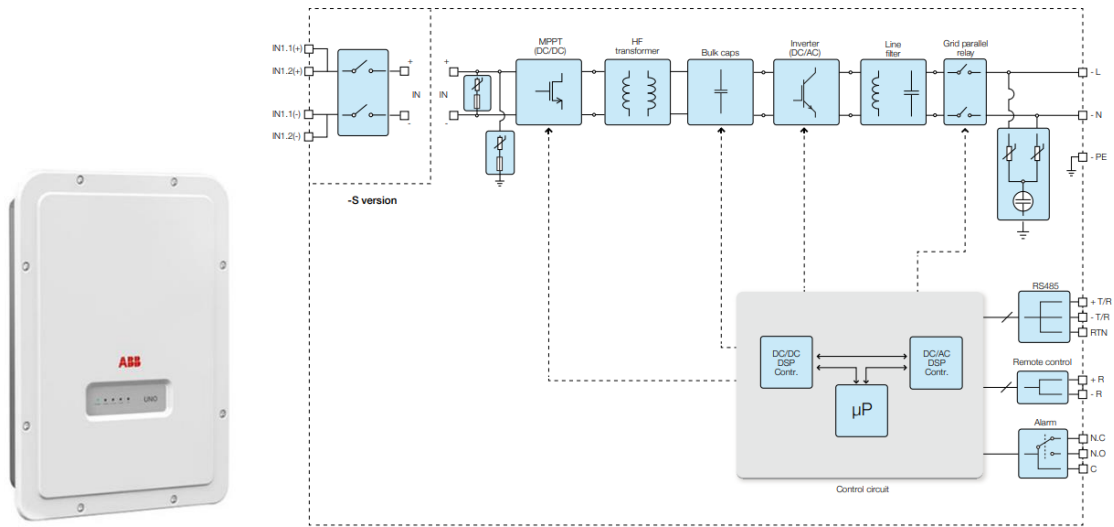
Figure 2.8: Picture and schematic representation of a commercial power inverter (ABB^{TM}) (25)

2.2 Solar irradiance to domestic hot water

The problem of producing heat from the solar irradiance has been solved by the technology of the solar thermal collectors. Their classification depends on the construction: the presence or absence of a glazing, the flat plate or tube glass configuration, the presence or absence of a concentrating surface.
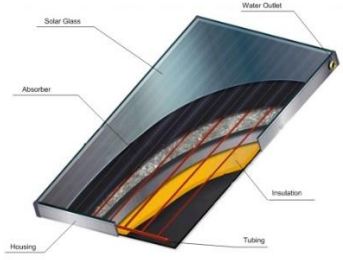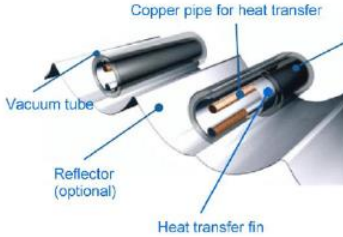
Moreover, a mean to store DHW and a backup source of heat have been investigated.

2.2.1 From solar irradiance to thermal energy

Technologies that convert directly solar irradiance into thermal energy go under the name of solar collectors. The main working principle is the indirect heating of a heat transfer fluid through a conductive surface, usually covered by a captive surface.

Even though its way of operating is simple, there are many different types that are used mainly in residential sector: those in Table 2.1 are the four most exploited (27).

Table 2.1: Different solar thermal collectors with correlated characteristics and representation. (27)

Collector type (Common field of application)	Characteristics	Picture
Unglazed collectors (**Swimming pools, evaporators for heat pumps**)	Metallic uncovered absorber. High performance at low temperatures (close to ambient temperature) and highly dependent of the wind speed Inexpensive. Sometimes designed for working under dew-point of ambient air (heat pumps).	
Flat plate (**Domestic hot water systems, combi systems and district heating**)	Consists of a metallic absorber and an insulated casing topped with glass plate(s). Good performance at higher temperatures (typical temperatures for domestic hot water).	
Vacuum tubes (**Domestic hot water systems, combined systems and district heating. Solar assisted cooling, process heat**)	Have less heat loss and perform better at high temperatures. A metallic absorber inserted in an evacuated glass tube, to withstand the pressure difference between the vacuum and the atmosphere (typical temperatures for domestic hot water and above).	
Stationary concentrating **e.g. CPCs** (**Domestic hot water systems, combined systems and district heating. Solar assisted cooling, process heat**)	Good performance at high temperatures. Low content of raw materials.	

In a solar thermal collector, the efficiency depends basically on the kind of technology used and, on a parameter, T_m^* called reduced temperature difference. To a low value of this parameter is associated a high solar irradiance as well a low difference of temperature between the fluid and the external environment. As can be stated from Figure 2.9, the two configurations that could guarantee higher efficiencies for DHW are the flat plate and the vacuum tube. However, since the cost of a flat configuration is lower than the evacuated tube one, this kind of thermal collector is a good compromise between an efficient and a cheap solution.
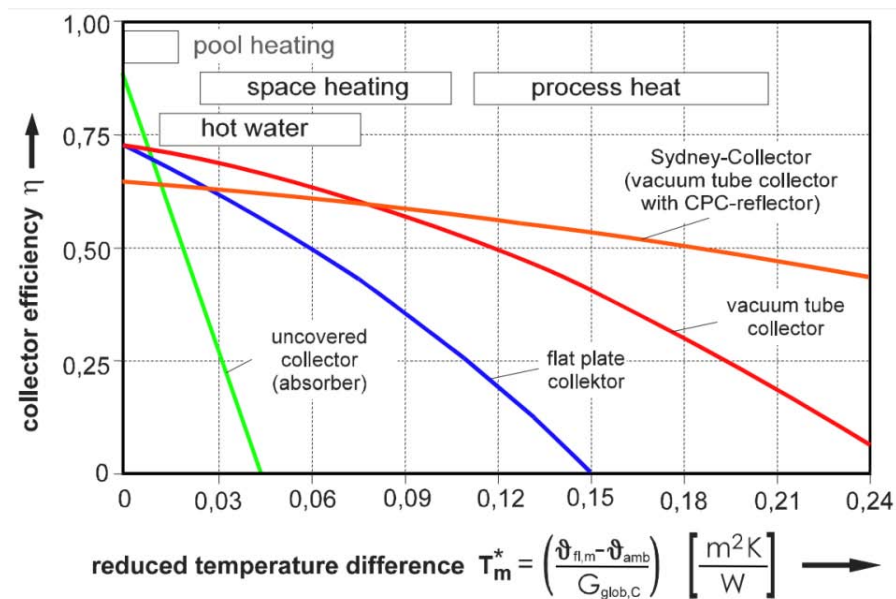
Figure 2.9: Efficiency of the four main types of solar thermal collector. (28)

2.2.2 Thermal storage and grid connection

The heat provided from a solar collector is often produced when the user does not require it and vice versa. Therefore, a TST is needed. Moreover, the heat furnished by the solar collector is often not enough to satisfy the load, so a backup unit is required. To accomplish the target an NGH connected to the natural gas pipeline has been coupled with the solar collector as input of the TST.

2.3   Solar irradiance to space heating & cooling

The problem of producing space heating and cooling for a residential user is seasonal because the two loads are separated in time, i.e. their usage never happens simultaneously. This means that a single component should be used in order to maximise its usage during the year. Heat pumps can supply both demands and are a well-known technology. As can be seen in Figure 2.10, their share has been rising in the past decades. The cause can be found in their high and still increasing efficiencies, compared to other technologies such as electric resistance heater or a condensing gas boiler. Nevertheless, electric heat pumps still meet less than 3% of heating needs in buildings globally, yet they could supply more than 90% of global space and water heating with lower CO_2 emissions (29).
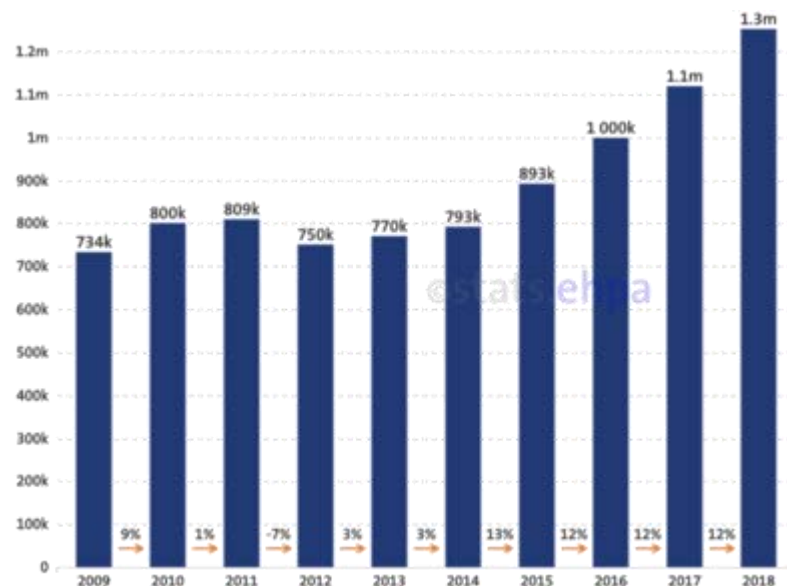
Figure 2.10: Sales development from 2009 to 2018 (EHPA) (33)

2.3.1 Heat pump principle & classification

A heat pump is a thermal machine that requires operating energy to convert heat from a certain level of temperature to another in two different manners, depending on the operative mode:

- In the winter case a low temperature energy from a heat source is converted into a high temperature energy to a heat sink (heating)

- In the summer case a high temperature energy from a heat source is converted into a low temperature energy to a heat sink (cooling)

Figure 2.11 shows the energy flows and concepts for heat pumps systems.
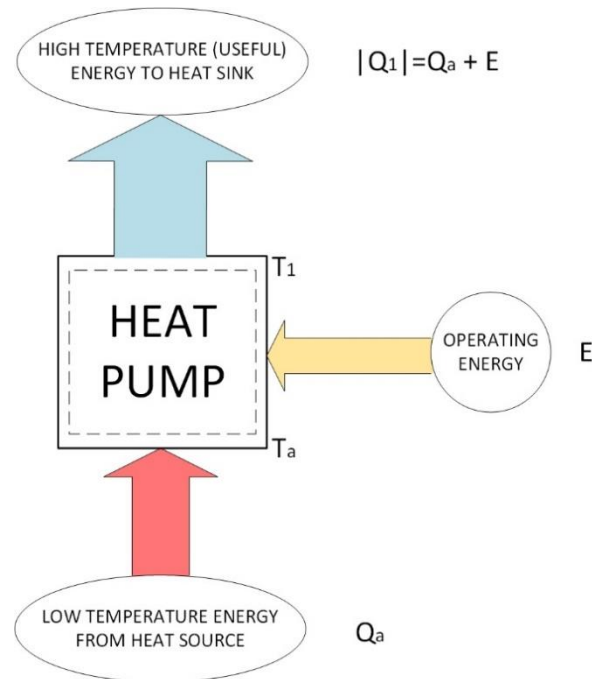
Figure 2.11: Operation concept of a heat pump: Q_a is the heat absorbed, $|Q_1|$ is in module the heat (or cold) produced, E is the operating energy provided from an external source.

The kind of energy required to make the machine work determines the type of the heat pump (30):

- Mechanical air or vapour compression (driven by electrical motors)
- High temperature thermal absorption (usually by burning natural gas or propane)
- Vapour thermocompression (by using an ejector)

The first ones are subdivided into 3 different types, depending on the fluids used to exchange energy with the source and with the sink:

- Air source to air
- Air source to water
- Ground source to water

For district and domestic usage, the most commonly adopted are the first ones (31). More specifically, in Europe the air source types are widely preferred (32).
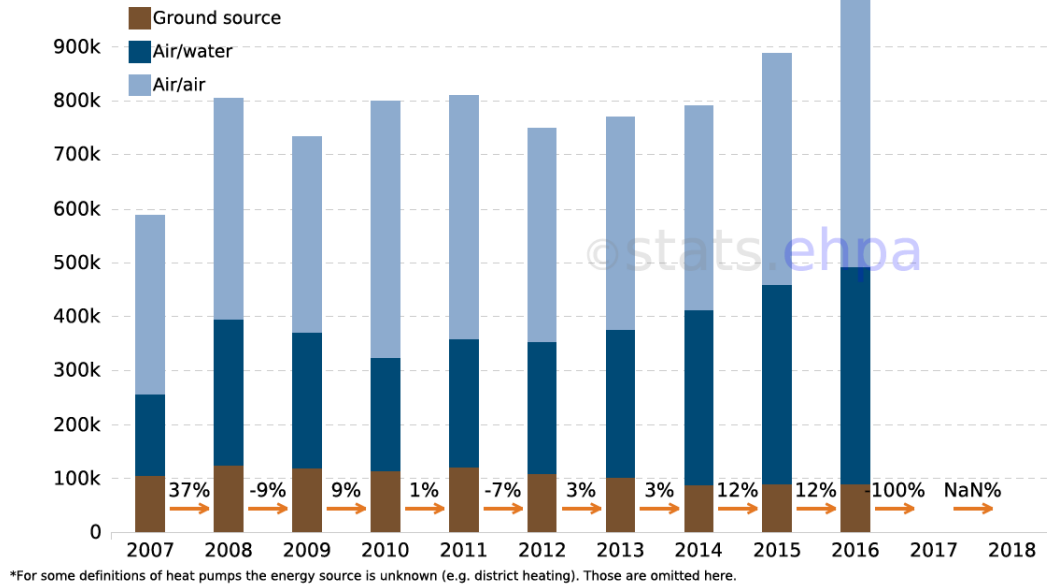
Figure 2.12: Sales development by source, from 2007 to 2016 (EHPA) (32)

Air and water are the two most common thermal vectors for their availability, but they are very different in terms of thermodynamic properties. Air is widely available and free of cost, but has worse thermal properties, i.e. lower specific heat, lower density and lower thermal conductivity. Instead distilled water is not as much available and has a non-negligible cost, but has better thermal properties, i.e. higher specific heat, higher density and higher thermal conductivity. Some of their properties are reported in Table 2.2.

Table 2.3: Thermal properties of air and water in standard conditions (34)

Thermal property at $T_{amb} = 288.15\ K$	Air	Water
Density $\rho\ [kg/m^3]$	1.225	999.1
Specific heat $c_p\ [kJ/(kg\ K)]$	1.007	4.186
Thermal conductivity $\lambda\ [W/(m\ K)]$	0.02476	0.589

From this evaluation, an air to water electrical driven heat pump seems to be a good compromise between economic and thermal efficiency.

2.3.2 Mechanical & thermal heat pumps thermodynamics

In energetic terms, the efficiency is described as the performance factor ε, expressed as the ratio between the useful energetic effect and the energy required to obtain it. Generically is defined as:

$$\varepsilon = \frac{|\dot{Q}_1|}{P} = \frac{|\dot{Q}_1|}{|\dot{Q}_1| - |\dot{Q}_a|} \tag{1}$$

where $|\dot{Q}|$ is the absolute value of the heat obtained in the sink, $|\dot{Q}_{amb}|$ is the absolute value of the overall heat absorbed from the source and P is the electric power needed for the compression of the working fluid. Depending on the season we are working in, we have two different kinds of performance factor:

- COP (Coefficient of Performance)
- EER (Energy Efficiency Rating)

According to operative parameters, the performance factors change throughout the year due to the fact that temperature and variable. Therefore, a seasonal performance factor is set (i.e. SCOP and SEER).

For an ideal reversible double-thermal heat pump, so with a working fluid of the cycle going exactly from the temperatures T_1 and T_a of the sink and the source respectively, would result:

$$\varepsilon^* = \frac{T_1}{T_1 - T_a} = \frac{1}{1 - T_a/T_1} \tag{2}$$

Which represents the maximum limit value that can be taken as reference by a real application; truly, in the common operative conditions at which the heat pumps work, it is difficult to reach the half of this value. From the equation it can be seen how the ideal performance factor grows the more the closer the two temperatures get, i.e. when the ratio T_a/T_1 aims at 1. The performance factor of real applications behaves obviously the same, which shows how a heat pump, to be effective, should operate between temperatures of the sink and of the source relatively close. In order to work as well as possible for a heat pump configuration the proper conditions are (according to their usage):

- In summer the source temperature should be as low as possible and the sink temperature as high as possible
- In winter the source temperature should be as high as possible and the sink temperature as low as possible

Therefore, for example, in the usage of a heat pump for hot water in winter space heating, a radiant panels underfloor or a fan coils system should be designed: as a matter of fact, these heat sources require water at a moderate temperature (35-45°C), rather than a radiators plant, which work with much hotter water (60-80°C).

The analysis of convenience of a heat pump heating, instead of a fossil fuels direct combustion requires the consideration of multiple technological and economic factors not easily generalizable (35). By speaking uniquely of the primary energy saved, PES, it can be seen (referring to mechanical heat pumps driven by an electric motor) that the electric energy unit given to the user roughly equals 3.3 units of thermal energy in terms of lower heating value, LHV, of the fuel burned in a thermal power station: this fact takes into account the conversion efficiency of the plant, the power losses of transformation and of distribution. The same 3.3 combustion units burned in a heater by the user, let available more or less 2.6 units of thermal energy usable in the heating process. Therefore, by only considering the PES, the heat pump is convenient whenever the performance factor > 2.6.

Regarding the *mechanical heat pumps*, the Figure 2.13 shows the plant scheme and the thermodynamic cycle in the $T - s$ diagram for a simple vapour compression heat pump. It has to be considered "real" the machine cycle $2 - 3 - 4 - 5$, extrapolated from the reference ideal one $2' - 3 - 4 - 5$ considering only the internal irreversibility in the compression. The diagram also shows how it is necessary that the evaporation temperature of the working fluid must take place at a $T_e < T_a$ and that the condensation temperature at a $T_c > T_1$ in order to occur the required heat exchanges.
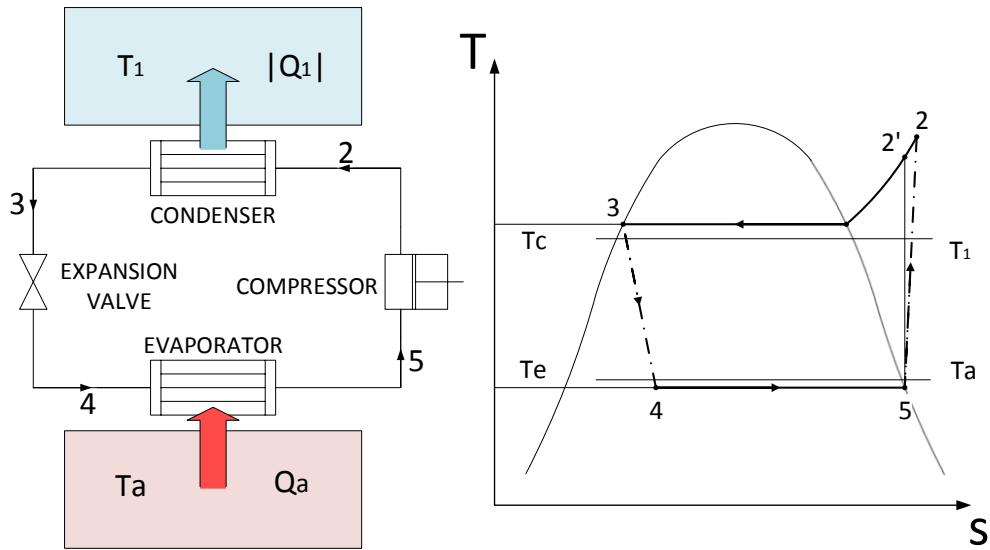
Figure 2.13: Schematic thermodynamic cycle and temperature-entropy (T-s) diagram of a mechanical heat pump

For the considered cycle, and in the same hypothesis of both kinetic and potential energy neglection at the extreme states of the single transformation, the value of the performance factor can be calculated as following:

$$\varepsilon = \frac{h_2 - h_3}{h_2 - h_5} \tag{3}$$

It is to be noticed from the Figure 2.13 how easy it is for a scheme as shown to change from heat production machine to a refrigerating one, for example just by commuting the function of the two heat exchangers by inverting the flow circulation of the working fluid by the action of a special four ways valve (or "cycle inversion valve"). This kind of machine are known also as invertible or reversible, and their use allows the satisfaction of both the space climatization requirements: working as a heat pump during the winter and as a refrigerating machine during the summer period.

The *thermal heat pumps*, on the other hand, use as drive force a thermal flow to a relatively high temperature (higher than the one at which must be available the useful heat $|\dot{Q}_1|$): because of that these are tri-thermal thermodynamic cycles, and so plants with three different thermal external interactions: to the two of the already mentioned must be summed the exchange of the heat $\dot{Q}_g$ at the temperature $T_g > T_1 > T_a$. According to the general definition, the expression of the performance factor for a thermal heat pump is:

34

$$\varepsilon_t = \frac{|\dot{Q}_1|}{\dot{Q}_g} \tag{4}$$

Where other eventual power requirements (i.e. pumps) are neglected. It can be seen how useless it is to try to compare the performance factors values of mechanical and thermal heat pumps, since the driving energy quality is totally different. For an ideal thermal heat pump, i.e. with all reversible operations, the first and second principle of thermodynamics allow writing:

$$|\dot{Q}_1| = \dot{Q}_g + \dot{Q}_a \tag{5}$$

$$\frac{\dot{Q}_g}{T_g} + \frac{\dot{Q}_a}{T_a} - \frac{|\dot{Q}_1|}{T_1} = 0 \tag{6}$$

From which can be evaluated immediately:

$$\varepsilon_t^* = \frac{|\dot{Q}_1|}{\dot{Q}_g} = \frac{T_1(T_g - T_a)}{T_g(T_1 - T_a)} \tag{7}$$

ε_t^* represents obviously the maximum value available for the performance factor of thermal heat pumps: real values are sensibly lower. By comparing the ideal values ε^* and ε_t^* it can be seen how the second one tends to the first when $T_g \rightarrow \infty$. The most common types of thermal heat pumps are the *adsorption* and *thermo-compression* ones. The working fluids that now find practical usage are still limited at the couples $NH_3 - H_2O$ or $H_2O - LiBr$.

2.3.3 Choice of the technology

In order to exploit the optimal technology that satisfies both space heating and cooling loads, a consideration on the two types of heat pumps must be done. The concept that lays within the choice is to match as well as possible the production of energy and the loads throughout the whole year. Therefore, the choice of the kind of heat pump depends mainly on the PV/T system.

In literature, many examples of drive a heat pump with a PV panel have been studied. In most solar electric chillers, the refrigeration system is realized by a vapor compression cycle.

In one of the first studies of solar electric cooling, Ayyash and Sartawi (1983) (57) compared the initial and operating costs of a PV-assisted VCC system and a solar absorption system. The results of the simulations showed that the solar electric system could be cost competitive.

Hartmann et al. (2011) (58) compared the performance of a solar electric system (a PV-driven mechanical compression chiller) and a solar thermal system (an adsorption chiller powered by flat-plate collectors) in terms of primary energy savings and their costs. Both systems were used to cover the heating and cooling loads of a typical building in two different European climates. A conventional compression chiller powered by the grid was used as a reference for the cost and energy savings calculations, with a nominal capacity able to cover the peak thermal load of the building. Both systems were more expensive than the conventional compression chiller. The solar electric system appeared to be a more competitive choice, being only 5% more expensive than the conventional chiller. In terms of the collector area, in order to achieve the same energy savings, the PV field area had to be six times smaller than the surface of the flat-plate collectors.

Beccali et al. (2014) (59)compared six different configurations. The reference system (system 1) was a conventional VCC system (with a nominal EER of 2.5) connected to the grid for cooling loads. For PV-assisted systems, three configurations were evaluated:

- The conventional chiller is simultaneously driven by PV panels and the grid.
- The conventional chiller is solely driven by PV panels.
- Partial-load standalone PV driving of the conventional chiller.

Two options were considered for a summer backup heat driven system:

- A backup natural-gas-fired burner to feed the absorption chiller generator.
- A conventional compression chiller to enhance the cooling production.

For hotter climates the optimal solution in terms of primary energy savings and payback time is a conventional chiller driven by both PV panels and the grid.

Calise et al. (2016) (60) developed a dynamic model and presented a thermo-economic analysis

for a polygeneration system consisting of PV/T collectors driving a water-to-water electric heat pump and a zeolite-water adsorption chiller. From an economic point of view the system is not competitive unless a generous subsidy is provided.

Bianchini et al. (2017) (61) investigated the potential of a PV/T system located in Forlì, Italy. The results indicated that PV cooling resulted in a 1–3% increase in the electric yield of the system. At an average outlet temperature of 40°C, the system was able to produce 835 kWh/m² of electricity and 1600 kWh/ m² of heat. On a yearly basis, the system was able to produce approximately 1360 kWh/y of electricity, while the respective thermal production ranged between 267–443 kWh/m², depending on the average inlet temperature of the cooling fluid. The investigated system was also economically compared with separate PV and flat-plate solar collectors. According to the results, the PVT system was able to be competitive when its installation costs were in the range of €3.700–4.700/kWp.

As already stated in the previous subchapters, the heat extracted from the PV/T hybrid collector has been exploited for DHW production. So, after all these considerations a preliminary choice of a mechanical heat pump driven by both the grid and the PV part of the PV/T system has been chosen.

2.3.4 Thermal storage

The working principle of the system is to produce heat and cold whenever the user requires them. In order to match the demand and the generation, the PV/T hybrid collector should produce whenever one of the two loads is required. However, the energy provided is often produced when the user does not require it and vice versa. Therefore, a TST is needed. Moreover, the energy furnished by the PV/T is often not enough to satisfy the load, so a backup unit is required. To accomplish the target, as already seen on the first chapter, the electricity grid has been chosen.

Conclusions

In this chapter the choice of each component of the system has been justified. A flat-plate water-based PV/T hybrid collector has been chosen as main component of the system, where the PV panel generates the power required and feeds the electrical driven HP, while the heat extracted from the thermal collector supplies DHW. In the end, two thermal storage tanks (TSTs) are used as means of energy storage, while the electric grid and a natural gas boiler (NGB) are meant to be used as backup for those situations in which the energy produced is not enough.

3. METHODS

The problem faced in this chapter is the operation analysis of a system in which the environmental data and the four loads curves are taken from a deterministic values database. However, in order to check if the system works correctly with the deterministic data, several simulations and different cases have been developed with fictious data.

The fundamental components are:

- PV/T hybrid collectors
- DC/AC power inverter
- Heat pump (HP)
- Two thermal storage tanks (TSTs)
- Natural gas heater (NGH)

The HP and the NGH are sized in function of the load curves: the HP refers to the maximum space heating or cooling load, while the NGH to the maximum DHW load. The designs of other elements such as the area of the PV/T hybrid collectors field and the volumes of the TSTs are left to be optimized as open system variables. However, for the initial simulations these values have been predetermined. Moreover, for the different cases analysis, other components have been introduced in substitution or in addition of the already mentioned. These are:

- PV panels
- Solar thermal collectors
- Battery energy storage system (BESS)

The initial sizing of the PV panels and the solar thermal collectors depended on the comparison with the PV/T hybrid collectors. The formers were designed in function of the nominal power produced by the latter: i.e. a certain area for the PV field was determined as much electrical power as the hybrid solution, and a different surface was calculated to produce the same amount of thermal power of the PV/T collectors field. On the other hand, the BESS was sized for stand-alone usage, i.e. with enough energy storage to supply the user even during the least sunny day of the year.

3.1 Model

The purpose of the model is to see how the system develops, i.e. how the energy transformations that happen in every component vary in function of the inputs and outputs set. This requires solving a problem of n constrained variables, m equations and $n - m$ unconstrained variables. The selection of the variables in subchapter 3.3 took into consideration the fact that some values need to be fixed in order to not overcharge the work of the optimization process. Moreover, some aspects of the system are useless for the optimization itself.

The model was built with the simulation tool Simulink; a program enhanced with Matlab which allows a modular sequential approach. The mass (MB) and energy (EB) balances are set in different modalities: the MB are simple, since are pre-fixed values that for simplicity in calculations do not change all over the system; while the EB for each load have been calculated separately.

Moreover, the equations linked to the performances of each component are required, so the values that characterize all the components are determined both at the design and at the off-design conditions.
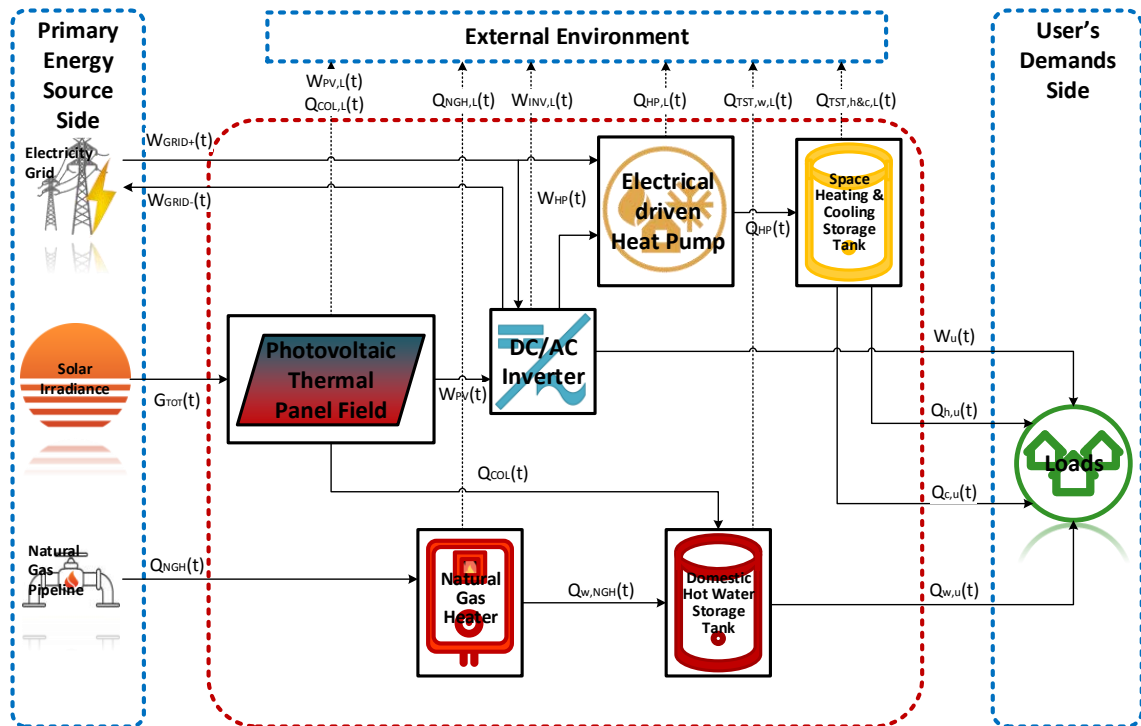
Figure 3.1: Flowsheet diagram of the original system.

3.2 Flowsheet of the system

As can be seen from Figure 3.1, the system is defined by its boundaries: everything that lies within them is considered to be part of it. In the flowsheet diagram of the system the red dashed line marks its edges. The blue dashed lines delimit three outer sides: the primary energy sources, the external environment and the user demands one. The first side consists in the supply of energy coming from outside, i.e. the solar irradiance that hits the panels, the electrical power from the grid to the user and to drive the heat pump, and the natural gas from the pipeline to the heater. Each black box represents a component of the system, while the lines that link them are divided into two kinds. The straight arrows show the direction of the flow of energy from a block to another, while the dashed ones represent the energy losses of each component towards the external environment. The only type of flow represented is the energy flow. This is because only the energy balances vary, since they depend on energetic variables. In addition, mass flow rates remain constant for each component; therefore, the mass balances are easily solvable and not much worthy to be introduced in the flowsheet.
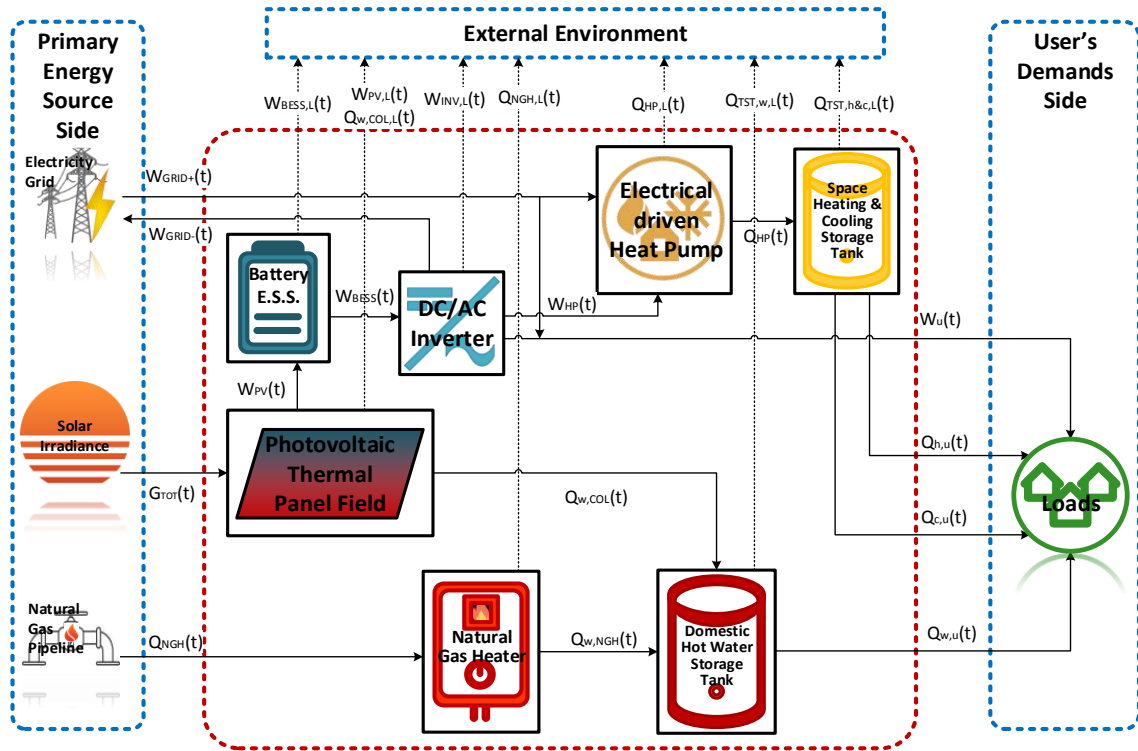
Figure 3.2: Flowsheet diagram of the original system with the introduction of the BESS

41

The flowsheet of the specific case of the PV/T original system with the introduction of the BESS is presented in Figure 3.2. This is the only other case represented because the other configuration is very similar to the main one in terms of representation. For the separated solution the PV/T hybrid collectors is split and replaced with two panels that are connected to the relatives flows of energy: a PV and a thermal one.

3.3 Inputs

A distinction must be made between the physical and the calculation inputs. The former are the flows of energy and mass that are required to solve the respective balances. The latter are the variables given at the beginning of the simulation in order to let the model run.

The physical inputs of this system are the flows coming from the primary energy source side, which take into consideration the electrical power to and from the grid, $\dot{W}^-_{GRID}$ and $\dot{W}^+_{GRID}$ respectively. the solar irradiance G_{TOT} and the mass flow rate of the natural gas from the pipeline $\dot{m}_{NGH}$. However, for the reason yet explained, the mass flow rate has been directly substituted by the thermal power provided by the pipeline $\dot{Q}_{NGH}$.

Once given $n = 72$ total number of variables, $m = 32$ equations of the system, the calculation inputs needed for the resolution of the problem are the pre-set unconstrained variables $n - m = 40$. These can be subdivided into three main categories: the environmental data, the variables set as parameter and the system variables. The environmental data given as input are the solar irradiance I_{TOT}, the ambient temperature T_{amb}, the wind speed u_w and the ambient pressure p_{amb}.

The variables set as parameters are the loads, the characteristic curves of all the components, and the constant parameters. The four loads considered are the electrical power $\dot{W}_u(kW)$, the domestic hot water $\dot{Q}_{w,u}(kW)$, the space heating $\dot{Q}_{h,u}(kW)$ and cooling $\dot{Q}_{c,u}(kW)$ demanded by the user. The characteristic curves of all the components are the transfer functions that allow converting one flow of energy into another. These are the efficiencies related to the PV section of the panel $\eta_{PV}(\%)$, to the thermal collector

$\eta_{col}(\%)$, to the heat pump $COP(kW/kW)$ (in heating mode) and $EER(kW/kW)$ (in cooling mode), to the NGH $\eta_{comb}(\%)$, to the inverter $\eta_{inv}(\%)$, to the charge-discharge of the BESS $\eta_{BESS}(\%)$, and the global heat exchange factor of the TSTs $U_{TST}[W/(m^2 K)]$. Moreover, some coefficients are taken for granted as constant values in the equations of the efficiencies.

3.3.1 System variables

The choice of the unconstrained variables of the system allows determining the sizing of the plant, which is the problem this work is requested to solve. Since the maximum values of the loads establish the design conditions of the HP and the NGB, these are chosen by comparing the requested values with commercially available solutions. The sizing of the inverter depends on the maximum power reached by the PV production. Regarding the other cases simulations, the sizing of the panels and collectors depended on the hybrid solution, while the design of the BESS depended on the worst ambient conditions. Moreover, all the mass flow rates and temperatures are set in function of the loads and of the environmental data. Therefore, the following are set as free system variables:

- A_{PVT} (m^2), the surface of the PV/T hybrid collectors field
- $Vol_W(m^3)$, the volume of the DHW load TST
- $Vol_{HP}(m^3)$, the volume of the TST coupled with the HP

However, for simulation purpose, all of these are predetermined, while during the optimization process are left free for the reasons already mentioned.

3.4   Outputs

As happened for the inputs, a distinction between physical and calculation outputs must be done as well.

The physical outputs are the four loads considered, i.e. the electrical power $\dot{W}_u$, the domestic hot water $\dot{Q}_{w,u}$, the space heating $\dot{Q}_{h,u}$ and cooling $\dot{Q}_{c,u}$ demanded by the user.

The calculation outputs are the objective functions of the optimization process. These functions take into consideration both the economical and energetic sustainability of the system. These are the payback period PB and the utilization coefficient of energy ε. However, these objectives are functions of the sizes of the component, of the energy produced and absorbed from outside the system. Therefore, a simulation of the system is needed to provide the input to the optimization process.

3.5   Independent variables

3.5.1 Unconstrained external conditions

Here are described the external conditions that do not depend on the components of the system but are needed for its resolution and are taken as input values. These deterministic values are taken from the simulation program EnergyPlus, which generates them by historical data. The values provided are hourly-based average of the quantity considered throughout the year and dependant on the location. Therefore, there are 8760 values for each external yearly condition. These are subdivided into two categories; both provided by the software: weather data and loads.

The former considers:

- T_{amb} = ambient temperature $(°C)$
- G_{TOT} = global solar irradiance (kW/m^2)
- u_w = wind velocity (m/s)

The latter are separated into the demands of:

- P_u = electrical power (kW)
- $\dot{Q}_{h,u}$ = space heating (kW)
- $\dot{Q}_{c,u}$ = space cooling (kW)
- $\dot{Q}_{w,u}$ = domestic hot water (kW)

The type of user considered is a district residential one, therefore a set of loads for each location has been taken for:

- Single-family building
- Multi-family building
- Utility building

The proportion in numbers of the load is of uttermost importance, therefore a proper ratio between the three types of buildings has been taken from EU Buildings Database of the European Commission (62). For the system studied, a district of 12 buildings resulted, divided into 4 single-family, 6 multi-family and 2 utility buildings.

3.5.2 Fixed performance of the components

The performances of components such as the PV/T hybrid collector, the heat pump and the inverter depend on external and operational conditions; therefore, are not to be considered as independent variables. However, four other different components have fixed performance, i.e. the two TSTs, the NGH and the BESS.

Their performance parameters are:

- The global heat exchanging factor for both the TSTs, $U_{TST} = 0.5\ W/m^2\ K$
- The combustion efficiency for the NGB, $\eta_{comb} = 85\ \%$
- The charge and discharge efficiency for the BESS, $\eta_{BESS} = 87\ \%$

For form purposes these are going to be fully presented on the components sections.

3.6   Equations of the model

3.6.1 Energy balances

The energy balances are the fundamental equations needed to solve the operation problem. One equation for each instantaneous load has been presented:

$$\dot{W}_{PV}(t) + \dot{W}^{+}{}_{GRID}(t) = \dot{W}^{-}{}_{GRID}(t) + \dot{W}_u(t) + \dot{W}_{HP}(t) + \dot{W}_{INV,L}(t) \qquad (8)$$

$$\dot{Q}_{HP}(t) = \dot{Q}_{h,u}(t) + \dot{Q}_{c,u}(t) + \dot{Q}_{TST,h\&c,L}(t) \qquad (9)$$

$$\dot{Q}_{w,COL}(t) + \dot{Q}_{w,NGH}(t) = \dot{Q}_{w,u}(t) + \dot{Q}_{TST,w,L}(t) \qquad (10)$$

Clearly, for the cases that considered the presence of the BESS, the first energy balance has been substituted by the following

$$\dot{W}_{PV}(t) + \dot{W}^{+}{}_{GRID}(t) =$$
$$= \dot{W}^{-}{}_{GRID}(t) + \dot{W}_u(t) + \dot{W}_{HP}(t) + \dot{W}_{INV,L}(t) + \dot{W}_{BESS,L}(t) \qquad (8b)$$

where $\dot{W}$ and $\dot{Q}$ represent the electrical and thermal power respectively, the subscripts h indicates the heating, c the cooling, u the user, PV the photovoltaic, HP the heat pump, L the energy dissipated or lost, INV the inverter, $GRID$ the grid, COL the collector, NGH the natural gas heater, $BESS$ the battery electric storage system.

3.6.2 Constrained external conditions: cell temperature and global irradiance on a tilted surface

As well as the unconstrained external conditions, these are average hourly based values that depend on the weather data and the location and are needed as input of the system. These two are the photovoltaic cell temperature and the global solar irradiance on an inclined plane.

An important parameter that affects the performance of a PV module is its *cell temperature*, thus the estimation of this temperature is of utmost importance. For the calculation of the PV cell temperature, the Faiman model (64) has been used:

$$T_{PV,cell}(t) = T_{amb}(t) + \frac{G_{TOT,\beta}(t)}{c_0 + c_1 * u_w(t)} \qquad (11)$$

where T_{amb} is the hourly ambient temperature of each location ($°C$), u_w is the wind speed (m/s) and c_0, c_1 are a set of constants dependent on the site location. The values of these constants are considered to be equal for both the considered locations due to their close to Mediterranean climate (65):

$$\begin{cases} c_0 = 41.86 \, W/Km^2 \\ c_1 = 3.95 \, Ws/Km^3 \end{cases} \qquad (12)$$

Second step towards the modelling of the PV modules is the calculation of their optimal tilt angle for maximizing annual solar irradiance on their surface. For this purpose, the annual meteorological data of two European cities (Athens and Vicenza) are used. By combining some of these data (global horizontal radiation, direct normal radiation and diffuse horizontal radiation) with the latitude, longitude and time zone meridian of each city, the hourly incident solar radiation for an optimal tilt angle is calculated throughout the whole year. The procedure is consequently elaborated. For each hour of the year, the next equations are used:

$$G_{TOT,\beta}(t) = G_{bT}(t) + G_d(t) * \frac{1 + cos\beta}{2} + G(t) * \rho' * \frac{1 - cos\beta}{2} \qquad (13)$$

where $G_{TOT,\beta}$ is the total incline solar irradiance on the PV module (W/m^2), I_{bT} is the direct incline solar irradiance (W/m^2), G_d is the diffuse horizontal radiation (W/m^2), β is the tilt angle (°) of the PV module, G is the global horizontal radiation and $\rho' = 0.2$ is a typical value of ground reflectance.

$$G_{bT}(t) = G_{bn}(t) * cos\theta \qquad (14)$$

where G_{bn} is the direct normal radiation (W/m^2) and θ is the incidence angle [°] which is calculated by the following equation for PV modules installed at northern hemisphere with south orientation:

$$cos\theta = sin\delta * sin(\varphi - \beta) + cos\delta * cos(\varphi - \beta) * cos\omega \qquad (15)$$

where φ is the latitude of the location [°], δ is the sun declination calculated by next equation [°] and ω is the hour angle (deviation from solar noon) [°]

$$\delta = 23.45 * \sin\left(\frac{360}{365} * (284 + n)\right) \tag{16}$$

$$\omega = 0.25 * (time(\min) \pm 4 * (L_{st} - L_{loc}) + EE - 12 * 60) \tag{17}$$

Where n is the day of the year, L_{st} is the meridian of the location time zone, L_{loc} is the longitude of each location and $-$ is for east longitudes while $+$ is for west. EE is a function of time [min] defined as follows:

$$EE = 9.87 \ \sin(2B) - 7.53 \ \cos(B) - 1.5 \ \sin(B) \tag{18}$$

$$B = 360 * \frac{n - 81}{364} \ (°) \tag{19}$$

3.6.3 PV/T hybrid collector

The type of PV/T used for this system is the water-based flat-plate collector, of which the characteristic parameters have been provided by DualSun®. From the solar irradiance absorbed, the main products of the panel are the electric and the thermal power. Respectively, the conversion depends on the PV effect and the heat exchanged between the environment and the selective surface. In order to have two different products, a separated modelling approach has been implemented. This allows also studying the comparison cases that exploit a separated solution or just one of the two solar parts. The method used to model the PV part of the PV/T system has been developed by Bellia et al. (66), while the one for the thermal part has been provided by UNI EN 12975-2006 (67), from which UNI EN ISO 9806 was developed.
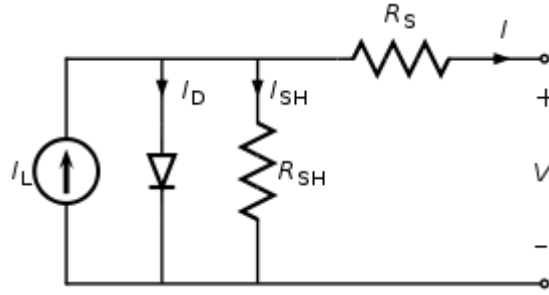
Figure 3.3: Circuit diagram of the operation of a PV solar cell

PHOTOVOLTAIC PART

The electrical behaviour of the PV cell has been studied by Bellia et al. (66) and has been presented on the circuit diagram of Figure 3.3. This depends mainly on the global solar irradiance, the cell temperature and the circuital parameters of the solar cell, which are reported in Table 3.1. For a single diode mode, the output current I_{module} of a single module can be estimated as following (69), by taking into consideration the series R_S and the shunt R_{SH} resistance:

$$I(t) = I_L(t) - I_D(t) * \left[\exp\left(\frac{V(t) + R_S * I(t)}{a_v(t)}\right) - 1\right] - \frac{V(t) + R_S * I(t)}{R_{SH}(t)} \qquad (20)$$

where:

- I_L is the photocurrent of a single module and is calculated from the following equation:

$$I_L(t) = \frac{G_T(t)}{G_{T,STC}} * \left(I_{sc,STC} + \mu_{sc}(T_{PV,cell}(t) - T_{PV,cell,STC})\right) \qquad (21)$$

where $G_{T,STC}$ is the solar irradiance at standard test conditions (STC), which is equal to $1000 \ W/m^2$, $I_{sc,STC}$ is the short circuit current at STC, μ_{sc} is the temperature coefficient of short circuit current, $T_{PV,cell}$ is the PV cell temperature and $T_{PV,cell,STC}$ is the cell temperature at STC and is equal to $T_{PV,cell,STC} = 298 \ K$.

- I_D is the reverse saturation current of a single module and is calculated from the following equation:

$$I_D(t) = I_{sc,STC} * \exp\left(\frac{-V_{oc,STC}}{a_v}\right) * \left(\frac{T_{PV,cell}(t)}{T_{PV,cell,STC}}\right)^3$$

$$* \exp\left(\frac{q * \varepsilon_g}{c_{ideal} * k} * \left(\frac{1}{T_{PV,cell}(t)} - \frac{1}{T_{PV,cell,STC}}\right)\right) \tag{22}$$

where $V_{oc,STC}$ is the open circuit voltage at STC and ε_g is the material band energy.

- a_v is the corrected thermal voltage, calculated from the following:

$$a_v(t) = N_s * c_{ideal} * k * \frac{T_{PV,cell}(t)}{q} \tag{23}$$

where N_s is the number of cells in the PV module, c_{ideal} is the ideality factor, $k = 1.3806 * 10^{-23} J/K$ is the Boltzmann constant and $q = 1.602 * 10^{-19} C$ stands for the electron charge.

- R_{SH} is the shunt resistance, estimated by the following expression:

$$R_{SH}(t) = \frac{V_{mp,STC} + I_{mp,STC} * R_S}{I_{sc,STC} * \left(1 - e^{\left(\frac{V_{mp,STC}+I_{mp,STC}*R_S-V_{oc,STC}}{a_v(t)}\right)} + e^{\frac{-V_{oc,STC}}{a_v(t)}}\right) - \frac{P_{STC}}{V_{mp,STC}}} \tag{24}$$

where the subscript mp refers to the maximum power operation.

Table 3.1: Characteristic parameters for a PV/T panel provided by DualSun® (68) and a common PV panel provided by Trinasolar® (80).

Parameter	DualSun	Tallmax	Unit
N_s	60	72	—
c_{ideal}	1.2	1.2	—
$I_{sc,STC}$	9.30	9.35	A
μ_{sc}	$4.8 * 10^{-4}$	$4.8 * 10^{-4}$	A/K
$V_{oc,STC}$	38.88	46.00	V
ε_g	$1.7944 * 10^{-19}$	$1.7944 * 10^{-19}$	J
R_S	0.19	$0.19 - - -$	Ω
$V_{mp,STC}$	31.95	37.60	V
$I_{mp,STC}$	8.77	8.91	A
$P_{mp,STC}$	280	335	W
Dimensions	1677x990x45	1960x992x40	mm

By applying a set of different values for the voltage of the module from 0 up to the open circuit voltage, the output currents are calculated, for a set of ambient temperature and solar irradiance for the aforementioned tilt angles. The voltage and current of the module are determined by finding the values that maximize the power output.

The voltage and the current produced are the products of the value of the single module by the number of panels in series and in parallel respectively.

$$V_{string}(t) = V(t) * N_{PV,series} \tag{25}$$

$$I_{parallel}(t) = I(t) * N_{PV,parallel} \tag{26}$$

The electrical power produced by the PV field is the product of the overall current intensity $I_{parallel}$ (A) and the potential difference between the edges of the string, i.e. its voltage V_{string} (V).

$$\dot{W}_{PV}(t) = V_{string}(t) * I_{parallel}(t) \tag{27}$$

Once determined the power output of the single PV panel, the efficiency η_{PV} can be evaluated for each timestep from the following equation:

$$\dot{W}_{PV}(t) = \eta_{PV}(t) * A * G_{TOT,\beta}(t) \tag{28}$$

where A is the overall surface of the PV field.

THERMAL PART

The first step towards the modelling of a solar thermal collector is the calculation of its efficiency. For this purpose, the following equation is used:

$$\eta_{col}(t) = a_0 - a_1 * \left(\frac{T_{col}(t) - T_{amb}(t)}{G_{TOT,\beta}(t)} \right)$$
$$- a_2 * G_{TOT,\beta}(t) * \left(\frac{T_{col}(t) - T_{amb}(t)}{G_{TOT,\beta}(t)} \right)^2 \tag{29}$$

where T_{col} is taken equal to the mean temperature of the collector, T_{amb} is the ambient temperature, $G_{TOT,\beta}$ is the global solar irradiance on the tilted PV/T module, a_0 is the optical efficiency of the collector and a_1 and a_2 are the heat loss coefficients of the

51

collector. According to the datasheet of a hybrid flat plate solar thermal collector and a common one, the values of these coefficients are reported in Table 3.2.

Table 3.2: Performance parameters of a PV/T hybrid collector (DualSun (67)) and a common solar flat plate collector (Vitosol, by Viessmann (81))

Parameter	DualSun	Vitosol	Unit
a_0	0.472	0.754	$-$
a_1	9.10	4.15	$W/K m^2$
a_2	0.0000	0.0114	$W/K^2 m^2$

According to the previous equation, in order to estimate the collector efficiency, the outlet temperature of the collector $T_{col,out}$ should be known. This temperature is the main output parameter needed from the modelling of the thermal collectors. Thus, an initial guess value is assumed ($T_{col,out} = T_{col,in}$) and the collector temperature is defined after iterations. Within every loop, the efficiency of the collector is estimated through its equation with the guessed value as an input. Then, the heat absorbed by the working fluid can be calculated as follows:

$$\dot{Q}_{w,COL}(t) = \eta_{col}(t) * A_{col} * G_{TOT,\beta}(t) \tag{30}$$

were for PV/T collectors $A_{col} = A$.

Hence, the temperature of the working fluid exiting the collector can be calculated from the following equation:

$$T_{col,out}(t) = T_{col,in}(t) + \frac{\dot{Q}_{col}(t)}{\dot{m}_{col} * c_{p,T_{col,in}}} \tag{31}$$

According to DualSun (68) the mass flow rate of the collector per square meter is steady and equal to:

$$\dot{m}_{col,m^2} = 0.0336 \ kg/(s \ m^2) \tag{32}$$

This procedure is terminated when the relative error between the outlet temperature of the collector and the guessed temperature is within an acceptable range. This range is defined as following:

$$error = \left| \frac{T_{col,out} - T_{guess}}{T_{guess}} \right| < 0.0075 \qquad (33)$$

If this condition is not met, the guessed value is increased by a step equal to 0.02°C until the error is lower than the restriction.

OVERALL PV/T SYSTEM

For simplicity in calculation, some additional values have been formulated, such as the overall area A and the total PV power produced:

$$A = A_1 * N_{panels} \qquad (34)$$

$$\dot{W}_{PV} = \dot{W}_{PV,1} * N_{panels} \qquad (35)$$

$$N_{panels} = N_{PV,series} * N_{PV,parallel} \qquad (36)$$

3.6.4 Inverter

The inverter is the component that allows tracking the maximum power point in PV generation (MPPT) and converts electric power from DC to AC. While the behaviour of a PV field can be changed by setting a certain number of panels, the number of panels in parallel depends on the maximum current the inverter manages to proceed. Its nominal power depends on the maximum power of the PV/T collector field, i.e. the maximum power generated defines the inverter size. Of course, the total power outcoming from the inverter is the product of the power of the single one multiplied by the number of parallel.

$$\dot{W}_{nom,INV} = \dot{W}_{nom,INV,1} * N_{PV,parallel} \qquad (37)$$

$$\dot{W}_{nom,INV} \geq \dot{W}_{PV,max} \qquad (38)$$

The output power depends on p_{output}, the ratio between the instantaneous power produced by the PV panel and the maximum power processable by all the inverters in parallel:

$$p_{output}(t) = \frac{\dot{W}_{PV}(t)}{N_{PV,parallel} * 1.25 * \dot{W}_{nom,INV}} \qquad (39)$$

where 1.25 is the ratio between the maximum and the nominal power of the inverter. The number of parallels in the PV field is equal to the number of inverters required. The inverter efficiency is calculated with Laukamp et al. and Jantsch et al. works (70) (71)

$$\eta_{inv}(t) = \frac{p_{output}(t)}{p_{output}(t) + 0.013 + 0.02 * p_{output}(t) + 0.05 * p_{output}(t)^2} \quad (40)$$

where 0.013 is the constant value that considers the absorption of current by the inverter whenever there is no solar irradiance, while the others are interpolation parameters.

The AC power produced as result of the PV panel production and the DC/AC inverter efficiency is

$$\dot{W}_{INV}(t) = \eta_{INV}(t) * \dot{W}_{PV}(t) \quad (41)$$

3.6.5 Heat Pump

The type considered is an air-water electrical driven heat pump. To this component is requested to satisfy the entire space thermal demand. For its design, the performance parameters are provided by Carrier datasheet (63), therefore the sizes linked were compared to the maximum space thermal loads. The device uses as refrigerant R410a, an ozone-friendly heat carrier fluid, has scroll compressors, low-noise fans and auto-adaptive microprocessor control. The sizes provided by Carrier were of 4, 6, 8, 12, 15, 17, 21, 26, 33 and 40 kW.

For calculation simplicity, whenever the maximum load cannot be satisfied by a single component, then more than one equal sized solution is adopted. In fact, as can be stated from the loads in the Results section, for Vicenza and Athens are designed three HPs of 33 kW each and two HPs of 40 kW respectively.

The data available from the heat pump are the values of coefficient of performance COP, energy efficiency ratio EER, heating produced $\dot{Q}_h$ and cooling produced $\dot{Q}_c$ are given as functions of the ambient temperature T_{amb}, the leaving water temperature LWT and the nominal power of the heat pump $\dot{Q}_{nom}$.

$$COP(t) = f\big(T_{amb}(t), LWT_h(t), \dot{Q}_{nom}\big) \ (kW_h/kW_e) \quad (42)$$

$$EER(t) = f\left(T_{amb}(t), LWT_c(t), \dot{Q}_{nom}\right) (kW_c/kW_e) \tag{43}$$

$$\dot{Q}_h(t) = f\left(T_{amb}(t), LWT_h(t), \dot{Q}_{nom}\right) (kW_h) \tag{44}$$

$$\dot{Q}_c(t) = f\left(T_{amb}(t), LWT_c(t), \dot{Q}_{nom}\right) (kW_c) \tag{45}$$

In order to get the electric power consumption of the HP in heating and cooling modalities respectively, the equations are:

$$\dot{W}_h = \frac{\dot{Q}_h(t)}{COP(t)} \ (kW_e) \tag{46}$$

$$\dot{W}_c = \frac{\dot{Q}_c(t)}{EER(t)} \ (kW_e) \tag{47}$$

The temperature of the water sent to the TST and then to space heating/cooling plants, like radiant panels or fan coils, is an important value of the system. According to the datasheet, a limited number of LWT is available, to which all the other parameters depend. Given the inputs of the external air temperature and the type of demand, these are the expression of the leaving water temperature:

$$LWT_h(t) = f\left(T_{amb}(t), \dot{Q}_h(t)\right) \tag{48}$$

$$LWT_c(t) = f\left(T_{amb}(t), \dot{Q}_c(t)\right) \tag{49}$$

Therefore, in order to exploit as much as possible the operations of the HP, the maximum thermal power available for a certain T_{amb} has been selected.

The performance values of the HP, i.e. the water flow rate $\dot{m}_{HP}$, the available thermal powers $\dot{Q}_h$ and $\dot{Q}_c$, and the performance factors COP and EER are loaded previously from the datasheet as inputs for the simulation.

3.6.6 Thermal Storage Tank

The thermal storage tank is the component of the model that allows the decoupling between the thermal energy produced and the one required. Two separated tanks have been used inside the model: one for the DHW and one for the space heating and cooling. Theoretically speaking, the tank should remain at a fixed temperature provided by a certain source of thermal energy. The values of temperature needed for the type of loads are reported in in Table 3.3.

For simplicity in calculation, the values of density ρ and specific heat at constant pressure c_p were predetermined and set as constant values in function of the set temperature and the pressure as reported in Table 3.3.

Table 3.3: Thermodynamic parameters of water inside the TST.

Case / Parameter	Temperature	Pressure	Density	Specific heat at constant pressure
	T_{TST} (°C)	p (bar)	ρ (kg/m³)	c_p [kJ/(kg K)]
Space cooling	10	2	999.73	4.19522
Space heating	40	2	992.25	4.17944
Domestic Hot Water	50	2	988.07	4.17841

However, in real conditions there is a non-negligible amount of energy loss due to the heat exchanged with the external environment. Two of the chosen system variables are the volumes of the storage tanks, so for modelling purpose the expression of the energy loss depends on the surface S, which is function of the volume Vol. The equation for the heat exchange exploits the global heat transfer coefficient U_{TST} ($W/(m^2 K)$) (30) and is used for three conditions:

- The heat loss of the DHW tank

$$\dot{Q}_{d,w}(t) = U_{TST} * S_W(Vol_W) * \left(T_{TST,w}(t) - T_{amb}(t)\right) \qquad (50)$$

- The heat loss of the heat pump tank in space heating mode

$$\dot{Q}_{d,h}(t) = U_{TST} * S_{HP}(Vol_{HP}) * \left(T_{TST,h}(t) - T_{amb}(t)\right) \qquad (51)$$

- The heat loss of the heat pump tank in space cooling mode

$$\dot{Q}_{d,c}(t) = U_{TST} * S_{HP}(Vol_{HP}) * \left(T_{amb}(t) - T_{TST,c}(t)\right) \qquad (52)$$

In order to have a real value of the global heat transfer coefficient, an experimental calculation has been made on an existing thermal storage tank in the National Polytechnical University of Athens, in the Department of Mechanical Engineering, Laboratory of Steam and Boilers Thermal Plants.

A set of measurements has been provided every 30 seconds, 4 temperatures at 4 different heights of the Solar- and Hot Water Buffer Tank PSF (72), the external room temperature and the pressure have been measured.

The model of the storage tank used the 4 probes as the number of mixing zones within the tank, supposing that each of them has a uniform temperature. The energy balance of each layer is then applied in order to model the mass and heat transfer between its boundary and the external environment. Since the storage tank model has been implemented for a night period of off-load an implicit method of discretization, which enhances the system solver stability, is used.

The storage tank was divided into a total number of $n = 4$ mixing zones, since this was the number of measurements available. For this number of mixing zones within the storage tank and for the measurement set time intervals ($\Delta t = 30s$) the following energy balances must be satisfied. The first mixing zone (element) refers to the top of the storage tank, while the last element refers to the bottom of the storage tank.

- Element n_1:

$$\frac{M_{st}}{n} c_p \frac{T_{st}(t+1,1) - T_{st}(t,1)}{\Delta t} = -U_l A_{st}(1)(T_{st}(t,1) - T_{amb}(t)) \qquad (53)$$

From which:

$$U_{TST}(1) = \frac{1}{A_{st}(1)} \frac{M_{st}}{n} \frac{c_p}{\Delta t} \frac{T_{st}(t,1) - T_{st}(t+1,1)}{(T_{st}(t,1) - T_{amb}(t))} \qquad (54)$$

- Elements n_j, $(j = 2:3)$:

$$U_{TST}(j) = \frac{1}{A_{st}(j)} \frac{M_{st}}{n} \frac{c_p}{\Delta t} \frac{T_{st}(t,j) - T_{st}(t+1,j)}{(T_{st}(t,j) - T_{amb}(t))} \qquad (55)$$

- Element n_{20}:

$$U_{TST}(n) = \frac{1}{A_{st}(n)} \frac{M_{st}}{n} \frac{c_p}{\Delta t} \frac{T_{st}(t,n) - T_{st}(t+1,n)}{(T_{st}(t,n) - T_{amb}(t))} \qquad (56)$$

The total mass of the storage tank has been calculated from its volume capacity as follows:

$$M_{st} = \rho_{wf} * V_{st} \qquad (57)$$

Finally, the surface of the mixing zones is calculated through the following equations:

- Elements n_1, n_4:

$$A_{st}(1) = A_{top} + \frac{h(2) - h(1)}{2} \tag{58}$$

$$A_{st}(4) = A_{bottom} + \frac{h(4) - h(3)}{2} \tag{59}$$

- Elements $n_j, j = 2:3$:

$$A_{st}(j) = \pi * D_{st} * \frac{h(j+1) - h(j-1)}{2} \tag{60}$$

where A_{top} and A_{bottom} are the area of the top and the bottom of the storage tank register respectively, D_{st} is the diameter of the storage tank and $h(j)$ is the height from the ground at which every probe has been set, as can be seen in Figure 3.4. The resulting value of U_{TST} is $1.892\ W/(m^2 K)$ while the overall surface $S\ (m^2)$ is a function of the volume Vol expressed in m^3, i.e. $S = 4.0572 * Vol + 2.0109$. The average values of pressure inside the storage tank and of room temperature were of $235.64\ kPa$ and $16.17\ °C$, respectively.

However, the value U_{TST} outcoming this procedure is more than three times bigger than the ones found in literature, which can bring to unreliable results. Therefore, the heat loss coefficient of the storage tank is assumed to be equal to $U_{TST} = 0.5\ W/m^2 K$, according to Bellos et al. (82).
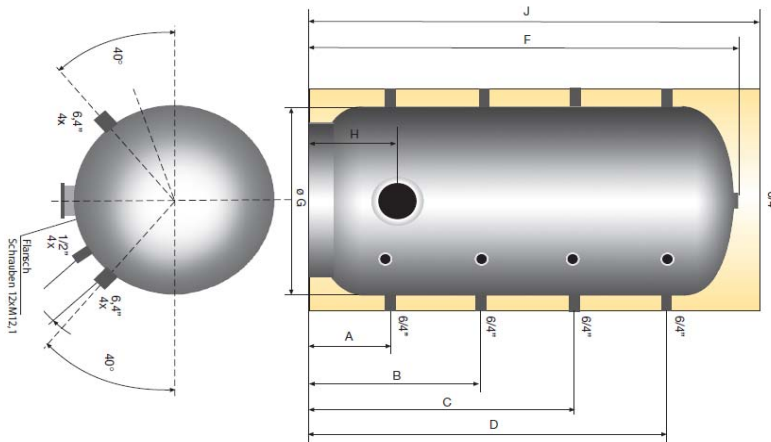

Figure 3.4: Technical representation of the TST

3.6.7 Battery Energy Storage System

The usage of an electrochemical device for the electric energy storage out coming the PV process requires considering the dynamic behaviour of the energy balance. In fact, the energy inside the battery varies in time: it is stored depending on the PV power production and it is released in function of the electric power demanded. These processes are respectively the charge and the discharge.

According to (26), the model of the total electric energy that is contained within the storage $E_{BESS}[kWh]$ at time t is

$$E_{BESS}(t) = E_{BESS}(0) + \int_0^t \left(\sqrt{\eta_{BESS}} * \dot{W}_{in}(t) - \frac{1}{\sqrt{\eta_{BESS}}} * \dot{W}_{out}(t) \right) dt \qquad (61)$$

where $E_{BESS}(0)$ is the energy contained in the battery at the initial time $t = 0$. The losses in charging and discharging the battery are taken into account using equal charging and discharging efficiencies, the product of which is the round-trip efficiency of the electric storage system ($\eta_{BESS} = \eta_{BESS}^+ * \eta_{BESS}^-$). The value of the round-trip efficiency is fixed at the mean value ($\eta_{BESS} = 0.87$) of those proposed in Refs. ((83) (84) (85)).

3.6.8 Natural Gas Heater

The condensing NGH is meant to be a backup device, so a component that provides heat whenever the thermal part of the PV/T hybrid collector is not able to satisfy entirely the DHW demand. Since there are many periods along the year in which the PV/T thermal production is null due to environmental conditions, e.g. during the night or in winter days, the NGH needs to satisfy the entire DHW load. That is why the maximum DHW load has been taken as reference. According to commercial sizes for a domestic NGH and the loads required in both locations, 1 NGH of 33 kW and 1 NGH of 40 kW were chosen for Athens and Vicenza respectively.

For simplicity in calculation, the operative modality of the NGH has been set as a simple on/off turning, where only a full or a null value of the already mentioned power were considered. There is no regulation in fuel mass flow rate, because it is not required from

other parameters inside the system. The fossil fuel considered is Natural Gas, but for the purpose of this work, it has been considered as Methane, i.e. CH_4.

However, since the values of combustion efficiency $\eta_{comb} = 85\,\%$ and lower heating value $LHV_{NG} = 50016\ kJ/kg$ have been set, the constant mass flow rate can be evaluated from the following (73):

$$\dot{Q}_{w,NGH} = \eta_{comb} * \dot{m}_{NG} * LHV_{CH_4} \tag{62}$$

Conclusions

The method of the problem solving has been presented in this chapter. The constrained and unconstrained variables have been defined. A system of $n = 72$ variables, $m = 32$ equations and $n - m = 40$ unconstrained variables resulted. The hourly environmental data and the district loads for the location of Athens and Vicenza throughout the year have been taken from determinist values. These, the energy balances and the performance of each component determined the instantaneous evolution of the system.

The area of the PV/T hybrid collector field and the volumes of the TSTs have been left as open variables, while the number and the nominal power of a single inverter can be determined only once the maximum PV field power has been set. The sizes of the HP and the NGB have been set.

4. DYNAMIC SIMULATION CONTROL

In this chapter the logic behind the control of the system is presented. The main concept is to match the loads with the production without forgetting the losses of each energy transfer. The model was built with the simulation tool Simulink; a program enhanced with Matlab which allows a modular sequential approach. The system studied has a dynamic behaviour, which requires this kind of solving approach, rather than a simultaneous one. The system has been modelled by implementing component by component and connecting all of them accurately.

The first configuration studied was the simplest one:

- The PV panel of the PV/T system provides electrical energy to the inverter, which either supplies it to the electrical driven heat pump for space heating and cooling, for a direct usage, or exchanges it with the grid;
- The thermal collector of the PV/T system in parallel with a backup NGH provides heat to the DHW load;
- Two different storages are included to decouple loads and production that are often shifted in time.

For a further comparison, two different solutions are considered. The first is the configuration of a separated solution, i.e. composed by common PV panels and solar thermal collectors instead of the hybrid ones. The second is the introduction of the BESS for the decoupling of the electric production and utilization.

4.1 Configuration parameters & set values

The configuration parameters set are linked to the solver and to the data import/export.

In the solver the simulation started at time $1s$ and stopped at time $3600 * 24 * 365 = 31536000\ s$ since the simulation has been developed all along the year and the unit value of the time is the second. The solver was the Ordinary Differential Equations 5 (Dormand-Prince), which is a fixed-step type. The fundamental sample time was firstly set at each

60 unit values, i.e. every minute. The periodic sample time was unconstrained, and each discrete rate has been treated as a separate task.

In the data import/export, the values saved outside of Simulink are given as a vector time-dependant, in which one value of the quantity considered at each time step has been taken, i.e. a vector of 1 column and $31536000/60 = 525600$ rows.

A representation of the overall system on Simulink platform, has been presented in Figure 4.1, where the coloured blocks represent the designed sizes of the main components. Figure 4.1a refers to the main case of a PV/T hybrid solution, while Figure 4.1b to the same case with the introduction of a BESS.
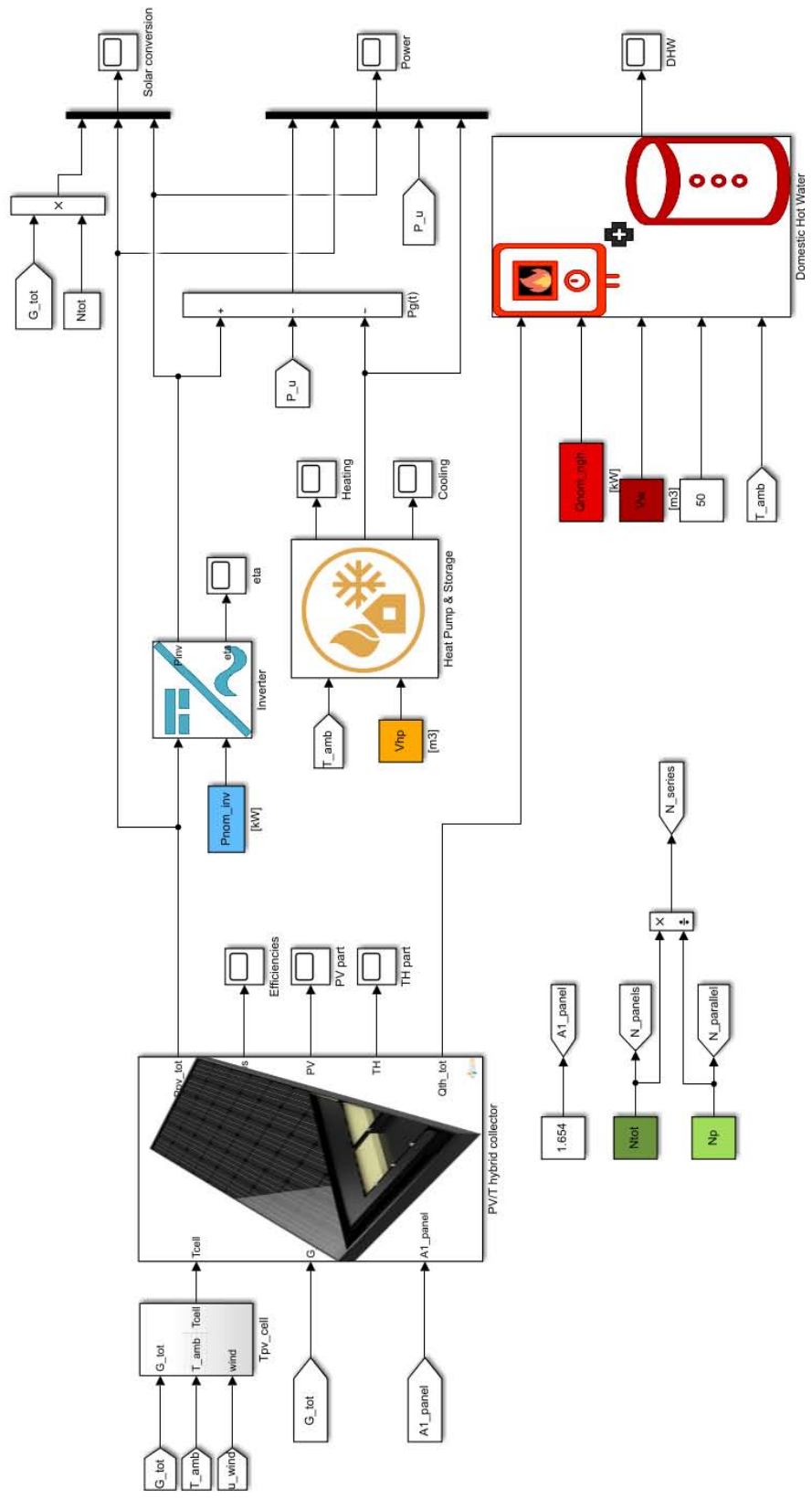
Figure 4.1a: Schematic representation of the overall PV/T hybrid system configuration in Simulink platform.
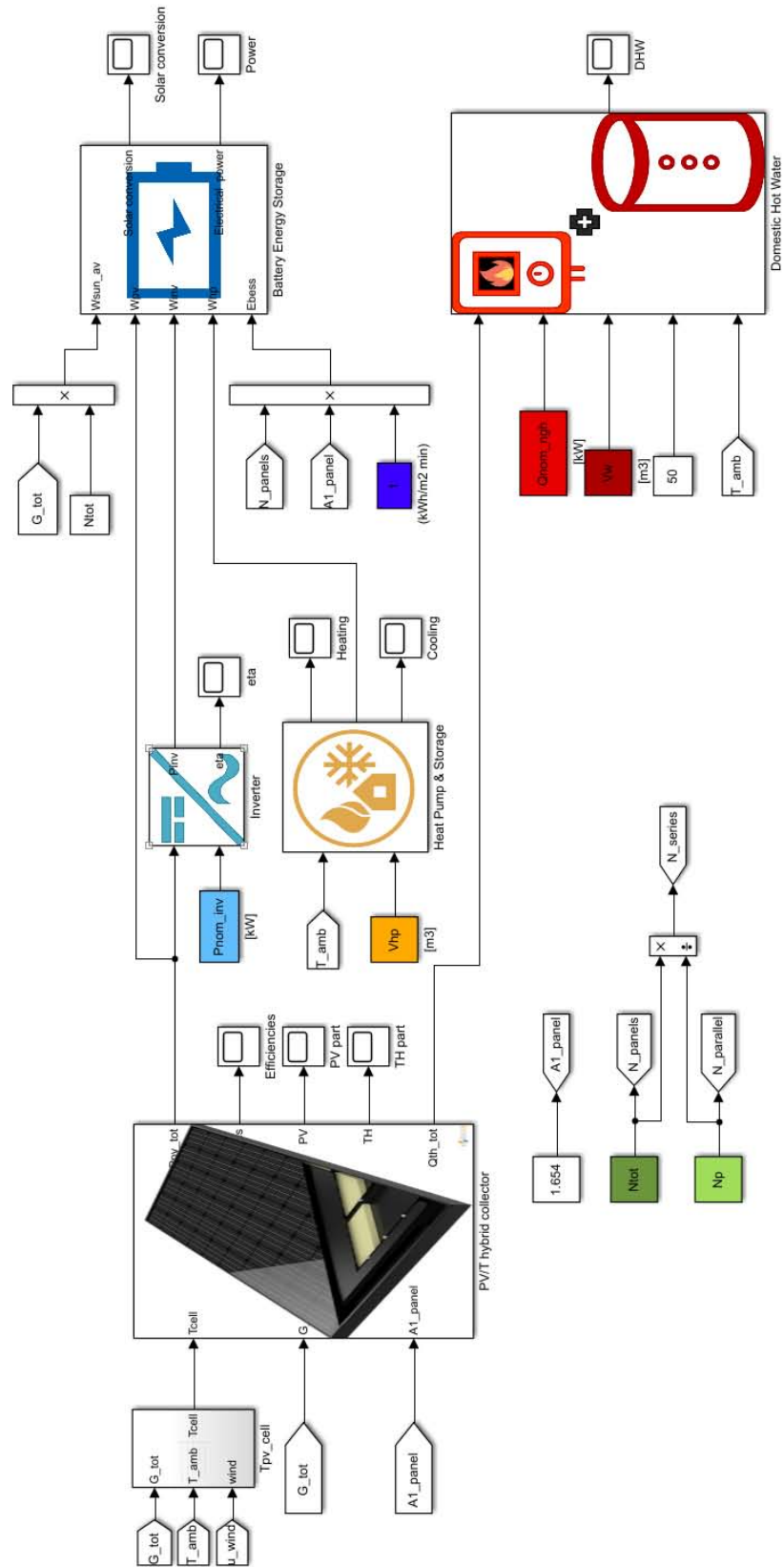
63

Figure 4.1b: Schematic representation of the PV/T system coupled with a BESS configuration in Simulink platform.

4.2 Power exchange control

As can be seen in Figure 4.1, the power control is the simple energy balance of the electrical power referred to Eq. 8, where the electrical power required by the simple usage and by the heat pump operation is subtracted from the power coming out from the inverter.

The outcome of this balance is the power exchanged with the grid: if $\dot{W}^{+}{}_{GRID}(t) > 0$ then the power is caught from the grid to supply the demand, while if $\dot{W}^{-}{}_{GRID}(t) > 0$ then the power is dispatched to the grid because a higher PV power than necessary has been produced.

For the cases in which also the battery was considered, a different configuration is adopted.

The PV/T system has been implemented to provide all the parameters necessary to the resolution of the problem. As shown in Figure 4.2, the electrical and the thermal part are separated. The resulting power of the PV part is then given as input of the inverter block of Figure 4.1.
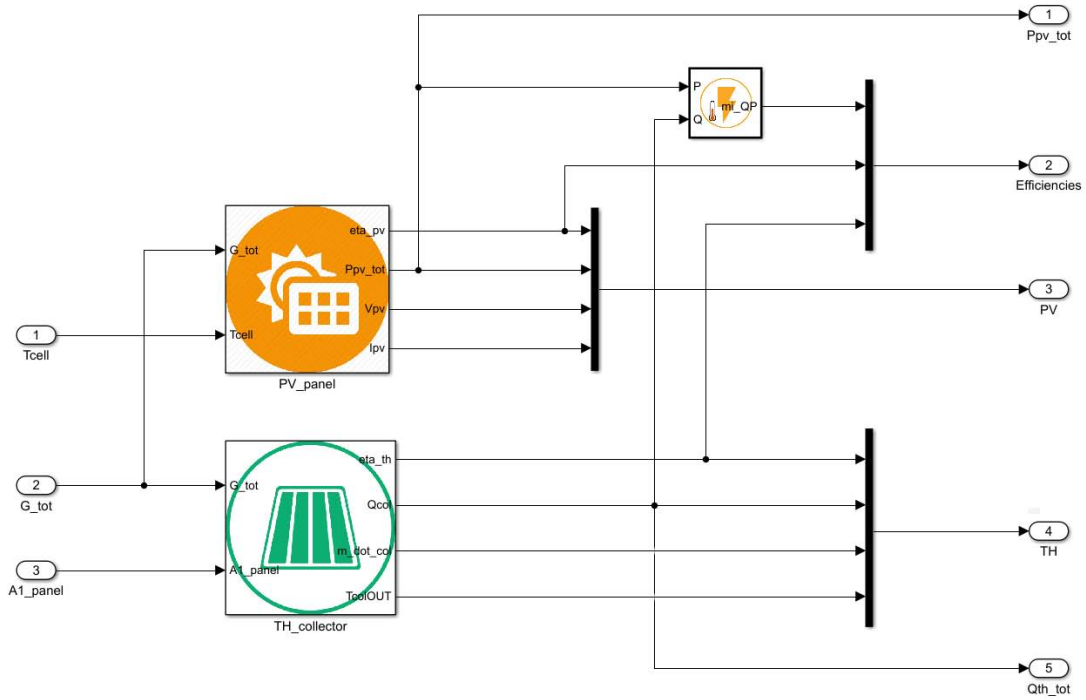
Figure 4.2: Flowsheet in Simulink platform of the PV/T system

4.3   Space heating & cooling control

The possibility to heat and cool a district of residential buildings by using the solar energy source is enhanced with the PV effect. The electrical power produced feeds directly the heat pump. The matching of demand and production is the common thread that links also the space conditioning control.

The control configuration of the HP is shown in Figure 4.3. The ambient temperature T_{amb} and the volume of the TST Vol_{HP} are external fixed values that work as input for the control. Moreover, two additional values for each load have been used for switching the modalities: the space heating $\dot{Q}_{h,u}$ and cooling $\dot{Q}_{c,u}$ demand. In order to have a continuity in the simulation of the heat pump, a further control on the kind of load has been set. The operation mode changes from winter to summer whenever the ambient temperature T_{amb} is higher than $20\ °C$.
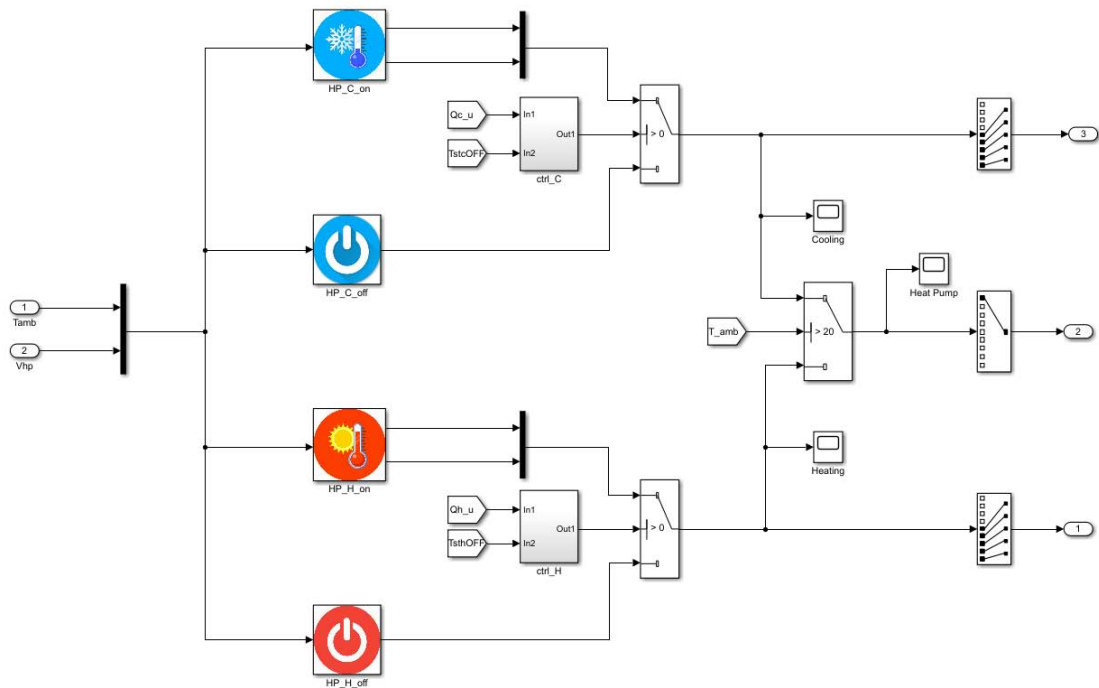
Figure 4.3: Control configuration of the heat pump in Simulink platform.

As can be seen from Figure 4.3, whenever the temperature rises beyond $20\,°C$, the HP turns into cooling mode, otherwise into heating mode. Whenever the load is non-null, or the temperature exceeds the range fixed for the type of load, then the HP is turned on and provides the heating or cooling thermal power available. This value is determined as function of the ambient temperature T_{amb}, the leaving water temperature LWT and the nominal power of the heat pump $\dot{Q}_{nom}$.

When the HP is working, the control hereby presented and pictured on Figure 4.4 has been followed. The component in which the main thermal flows for space conditioning convey into, is the TST. The energy balance of the heat exchanged must be respected, but its evolution changes every time-step of the simulation, i.e. every 60 seconds. While the loads and production values are hourly, the heat losses change more rapidly. Thus, they must be calculated more precisely in order to converge to a solution. The temperature of the TST has been taken as control parameter for the same reason. Its calculation has been determined as follows.

The internal energy of the system varies over time and is equal to the energy balance that regards the system, i.e. the tank. The following equation is adopted for both type of space conditioning loads.

67

$$\frac{dU(t)}{dt} = \sum \dot{Q} \begin{cases} \dot{Q}_{HP}(t) \\ \dot{Q}_u(t) \\ \dot{Q}_d(t) \end{cases} \qquad (63)$$

By rearranging Eq. 63, taking as example the cooling mode, the following is obtained:

$$\frac{dT_{TST,c}(t)}{dt} = \frac{1}{\rho * Vol_{HP} * c_p} \sum \dot{Q}_c(t) = \frac{1}{\rho * Vol_{HP} * c_p} \left(\dot{Q}_c(t) - \dot{Q}_{c,u}(t) - \dot{Q}_{c,d}(t) \right)$$

And integrating the previous one leads to:

$$T_{TST,c}(t) = T_{TST,c}(0) + \int_0^t \frac{1}{\rho \, Vol_{HP} \, c_p} \sum \dot{Q}_c(t) \, dt$$

where the temperature at starting time $T_{TST,c}(0)$ has been set as the ambient temperature at that moment. The set of temperature values required for heating were between 35 and 45 °C, whereas those for cooling vary between 5 and 15 °C.

$$35\,°C < T_{TST,h} < 45\,°C \qquad (64)$$
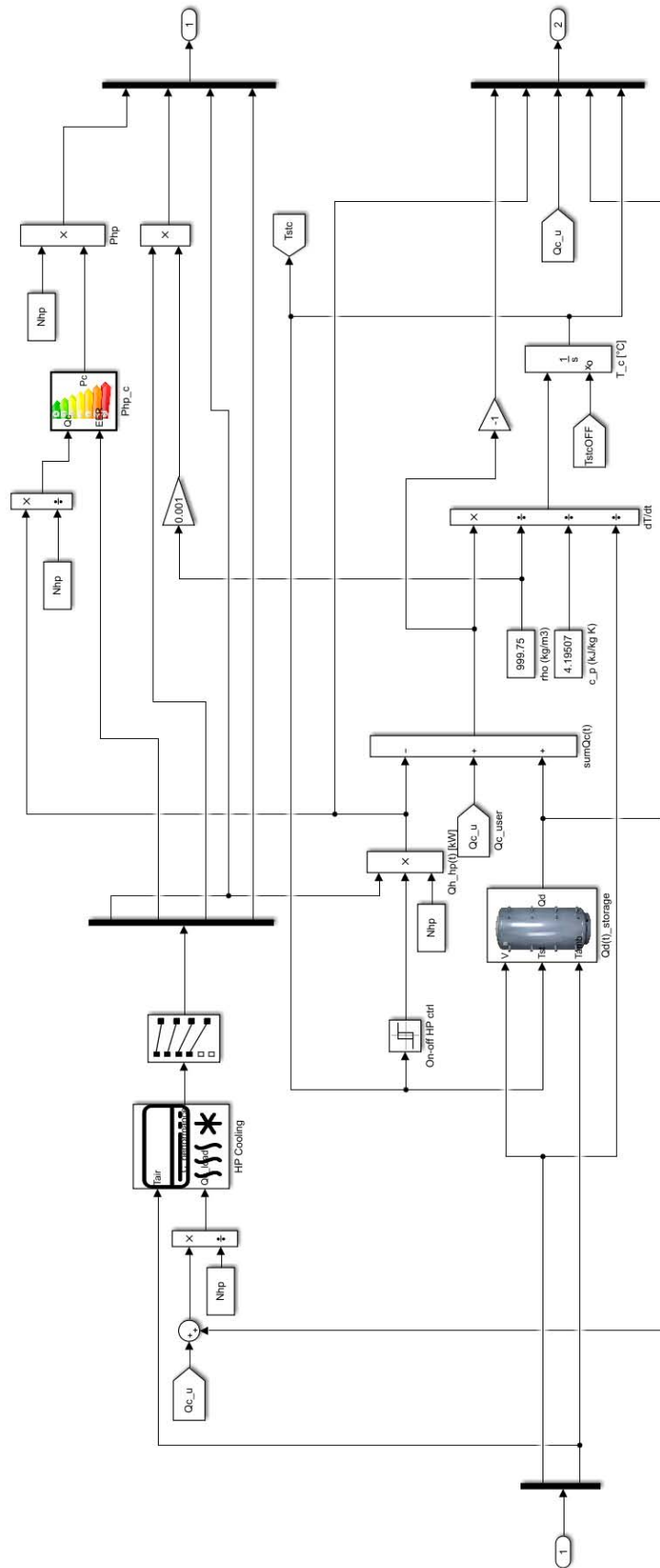$$5\,°C < T_{TST,c} < 15\,°C \qquad (65)$$

Figure 4.4: Control scheme of the heat pump switched on during the cooling mode in Simulink platform.

When the system is switched off, the values of thermal production, thermal load and electric consumption of the heat pump are null, while the temperature has been left free of evolving depending on the thermal dispersion of the TST as can be easily seen on Figure 4.6. The system switches on whenever the temperature $T_{TST,OFF}$ goes below 35 °C or over the 15 °C in summer, while it switches off whenever the temperature $T_{TST,ON}$ exceeds the 45 °C in winter or falls under the 5 °C in summer. In these ranges, water density has an almost constant behaviour, so to reduce calculation effort two constant values have been set, i.e. the ones proposed in Table 3.3.

Once determined the operative mode and if the HP is switched on or off, the performance parameters are available. Moreover, the electrical power absorbed by the HP, which is needed for the electrical energy balance, can be determined from the thermal power produced and the performance factor: i.e. $\dot{Q}_h(t)$ and COP in winter and $\dot{Q}_c(t)$ and EER in summer (Eqs. (46) and (47)).
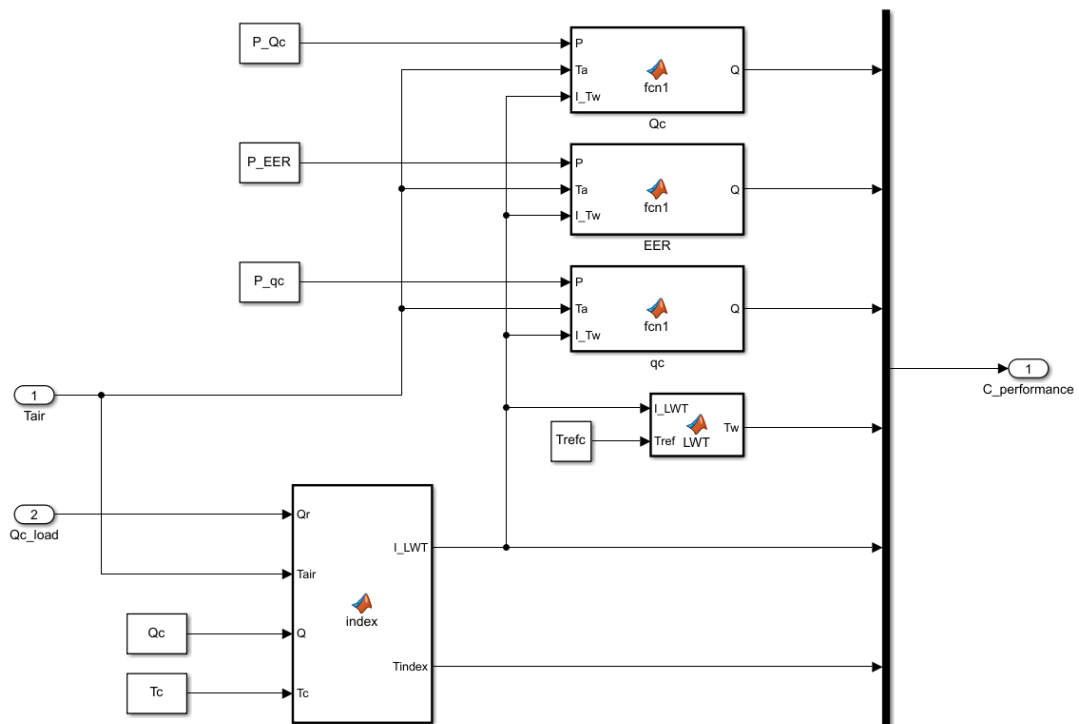

Figure 4.7: Energy conversion of the heat pump during the cooling mode taken from Simulink platform.

4.4　Domestic hot water control

The DHW produced by the thermal collector of the PV/T system is often not enough to fulfil the demand of the user. Thus, an NGH connected to the natural gas pipeline works as a backup of the system. The energy balance related to the DHW thermal flow is exchanged in the TST. The evolution of the heat exchanged changes every time-step, i.e. in the simulation every minute (60 seconds). The loads and the production values are taken every hour, but the heat loss requires a faster calculation in order to let the simulation converge. The temperature of the TST has been taken as control parameter. Its calculation has been determined as follows.

The internal energy of the system varies over time and is equal to the energy balance that regards the system, i.e. the tank.

$$\frac{dU_w(t)}{dt} = \sum \dot{Q} \begin{cases} \dot{Q}_{w,COL}(t) \\ \dot{Q}_{w,NGH}(t) \\ \dot{Q}_{w,u}(t) \\ \dot{Q}_{w,L}(t) \end{cases} \tag{66}$$

By rearranging Eq. 66, the following is obtained:

$$\frac{dT_{TST,w}(t)}{dt} = \frac{1}{\rho_w * Vol_W * c_{p,w}} \sum \dot{Q}_w(t)$$

$$= \frac{1}{\rho_w * Vol_W * c_{p,w}} \left(\dot{Q}_{w,COL}(t) + \dot{Q}_{w,NGH}(t) - \dot{Q}_{w,u}(t) - \dot{Q}_{w,L}(t) \right)$$

And integrating the previous equation leads to:

$$T_{TST,w}(t) = T_{TST,w}(0) + \int_0^t \frac{1}{\rho_w * Vol_W * c_{p,w}} \sum \dot{Q}_w(t) \, dt$$

where the temperature at starting time $T_{TST,w}(0)$ has been set as the ambient temperature at that moment. The set of temperature values required for a DHW usage is between $45\,°C$ and $55\,°C$, which is also the range of temperature set for the NGH. However, when it comes to the range of temperature of the thermal collector's part, a higher maximum value

has been considered in order to exploit the maximum heat from solar irradiance. Nevertheless, an edge must be set to avoid stagnation.

The PV/T hybrid collector has a low stagnation temperature of $80\,°C$, while a common flat plate solar collector can reach higher temperatures of $130\,°C$. This is due mainly to the difference in the maximum operating pressures: while for the hybrid solution this is $1.2\,bar$, for a common solution it is of $6\,bar$. For both types a safety margin of $5\,°C$ has been chosen, therefore the range of temperatures of the PV/T thermal collector is

$$45\,°C < T_{COL} < 75\,°C \tag{67}$$

And for a common one is

$$45\,°C < T_{COL} < 125\,°C \tag{68}$$

The system switches on when the temperature goes below $45\,°C$, while it switches off at two different stages: the solar thermal collector when the temperature exceeds the upper limit yet defined, while the NGB when the temperature exceeds the $55\,°C$.
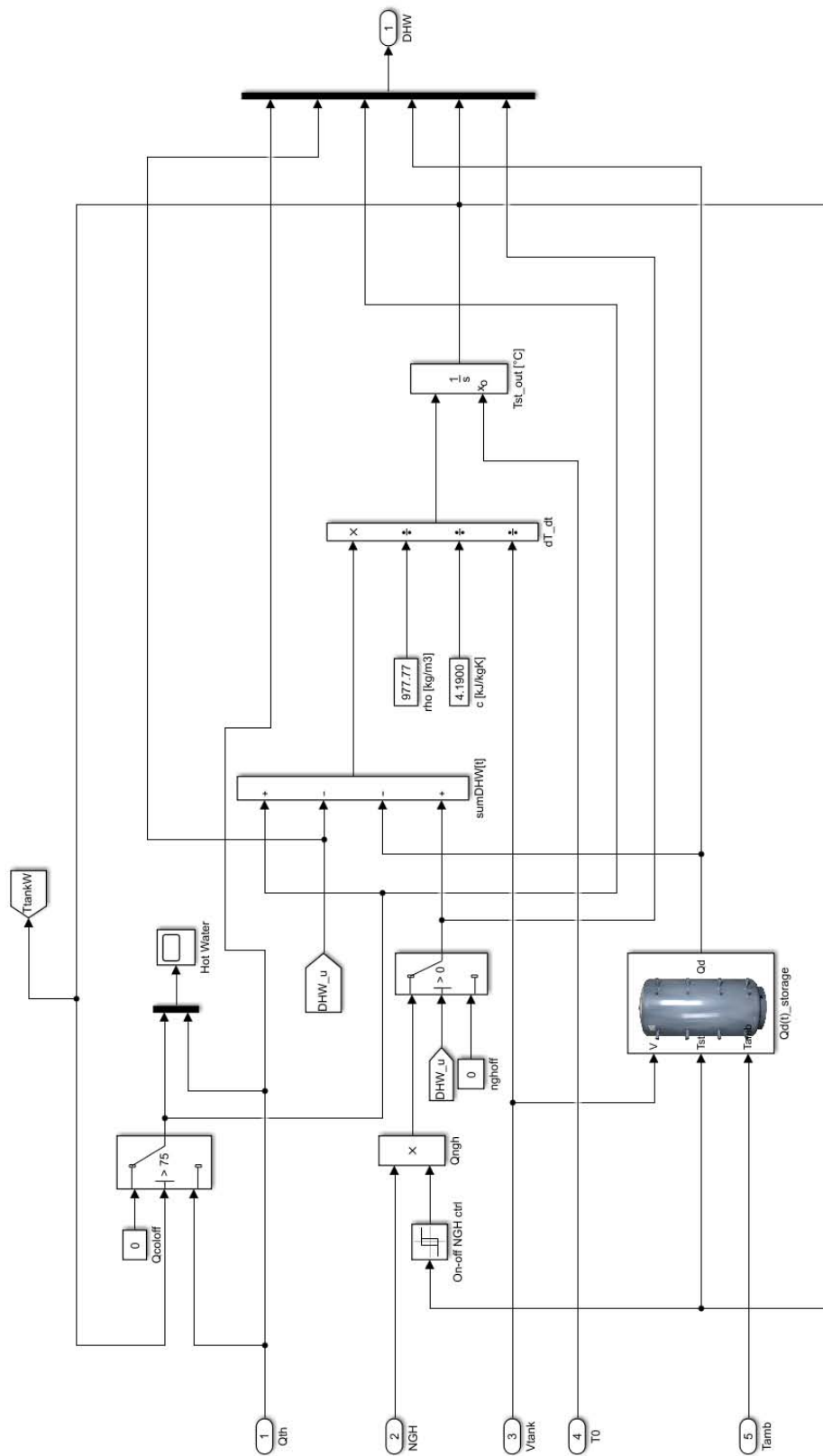
Figure 4.8: Control scheme of the DHW with both the solar thermal collector and the natural gas heater dependant on the temperature inside the TST as built in Simulink.

5. OPTIMIZATION PROBLEM

The optimization problem faced on this section is the minimization of a two-objective time-dependant function. This function relates to economic and energetic aspects. The determination of the Pareto front depends on a set of constraints and boundary conditions stated a priori.

5.1 Multi-objective optimization

The multi-objective optimization problem with inequality constraints can be formulated as follows (74).

$$\text{Find} \qquad X = \begin{Bmatrix} x_1 \\ x_2 \\ \vdots \\ x_n \end{Bmatrix} \qquad (69)$$

which minimizes $\qquad f_1(X), f_2(X), \cdots, f_k(X) \qquad$ (70)

subject to $\qquad g_j(X) \leq 0, \qquad j = 1, 2, \cdots, m \qquad$ (71)

where k denotes the number of objective functions to be minimized. Any or all of the functions may be nonlinear. The multi-objective optimization problem is also known as a *vector minimization problem*. In general, it does not exist any vector X that minimizes all the k objective functions at the same time. For this purpose, the concept of the Pareto optimum solution is used in multi-objective optimization problems. A feasible solution X is called Pareto optimal if there is no other feasible solution Y such that $f_i(Y) \leq f_i(X)$ for $i = 1, 2, \cdots, k$ with $f_j(Y) < f_i(X)$ for at least one j. In other words, a feasible solution X is called Pareto optimal if no other feasible solution Y has a performance at least equal in all the objectives, but strictly better in at least one of them. The objective function values corresponding to the set of Pareto optimal solutions, representing the best possible trade-off among the objectives, are called the *Pareto front*.

The optimization problem faced in this work regards the interactions with the world outside the system boundaries. Therefore, it considers economic, energetic and environmental aspects. Investment, operational and maintenance costs are fundamental for the realization of the system; thermodynamic laws impose how the energy conversions

happen; and the fossil fuels directly and indirectly burnt are linked to the emission of pollutants into the environment. In order to cope with all these perspectives, an integrated approach is required.

5.1.1 Single- and multi-objective approaches

The Pareto approach is not the only possible way to deal with multi-objective optimization (10). In fact, single-objective approaches do not necessarily deal with fewer objectives than multi-objective approaches since they can weigh explicitly or implicitly multiple objectives into an overall single-objective function. The different optimal solutions on the Pareto front can then be obtained by varying the weight coefficient.

Nevertheless, multi-objective optimization processes allow having a wider range of points of view than the single-objective ones. Also, they can provide a whole spectrum of solutions that can chose the best one by considering simultaneously more than a single objective. As a matter of fact, the objectives compete with one another, and a unique solution for all of them cannot be found. Therefore, the concept of Pareto front must be introduced to assess whether a solution is optimal or not. The same range of optimal solutions could be obtained by a single-objective approach weighting explicitly or implicitly the three objectives into an overall single-objective function and varying the weight coefficients. However, this method needs a higher computational effort since an optimization run is required per each combination of the weight coefficients. On the other hand, a multi-objective approach finds the final solution in a single run of the optimization algorithm.

5.1.2 Multi-objective evolutionary algorithms

The solutions of a multi-objective optimization should follow two goals: to be close to the true Pareto optimal set; and to be widely different from each other, in order to cover the entire Pareto optimal set. Classic optimization methods are not well-suited for the Pareto approach to multi-objective optimization for three main reasons (75):

- most of them are unable to find multiple solutions in a single run, so they have to be applied as many times as the number of Pareto-optimal solutions required;

- the solutions found through the repeated application of these methods are not guaranteed to be widely different from each other;
- most of them are unable to handle problems having multiple optimal solutions.

The class of search algorithms that implement the Pareto approach for multi-objective optimization in the most straightforward way is the class of multi-objective evolutionary algorithms (MOEAs). MOEAs have been developed over the past decade (76); severe tests on complex mathematical problems and on real-world engineering problems have shown that they can eliminate the above cited difficulties of classical methods. An evolutionary algorithm is a hybrid stochastic/deterministic optimization tool that imitates the natural evolution of biological organisms, i.e. a randomly initialized population of individuals (a set of points in the search space) evolves following the Darwinian principle of survival of the fittest. New individuals are created using some simulated evolutionary operators, such as crossover and mutation, and the probability of survival for these newly generated solutions depends on their fitness, that is on how well they perform with respect to the objective(s) of the optimization problem. Since MOEAs use a population of solutions during the search, a single run will find multiple Pareto-optimal solutions; moreover, by adding a diversity-preserving mechanism to the algorithm, widely different Pareto-optimal solutions can be found.

In Toffolo et al. (9) an evolutionary-based procedure was presented for the exergetic and economic design optimization of thermal systems. The proposed multi-objective evolutionary algorithm was shown to be a powerful and effective tool in finding the set of the best trade-off solutions between the two competing objectives. The algorithm, improved by an innovating diversity preserving mechanism, converged to the Pareto optimal set and adequately spread the solution over it. The analysis of the optimized solutions shows also that the economic minimum is not the only solution that should be considered in the decision-making process.

5.2 Optimization functions

The main purpose in the design of every energy system is its sustainability. This characteristic not only refers to the ability to supply energy to the user, but also to the affordability of the system and its efficiency. Therefore, the optimization objectives chosen in this work regard economic and energetic aspects.

5.2.1 Payback period

The payback period (PB) is a widely known economic parameter that gets more useful when long-term cash flows are difficult or not necessary to forecast (77). That is, over a period of several years before to reach the breakeven point. Thus, it is a valid tool for the goal of this work. PB is usually measured as the time from the start of production to recovery of the capital investment. The simple payback period (SPB) is the time taken for the cumulative net cash flow C_{CF} from the start-up of the plant to equal the depreciable fixed capital investment C_{FC}. Considering that the common period of analysis is the year, the PB can be expressed as the value of t that satisfies the equation

$$\sum_{t=0}^{SPB} c_f(t) + \sum_{t=0}^{SPB} s_f(t) = C_{FC} \tag{72}$$

where $c(t)$ is the net annual cash flow of the system, $s(t)$ is the net annual salvage flow and C_{FC} is the fixed capital cost.

The SPB thus measures the time required for the cumulative project investment and other expenditure to be balanced by the cumulative income. Consequently, it is possible to calculate it by dividing the total amount of the initial cost by the sum of the total net cash flow $C_F(\text{€})$ and the total salvage $S_F(\text{€})$ at each time interval taken into consideration.

$$SPB = \frac{C_{FC}}{C_F + S_F} \ (years) \tag{73}$$

FIXED CAPITAL INVESTMENT

The fixed capital investment takes into consideration the cost of each component of the system $C_{component}$ and the cost for the installation $C_{installation}$. The former regards the

selling price of the single devices, while the latter takes into account the installation, the cables and the pipes costs.

$$C_{FC} = \sum C_{component} + \sum C_{installation} \ (\text{€}) \tag{74}$$

NET CASH FLOW

The net cash flow C_{CF} is the annual result of the subtraction between the energy production income C_{prod} and the operational C_{cons}, maintenance C_{main} and eventual fees C_{fee} costs. The overall period considered is the total number of hours of the year, i.e. 8760.

$$C_{CF} = C_{prod} - C_{cons} - C_{main} - C_{fee} \ (\text{€}) \tag{75}$$

The annual income due to energy production regards only the overall electric energy produced and depends on the national feed-in tariff system. In general, it can be expressed as the product of the sale price $c_{el,s}(\text{€}/kWh)$ and the hourly electrical power produced $\dot{W}_{prod}(kWh)$.

$$C_{prod} = c_{el,s} * \sum_{t} \dot{W}_{prod}(t) \tag{76}$$

The operational costs are defined as the energy consumption, i.e. of the electricity and natural gas absorbed from the national networks. These values depend on the local tariffs too. In general, they can be expressed as the product of the purchase price for electricity $c_{el,p}(\text{€}/kWh)$ and natural gas $c_{gas}(\text{€}/kWh)$ and the hourly electrical power absorbed by the grid $\dot{W}_{cons}(kWh)$ and the heat taken from the natural gas pipeline $\dot{Q}_{cons}(kWh)$ respectively.

$$C_{cons} = c_{el,buy} * \sum_{t} \dot{W}_{cons}(t) + c_{gas} * \sum_{t} \dot{Q}_{cons}(t) \tag{77}$$

Finally, C_{main} is taken as a percentage of the investment of each component, while C_{fee} is a fixed value for each country.

SALVAGE

The annual salvage is the cost that the user would have paid if the PV/T system was not implemented. This means that for each load a different solution is adopted. In particular, only natural gas from the pipeline is exploited to fulfil the heating demand, i.e. space heating $\dot{Q}_{h,u}(kWh)$ and DHW $\dot{Q}_{w,u}(kWh)$; while only electricity from the grid is used to supply power $\dot{W}_u(t)$ and space cooling $\dot{Q}_{c,u}(kWh)$ to the user. The heat is provided by burning the natural gas in a condensing boiler, while the cool is supplied by an electric driven chiller. The overall period considered is the total number of hours of the year, i.e. 8760.

$$S_{CF} = c_{gas} * \sum_t \left(\frac{\dot{Q}_{h,u}(t)}{\eta_{comb}} + \frac{\dot{Q}_{w,u}(t)}{\eta_{comb}} \right) + c_{el,buy} * \sum_t \left(\frac{\dot{Q}_{c,u}(t)}{SEER} + \dot{W}_u(t) \right) \tag{78}$$

where the performance factors are the efficiency η_{comb} for the boiler and the seasonal energy efficiency ratio $SEER$ for the chiller. Their values are 0.85 and 3.5 respectively.

DISCOUNTED VALUES

The form of PB expressed in Eq. 73 might be of easy interpretation but does not consider the value of money over time. For this reason, both the cash and salvage flows must be actualized by using a discount rate. The discount rate expresses the time value of money and can make the difference between whether an investment project is financially viable or not. Thus, it is introduced for a period that is comparable with the duration of the system.

$$C_{CDF} = \sum_{i=1}^{n} C_{DF} = \sum_{i=1}^{n} \frac{C_F}{(1+r)^i} \qquad S_{CDF} = \sum_{i=1}^{n} S_{DF} = \sum_{i=1}^{n} \frac{S_F}{(1+r)^i} \tag{79}$$

where r is the discount rate, $1/(1+r)^i$ is the discount factor at the year i, C_{DF} and S_{DF} are the discounted cash and salvage flows respectively, and C_{CDF} and S_{CDF} are the cumulative discounted cash and salvage flows respectively. The total number of years n represents the duration of the system, and for this work its value is $20 \ years$. Since the SPB is a time value as well, in order to find a discounted payback period PB the net present value NPV needs to be determined. As shown in Eq. 80, the NPV is expressed as

the sum of C_{CDF} and C_{CDF} to which C_{FC} is subtracted. The year when the NPV reaches the null value is the researched DPB.

$$NPV = -C_{FC} + \sum_{i=1}^{PB} C_{DF} + \sum_{i=1}^{PB} S_{DF} \qquad (80)$$

Eq. 80 allows finding a more suitable payback period, focused not just on the expected earnings, but also on the dependency of these on time.

As can be seen from these expressions, the determination of four parameters is important for the financial feasibility of the investment, i.e. the price of electricity, the price of natural gas, the feed-in tariff and the discount rate. Therefore, a further sensitivity analysis will be developed. The actual values of these parameters are reported in Table 5.1.

Table 5.1: Prices of energy and discount rate taken in Athens and Vicenza.

	ELECTRICITY PRICE $c_{el,buy}\left(\dfrac{c€}{kWh}\right)$	NATURAL GAS PRICE $c_{gas}\left(\dfrac{c€}{kWh}\right)$	FEED-IN TARIFF $c_{el,s}\left(\dfrac{c€}{kWh}\right)$	DISCOUNT RATE $r\ (\%)$
ATHENS	16.50	5.55	8.00	6.00
VICENZA	23.01	7.69	4.90	6.00

The evolutionary algorithms work by choosing initial random values of the population, which means that it can evaluate also negative values. A negative value of PB represents a nonsense, because it would mean that the system is not economically convenient. In order to avoid useless values in the algorithm optimization research, whenever the value of the denominator $C_{DF} + S_{DF}$ was negative, it was forced to have a close-to-zero value, i.e. $C_{DF} + S_{DF} = e^{-\frac{C_{DF}+S_{DF}}{10000}}$.

5.2.2 Global utilization factor

The system behaves under the laws of thermodynamics, and a way to evaluate how well it works is to calculate the global utilization factor ε. Since the PV/T hybrid collector cogenerates heat and electrical power, a common overall efficiency is not the best option for this system. Moreover, additional components within the system are required for the

conversion of energy into different kinds, which consume energy of different natures themselves. A way to relate the different types of energy consumed is to resort to the primary energy consumption. This considers the raw material used to supply energy to the user. Also, this factor considers indirectly environmental aspects. In fact, the more fossil fuel is burned, the more pollution the combustion generates.

The fossil fuels other than natural gas burned to produce electric energy result in the emission of enormous amounts of compounds and particulates that have negative impacts on human health (EIA, 1999). However, during natural gas combustion, the emissions of sulphur dioxide are negligible and emissions of nitrous oxide and carbon dioxide are lower, which consequently helps to reduce problems associated with acid rain, the ozone layer, or greenhouse gases (78). The most environmentally friendly fossil fuel is methane, which represents the 96.0% in volume of natural gas (79). According to the ideal combustion of methane, for a single molecule of CH_4 a molecule of CO_2 is produced (73). Its chemical reaction shows that even the least polluting among the fossil fuels has an impact on the environment for every burnt molecule.

Also, since the objective of the system is to exploit the solar energy available, it is better to depend from the grid or the pipeline as little as possible. Everything summed up, not only the less fossil fuel is consumed, the more efficient the system is, but also the more benefit the environment gets. For this reason, this factor is adopted. It is defined as the ratio between all the useful forms of energy produced and all the primary energy that has been consumed. With this definition, the global utilization factor in Eq. 81 is set.

$$\varepsilon = \sum_{t=0}^{8760} \frac{\dot{W}_u(t) + \dot{Q}_{c,u}(t) + \dot{Q}_{h,u}(t) + \dot{Q}_{w,u}(t)}{\frac{\dot{W}_{GRID}^+(t)}{\eta_{trans} * \eta_{conv}} + pec_{NG} * \frac{\dot{Q}_{w,NGH}(t)}{\eta_{comb}} + G_{TOT}(t) * A} \tag{81}$$

In the numerator there are all the powers required by the user $(\dot{W}_u(t), \dot{Q}_{c,u}(t), \dot{Q}_{h,u}(t), \dot{Q}_{w,u}(t))$. The surplus of electrical power produced and sold to the grid $\dot{W}_{GRID}^-(t)$ is not considered for the purpose is to match the production of energy with its direct utilization inside the system. In the denominator the power absorbed from the grid $\dot{W}_{GRID}^+(t)$ is divided by the efficiency of transmission η_{trans} and conversion η_{conv} of electric energy. This is added to the gas withdrawn from the pipeline and the

global solar irradiance $G_{TOT}(t)$ that reaches the total surface of the panels A. The overall natural gas used is calculated as the specific primary energy consumed to transport it pec_{NG} multiplied by the energy consumed $\dot{Q}_{w,NGH}(t)$ and divided by the combustion efficiency η_{comb}. The efficiency values for the two locations are reported in Table 5.2.

The multi-objective optimization algorithm solves a minimization problem, while the purpose is to have the highest global utilization. Therefore, the objective function linked to the energetic aspect implemented in the optimization algorithm is $-\varepsilon$.

Table 5.2: Specific primary energy consumption in the pipelines and efficiencies of the electric conversion and transmission grid for the Greek and Italian systems.

	pec_{pipe}	η_{conv}	η_{trans}
Greece	1.1743	0.425	0.91759
Italy	1.1743	0.465	0.93006

5.3 Decision variables & boundaries

The decision variables adopted are the ones chosen in section 3, i.e. the overall surface of the PV/T hybrid collectors A, and the volumes of the TSTs for the space thermal conditioning V_{HP} and for the sanitary water V_w. For the separated solution case, the overall surface was separated in two different decision variables: the surface of the PV panels A_{PV} and the one of the thermal collectors A_{COL}. The upper and lower boundaries connected to this were set to let the optimization evolutionary algorithm work with higher precision and lower computational effort. These values are reported in Table 5.3.

Table 5.3: Lower and upper boundaries of the decision variables for the hybrid and the separated solution respectively.

Hybrid solution	$A\ (m^2)$	$Vol_{HP}\ (m^3)$	$Vol_w\ (m^3)$
Lower boundary	50	0.5	0.5
Upper boundary	500	5	5

Separated solution	$A_{PV}\ (m^2)$	$A_{COL}\ (m^2)$	$Vol_{HP}\ (m^3)$	$Vol_w\ (m^3)$
Lower boundary	50	50	0.5	0.5
Upper boundary	500	500	5	5

5.4   Genetic algorithm

Several methods have been developed for solving a multi-objective optimization problem. Evolutionary algorithms are well suited for this purpose, and genetic algorithms (GAs) belong to this category (80).

The genetic algorithm can be used to solve problems that are not well suited for standard optimization algorithms, including problems in which the objective function is discontinuous, discrete, stochastic, or highly nonlinear. The genetic algorithms are based on the principles of natural genetics and natural selection stochastic methods that can find the global minimum with a high probability. Philosophically, GAs are based on the survival-of-the-fittest principle of nature. The basic elements of natural genetics, i.e. reproduction, crossover, and mutation, are used in the genetic search procedure. GAs differ from the traditional methods of optimization in the following aspects:

- A population of points (trial design vectors) is used for starting the procedure instead of a single design point. Since several points are used as candidate solutions, GAs are less likely to get trapped at a local optimum.

- GAs use only the values of the objective function. The derivatives are not used in the search procedure.

- In GAs the design variables are represented as strings of binary variables that correspond to the chromosomes in natural genetics. Thus, the search method is applicable for solving discrete and integer programming problems. For continuous design variables, the string length can be varied to achieve any desired resolution.

- The objective function value corresponding to a design vector plays the role of fitness in natural genetics.

- The algorithm repeatedly modifies a population of individual solutions. At each step, the genetic algorithm randomly selects individuals from the current population and uses them as parents to produce the children for the next generation. Over successive generations, the population "evolves" toward an optimal solution.

5.4.1 Fitness function and constraints for GA

Since GAs are based on Darwin's theory of survival of the fittest, they try to maximize a "fitness function". This fitness function, $F(X)$, can be taken to be same as the objective function $f(X)$ of an unconstrained maximization problem so that $F(X) = f(X)$. A minimization problem can be transformed into a maximization problem before applying the GAs. Usually the fitness function is chosen to be nonnegative. The commonly used transformation to convert an unconstrained minimization problem to a fitness function is given by Eq. 82.

$$F(X) = \frac{1}{1 + f(X)} \tag{82}$$

Eq. 82 does not alter the location of the minimum of $f(X)$ but converts the minimization problem into an equivalent maximization problem. A general constrained minimization problem can be stated as:

$$\text{Minimize } f(X)$$

subject to $\qquad g_i(X) \leq 0, \qquad i = 1, 2, \ldots, m$

and $\qquad h_j(X) = 0, \qquad j = 1, 2, \ldots, p$

where $g_i(X)$ and $h_j(X)$ are the constraints.

5.4.2 Genetic operators

The algorithm begins by creating a random initial population. Then it creates a sequence of new populations. At each step, the genetic algorithm uses the current population to create the children that make up the next generation. The algorithm selects a group of individuals in the current population, called parents, who contribute their genes, i.e. the entries of their vectors, to their children. The algorithm usually selects individuals that have better fitness values as parents. The genetic algorithm creates three types of children for the next generation: elite, crossover or mutation children.

Elite children are the individuals in the current generation with the best fitness values. These individuals automatically survive to the next generation.

Crossover children are created by combining pairs of parents in the current population. At each coordinate of the child vector, the default crossover function randomly selects an entry, or gene, at the same coordinate from one of the two parents and assigns it to the child. For problems with linear constraints, the default crossover function creates the child as a random weighted average of the parents.

Mutation children are generated by randomly changing the genes of individual parents. By default, for unconstrained problems the algorithm adds a random vector from a Gaussian distribution to the parent. For bounded or linearly constrained problems, the child remains feasible.

Conclusions

A multi-objective optimization problem was faced. An evolutionary algorithm seemed to be the best approach to find the Pareto front in the minimization of the nonlinear functions involved. The genetic algorithm was chosen among this category. This optimization tool was used in Matlab® that allows minimizing an undefined number of multi-objective functions. The functions taken under study considered both the economic and energetic aspects: the payback time PB and the usage factor ε.

6. PRESENTATION OF THE RESULTS

Here the logic behind the control of the system is presented. The main concept is to match the loads and the production. The model was built with the simulation tool Simulink; a program enhanced with Matlab which allows a modular sequential approach. The system studied has a dynamic behaviour, which requires this kind of solving approach, rather than a simultaneous one. The system has been modelled by implementing component by component and connecting all of them accurately.

The first configuration studied was the simplest one:

- The PV panel of the PV/T system provides electrical energy to the inverter, which either supplies it to the electrical driven heat pump for space heating and cooling, for a direct usage, or exchanges it with the grid;
- The thermal collector of the PV/T system in parallel with a backup NGH provides heat to the DHW load;
- Two different storages are included to decouple loads and production that are often shifted in time.

The simulation is the fundamental step before the optimization process: the outputs of the system are the inputs of the objective functions. The objectives are yearly based; therefore, an annual simulation is needed to solve the optimization problem. Deterministic values for the loads are taken from the simulation program EnergyPlus, which generates them by historical data. The values provided are hourly-based average of the quantity considered throughout the year and dependant on the location. Therefore, there are 8760 values for each external yearly condition. However, a base case simulation has been developed at the beginning in order to check if the system behaves properly.

6.1 Base case simulation

In order to cover the most disparate alternatives, the base case simulation was divided into three subcases: on constant standard conditions, on a summer day and on a winter day. As already stated, the sizes of the natural gas heater $\dot{Q}_{NGH,nom}(kW)$ and the heat pump $\dot{Q}_{HP,nom}(kW)$ are designed in function of the maximum thermal power demanded by the user in terms of DHW and space conditioning respectively. On the other hand, the sizes of the other components are defined in order to solve the problem, i.e. the area if the panels $A_{PVT}(m^2)$ and the volumes of the heat pump $Vol_{HP}(m^3)$ and the hot water $Vol_W(m^3)$ storage tanks are predefined. The inverter $\dot{W}_{inv,nom}(kW)$ is designed on the maximum power output of each string of the photovoltaic part of the hybrid collectors field; therefore, it depends directly on A_{PVT}.

6.1.1 Constant standard conditions

This first simulation was made to verify the performance of the main component, i.e. the PV/T hybrid collector. The constant standard conditions (STC) are the environmental parameters defined as follows:

- $T_{amb} = 25\,°C$
- $G_{tot} = 1000\,W/m^2$
- $u_w = 1\,m/s$

Moreover, a cell temperature equivalent to the ambient temperature $T_{cell} = 25°C$ and a usage temperature for the thermal collector must be set. Two different values of usage temperature are set for the heat carrier fluid: in the standard case $T_w = 25°C$, while for the DHW production of $T_w = 50°C$. In these conditions the values expected are the nominal electrical and thermal power produced. From Table 1 some values can be compared to the nominal ones. As can be seen, the electrical values are close to the ones of the datasheet. In particular, the photovoltaic efficiency is the only parameter slightly different from the given one. That is because the surface considered for its calculation is narrower than the one used, which is also the same adopted for the thermal efficiency. As can be stated from the Figures, the reference value of temperature for the thermal efficiency is the mean temperature inside the collector T_{mean}, which is calculated as the average value between the inlet and outlet temperatures of the heat carrier fluid.
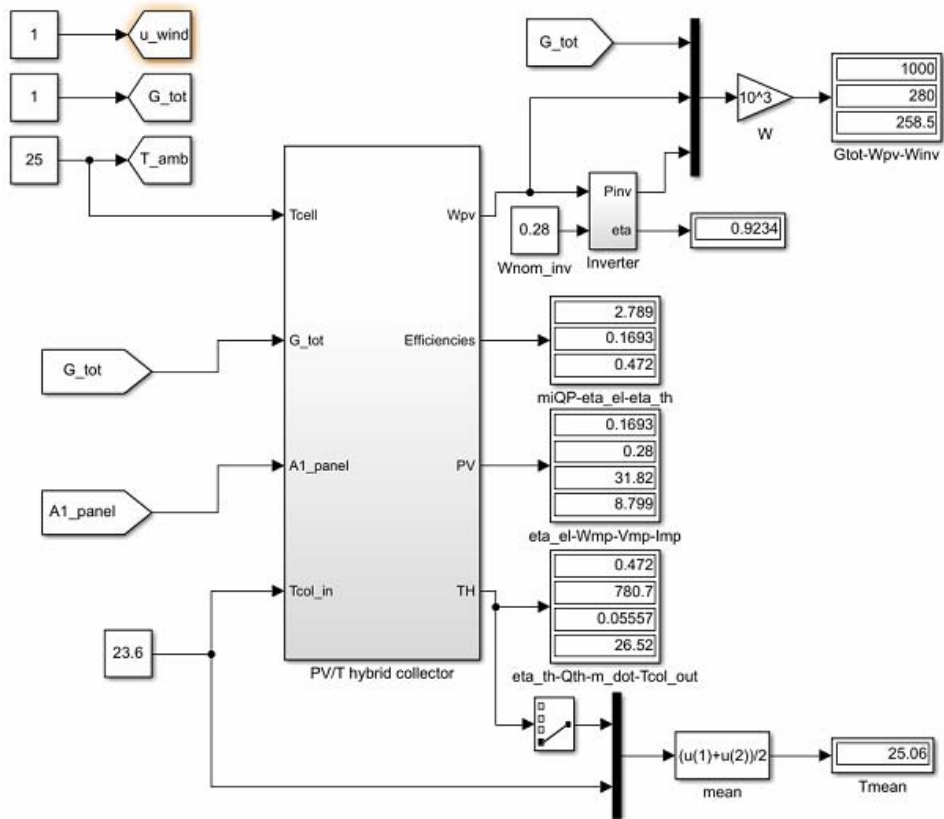
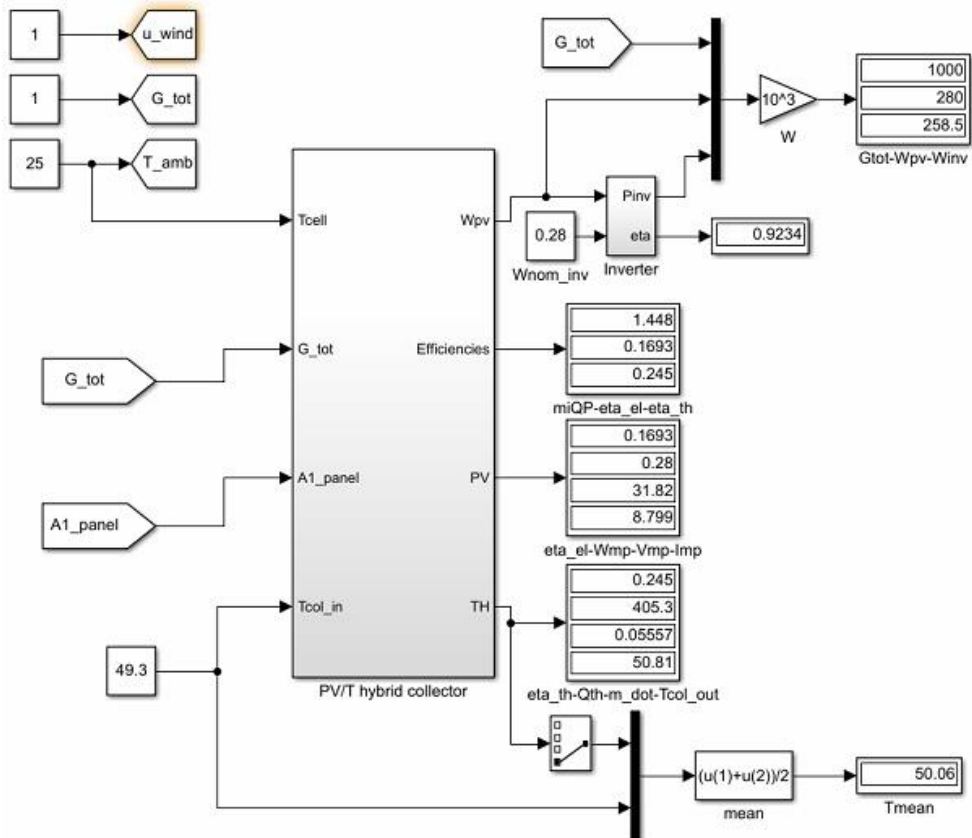*Figure 6.1: Operational diagram of the PV/T in standard conditions*

Figure 6.2: Operational diagram of the PV/T in standard conditions

Table 6.1: comparison between nominal and computed values of the PV/T hybrid collector

Parameter	Nominal Value	Simulated Value	Relative difference
Nominal electric power (W)	280	280	-
Module efficiency (%)	17.2	16.93	1.57 %[*]
Rated Voltage V_{MPP} (V)	31.95	31.82	0.41 %
Rated Current I_{MPP} (A)	8.77	8.79	0.23 %
Thermal power (@STC) (W)	780	780.7	0.09 %
Efficiency (@STC) (%)	47.2	47.2	-
Heat-Power ratio μ_{QP}(@STC) (-)	2.786	2.789	0.11 %
Thermal power ($T_w = 50°C$) (W)	404	405.3	0.32 %
Efficiency ($T_w = 50°C$) (%)	24.43	24.5	0.29 %
Heat-Power ratio μ_{QP}($T_w = 50°C$) (-)	1.443	1.448	0.35 %

[*]This relatively wide difference is due to the different area selected for the determination of the efficiency: while in the datasheet the value taken was the overall area, i.e. 1.6602 m², the one used for this comparison was the captative area of the absorber, i.e. 1.654 m².

Table 6.2: Separated solution characteristics

Parameter	Nominal Value	Simulated Value	Relative difference
Nominal electric power (W)	335	335	-
Module efficiency (%)	17.2	17.23	0.17 %
Rated Voltage V_{MPP} (V)	37.6	37.61	0.03 %
Rated Current I_{MPP} (A)	8.91	8.906	0.04 %
Thermal power (@STC) (W)	1749.3	1749	0.02 %
Efficiency (@STC) (%)	75.4	75.39	-
Heat-Power ratio μ_{QP}(@STC) (-)	5.222	5.221	0.02 %
Thermal power ($T_w = 50°C$) (W)	1492.1	1492	-
Efficiency ($T_w = 50°C$) (%)	64.3	64.32	0.03 %
Heat-Power ratio μ_{QP}($T_w = 50°C$) (-)	4.454	4.455	0.02 %

The electrical power produced by the PV module, once set all the parameters (e.g. the cell temperature), is mainly dependent on the operational voltage and the global irradiance hitting the panel. This can be well seen on Figure 6.3, in which $\dot{W}_{PV}$ was taken also for lower values of G_{tot}. Also, a difference in power output would happen if a different cell temperature was set. In the same figure listed below, it can be noticed that with high solar irradiance, the output current and thus the power production is increased. The maximum power output is observed when the voltage of the short circuit equals to $V_{sc} = V_{mp,STC} = 31.95\ V$. The side values over the right edge of the minimum current are calculations failures, thus are not to be considered.

On the other side of the hybrid collector, the thermal power produced by the solar collector vary in function of the operating temperature and so does the thermal panel efficiency, as can be noticed from Figure 6.4.
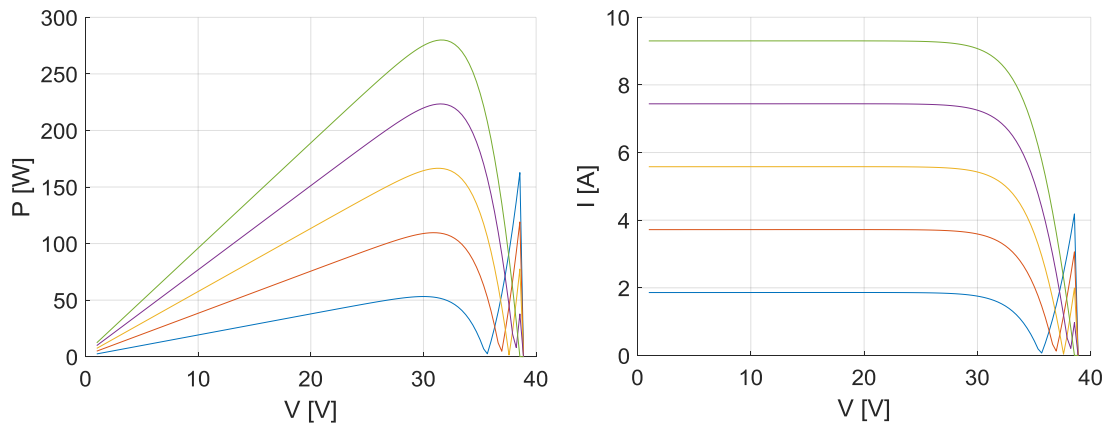

Figure 6.3: On the left side: Power-Voltage characteristic curve at STC for different solar irradiance values

On the right side: Current-Voltage characteristic curve at STC for different solar irradiance values

In the same figure, the efficiency of the thermal component of the PV/T collector is depicted as a function of the heating utility temperature of its working fluid in STC conditions ($T_{amb} = 25°C$, $G_T = 1000\ W/m^2$). This efficiency is very low compared to that of conventional solar thermal collectors, as the PV module absorbs most of the solar radiation and heat for electricity production.

The inverter varies its efficiency by changing the power output ratio, i.e. the value of $\dot{W}_{PV}$ referred to the inverter nominal value $\dot{W}_{inv,nom}$. The evolution of the efficiency curve η_{INV} in function of the power output ratio p_{output} is reported in Figure 6.5.
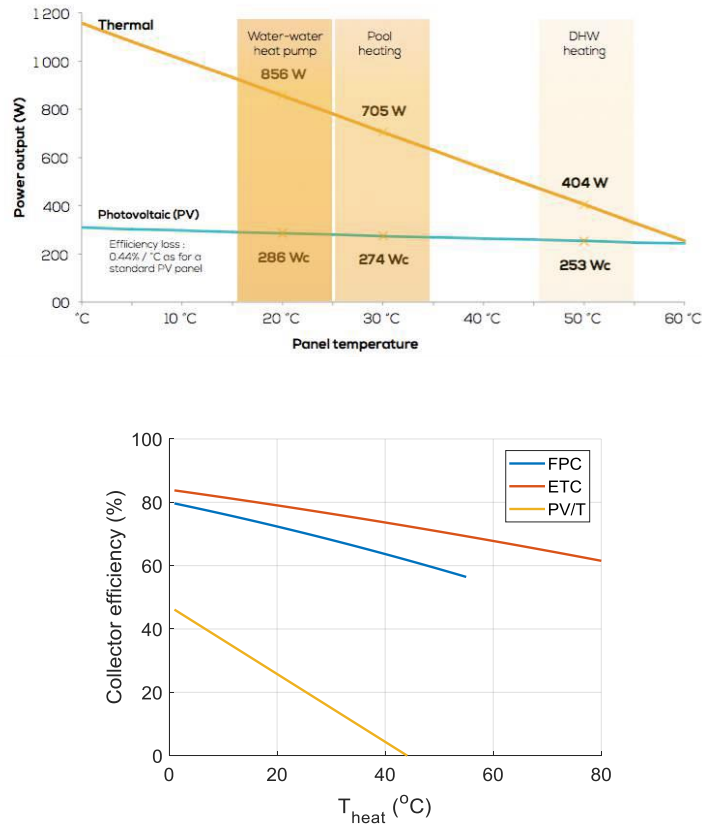

Figure 6.4: On the upper side: power output as a function of the water in the panel by application (from DualSun datasheet). On the lower side: efficiency of the thermal component of the PV/T as a function of heating utility temperature, compared to the ones of a Flat Plate Collector (FPC) and an Evacuated Tube Collector (ETC).

The heat pump is a component that varies its performances in function of the type of thermal demand, designed thermal power $\dot{Q}_{HP,nom}$, the water outlet temperature LWT and the ambient temperature T_{amb}. This variation is reported for a $\dot{Q}_{HP,nom} = 40 \; kW$ in Figure 6.6.
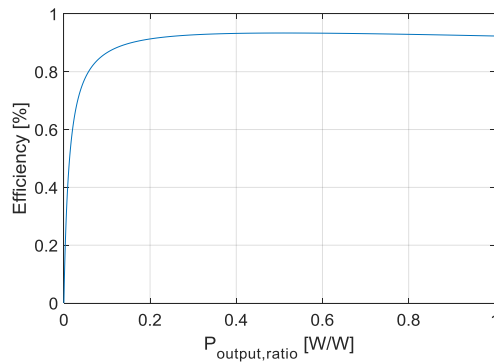
Figure 6.5: Efficiency graph of the DC/AC inverter as function of the power output ratio

The natural gas heater varies its efficiency in function of the water inlet temperature, but since this value is almost constant the efficiency is taken as a constant parameter. For the same reason, the charge and discharge factors of the battery are constant as well.
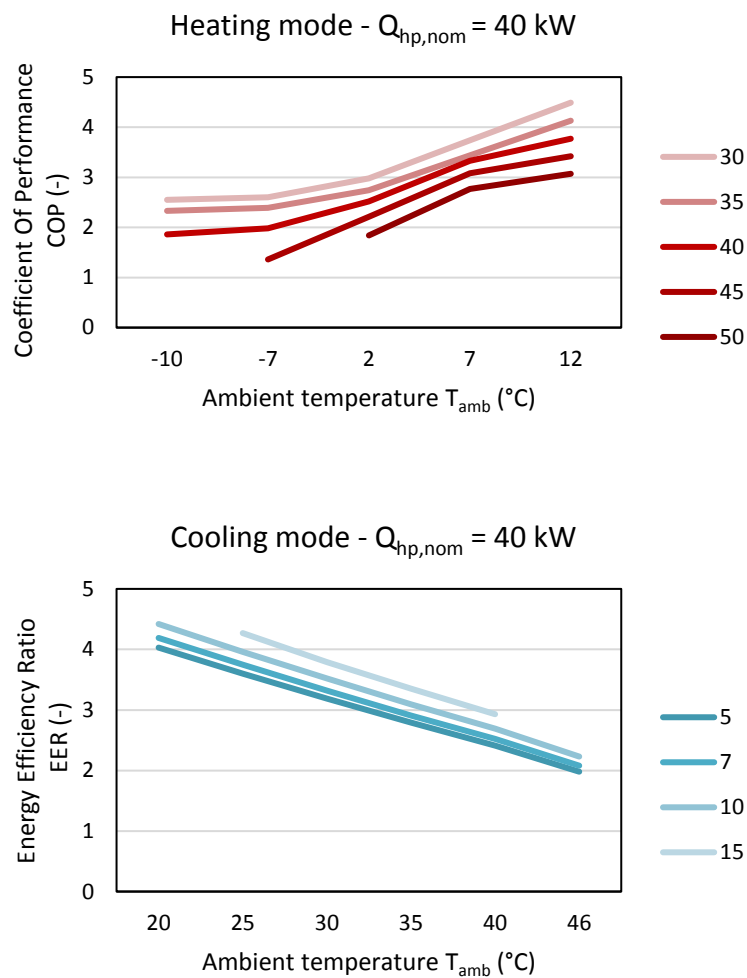

Figure 6.6: Heat pump performance factors at a predefined nominal thermal power and in function of the ambient temperature T_{amb} and the outlet water temperature LWT. Upper side: heating mode. Lower side: cooling mode.

6.1.2 Summer day simulation

On a summer day simulation, the space heating load is null, while the space cooling, the electrical power and the DHW loads are stair functions. The values of temperature and irradiance are variable, but for simplicity in calculation the first is a sinewave while the second a triangular function. The speed of the wind was set constant at $1\ m/s$.

The size of each component is reported in Table 2. As can be seen, while the gas heater and the heat pump are designed in function of the maximum thermal demand, the area of the PV/T field was taken to provide nominally the double of the electrical power requested by the user. In fact, electric energy is required always throughout the day, which means that electricity from the grid must be absorbed when no photovoltaic energy is produced.

Table 6.3: Design variables of the components for a daily base case simulation.

Component size parameter	Number of components	Value of each component
A_{PVT}	200	$1.654\ m^2$
Vol_{HP}	1	$1\ m^3$
Vol_W	1	$1\ m^3$
$\dot{Q}_{HP,nom}$	3	$40\ kW$
$\dot{Q}_{NGH,nom}$	1	$38\ kW$
$\dot{W}_{inv,nom}$	10	$5.6\ kW$

The space cooling load is made of three steps: from 00.00 to 08.00 at the lowest level $\dot{Q}_{c,u} = 30\ kW$, from 08.00 to 16.00 at an intermediate $\dot{Q}_{c,u} = 60\ kW$ and from 16.00 to 20.00 at a higher demand of $\dot{Q}_{c,u} = 90\ kW$. The remaining time the load is at the lowest level. The control on the space cooling is made in function of the demand of thermal power and of the temperature inside the TST.

The electrical power load is made of three steps as well: from 00.00 to 08.00 at the lowest level $\dot{W}_u = 14\ kW$, from 08.00 to 16.00 at an intermediate $\dot{W}_u = 21\ kW$ and from 16.00 to 20.00 at a higher demand of $\dot{W}_u = 28\ kW$. The remaining time the load is at the lowest level.

The hot water load is made of three steps too: from 00.00 to 08.00 at the lowest level $\dot{Q}_{w,u} = 0\ kW$, from 08.00 to 12.00 at the highest $\dot{Q}_{w,u} = 10\ kW$ and from 16.00 to 20.00 again at $\dot{Q}_{w,u} = 10\ kW$. The remaining time the load is null.

Temperature is a sinewave raised from zero at $30°C$, its amplitude is of $10°C$ and gets its maximum at noon, therefore is shifted of $-\pi/2$. Solar irradiance is a triangular function that rises from 06.00 to 12.00 and decreases from 12.00 to 18.00: its peak is at $1\ kW/m^2$. The rest of the time its value is null.

The results of the simulation are hereby reported.

Figure 6.7a shows the development of the electric power inside the PV/T hybrid system throughout the summer day. The power produced by the PV/T hybrid collector $\dot{W}_{PV}$ reaches its peak at solar noon, and so does the inverter $\dot{W}_{INV}$. The power exchanged with the grid $\dot{W}_g$ is the difference between the converted photovoltaic power of the inverter $\dot{W}_{INV}$ and the ones absorbed by the heat pump $\dot{W}_{HP}$ and directly provided to the user $\dot{W}_u$.
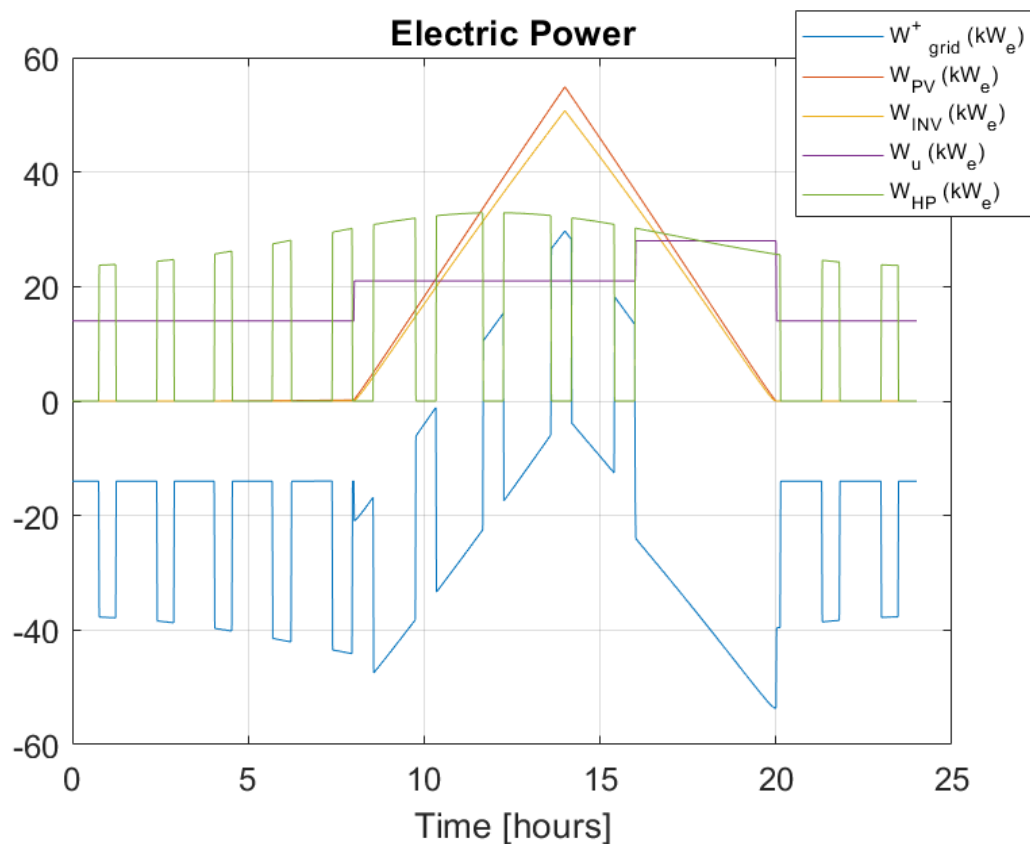

Figure 6.7a: Trend of the electric power inside the PV/T hybrid system for a summer day simulation
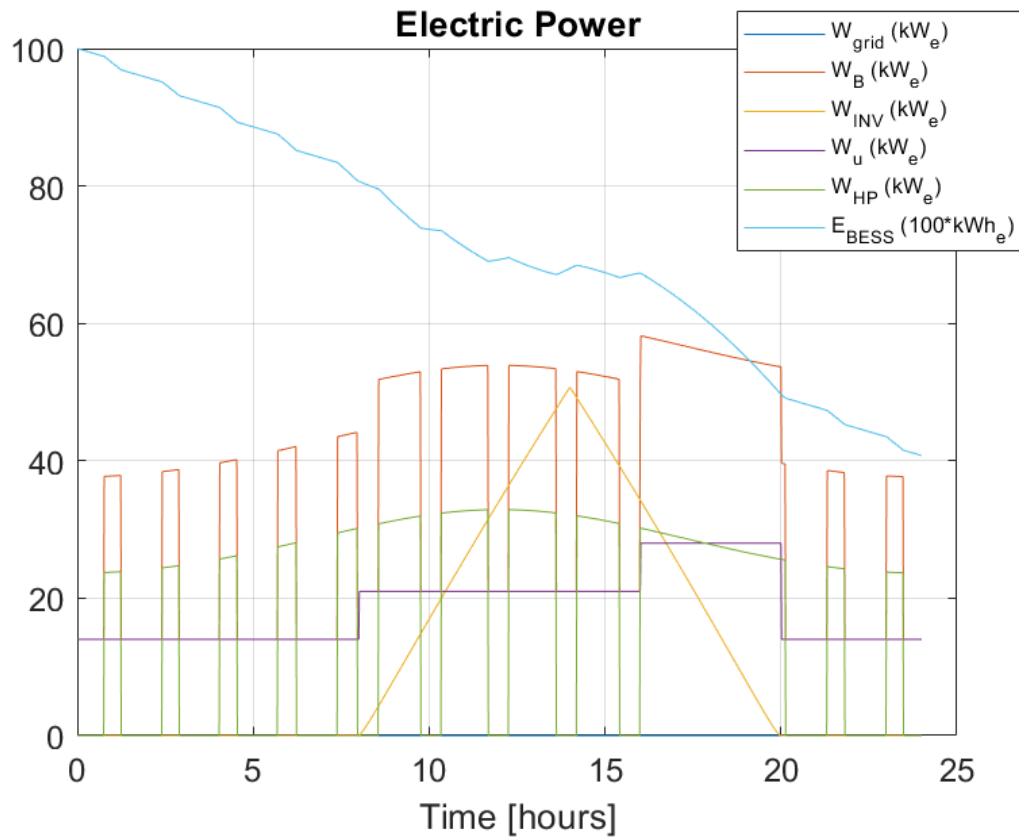
94

Figure 6.7b: Trend of the electric power inside the PV/T hybrid system coupled with a BESS for a summer day simulation.

The heat pump behaviour is an on-off switching that depends on the space conditioning required: when it is on, the electrical power absorbed for the maximum power available is provided, otherwise the electrical power absorbed is null. As can be stated from the graph representing the power output, $\dot{W}_g$ is mainly negative. This is due to the absorption of electricity by the heat pump $\dot{W}_{hp}$, which has indeed a greater amount than the one demanded directly by the user $\dot{W}_u$. Therefore, the PV/T field is not able to provide enough energy $\dot{W}_{PV}$ to cover the main loads.

Figure 6.7b shows the behaviour of the hybrid system coupled with a BESS. The energy stored inside the battery provides the electric power demanded throughout the day as a sum of the heat pump and the direct use. Part of the energy consumpted is integrated by the PV production. However, this is not enough to charge the battery at its starting level.
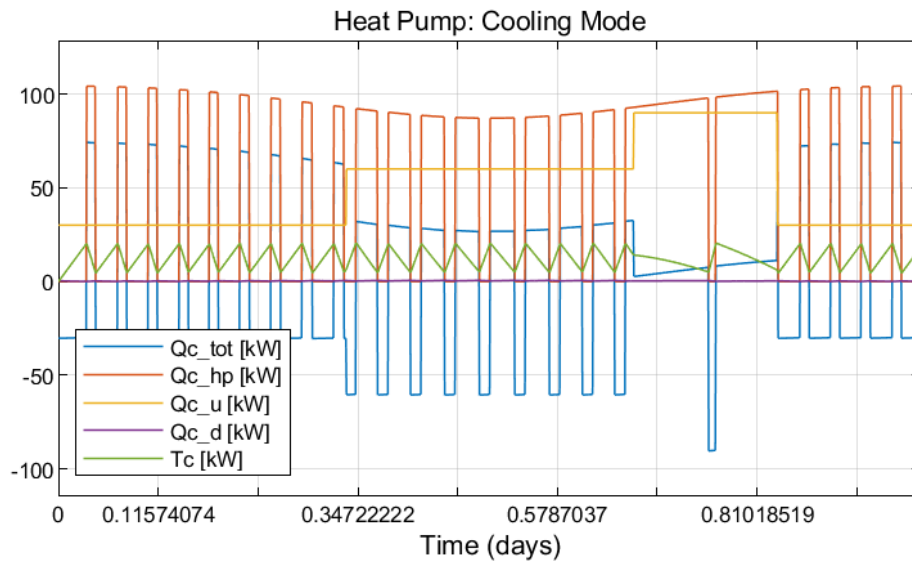
Figure 6.8a: Trend of the thermal power exchanged and temperature development inside a 1 m³ volume TST for space conditioning on a summer day simulation.
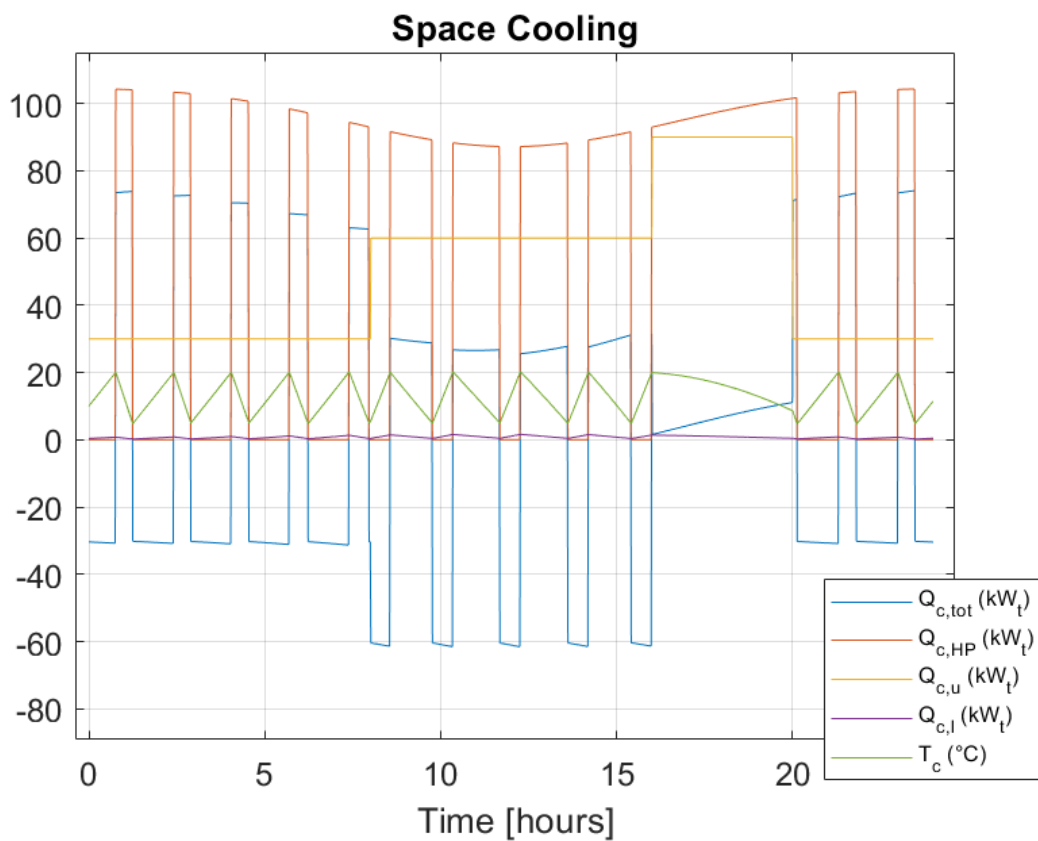

Figure 6.8b: Trend of the thermal power exchanged and temperature development inside a 2 m³ volume TST for space conditioning on a summer day simulation.

The behaviour of the space cooling is shown in Figure 6.8a and 6.8b. The available cooling load of the HP varies in dependence of the outside ambient temperature: lower

when it is hotter, higher when it gets colder. The temperature inside the storage tank T_c is constantly maintained between 5 and 15 °C: due to the space cooling required and difference of temperature between the TST and the external environment, there is a thermal loss that rises the temperature of the TST. Whenever T_c reaches the highest limit, then the heat pump switches on. On the other hand, in order to avoid freezing temperatures, the heat pump is switched off when gets to the lowest limit. It can be seen how temperature decreases more rapidly when the demand of thermal power of the user gets higher. In Figure 6.8a is shown the behaviour of the system with a 1 m³ volume TST, while in Figure 6.8b with a 2 m³. The switching of the heat pump is more rapid in the first than in the second due to the worse thermal capacity of the storage. In fact, the higher amount of water present in the second case determines a slower temperature variation.

The trend of the thermal power linked to the DHW is shown in Figure 6.9 and Figure 6.10.
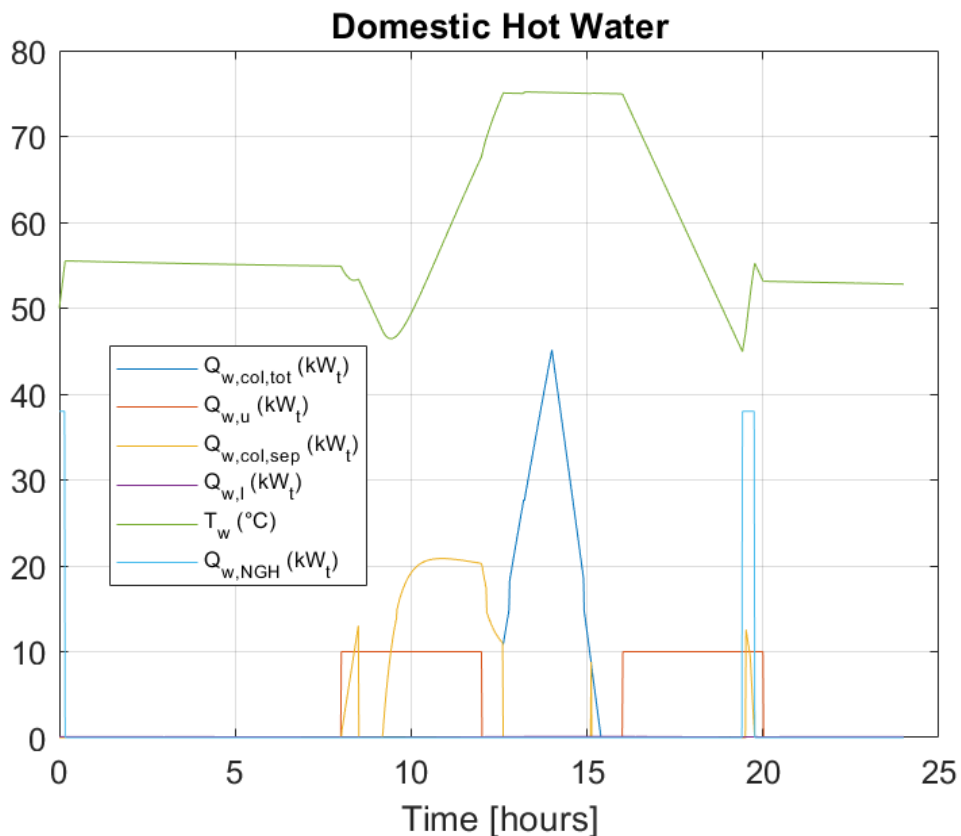

Figure 6.9: Trend of the thermal power exchanged and temperature development inside a 1 m³ volume TST for domestic hot water on a summer day simulation.
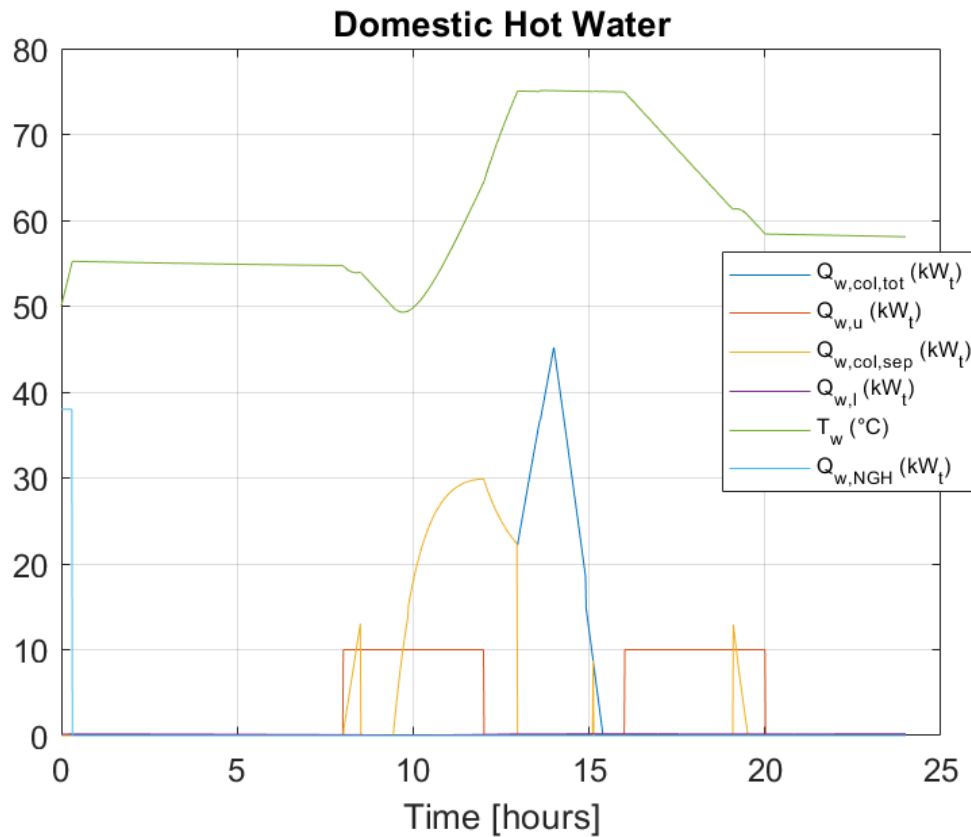
Figure 6.10: Trend of the thermal power exchanged and temperature development inside a 2 m³ volume TST for domestic hot water on a summer day simulation.

This varies along with the solar thermal production, and the control parameter is the storage temperature T_w. As stated in section 4.4, the temperature must lie in a range between the minimum temperature to avoid bacteria formation like legionella, and the maximum for stagnation problems of the collector. Within this range temperature is free to evolve. While the user is exploiting the hot water, the temperature lowers: when it reaches the lower boundary, if the support of the solar collector is not enough, the NGH intervenes and provides the necessary heat. In Figure 6.9 it is visible only for a narrow period around 20.00. When there is no DHW demand and the solar energy is available, T_w rises until it reaches the top of the affordable temperature. At this point, as can be seen by confronting Figure 6.9 and 6.10, part of the energy available cannot be used by the system but needs to be dissipated to the external environment for not compromising the thermal collector. This happens during the most irradiated hours of the day. However, the presence of a different volume of TST changes the availability of the solar resource: in Figure 6.10, where the volume is of 2 m³ instead of 1 m³, the operation of the NGH is not required.

6.1.3 Winter day simulation

On a winter day simulation, the space cooling load is null, while the space heating, the electrical power and the DHW loads are stair functions. The values of temperature and irradiance are variable, but for simplicity in calculation the first is a sinewave while the second a triangular function. The speed of the wind was set constant at $1\ m/s$. The size of each component is reported in Table 2 like in the summer day simulation.

The space heating load is a stair function of three steps: from 00.00 to 08.00 the highest level $\dot{Q}_{h,u} = 80\ kW$, from 08.00 to 16.00 a lower $\dot{Q}_{h,u} = 40\ kW$ and from 16.00 to 20.00 an intermediate demand of $\dot{Q}_{h,u} = 60\ kW$. The remaining time the load is at the lowest level.

The electrical power load is made of three steps as well: from 00.00 to 08.00 at the lowest level $\dot{W}_u = 14\ kW$, from 08.00 to 16.00 at an intermediate $\dot{W}_u = 21\ kW$ and from 16.00 to 20.00 at a higher demand of $\dot{W}_u = 28\ kW$. The remaining time the load is at the lowest level.

The hot water load is made of three steps too: from 00.00 to 08.00 at the lowest level $\dot{Q}_{w,u} = 0\ kW$, from 08.00 to 12.00 at the highest $\dot{Q}_{w,u} = 38\ kW$ and from 16.00 to 20.00 again at $\dot{Q}_{w,u} = 38\ kW$. The remaining time the load is null.

Temperature is a sinewave raised from zero at $5°C$, its amplitude is of $10°C$ and gets its maximum at noon, therefore is shifted of $-\pi/2$. Solar irradiance is a triangular function that rises from 06.00 to 12.00 and decreases from 12.00 to 18.00: its peak is at $1\ kW/m^2$. The rest of the time its value is null. Hereby are presented the results.

The electric power exchanged evolves in the same way it did during the summer day, as shown in Figure 6.11. During the day the power exchanged with the grid is mostly negative, which means that is absorbed: only close to solar noon it is alternatively transmitted to the grid, i.e. when PV production is higher. When the heat pump is switched on the power is absorbed suddenly and depends on the thermal power available at the external conditions. As shown in Figure 6.12, the heat pump starts providing heat since the beginning because of the initial condition.

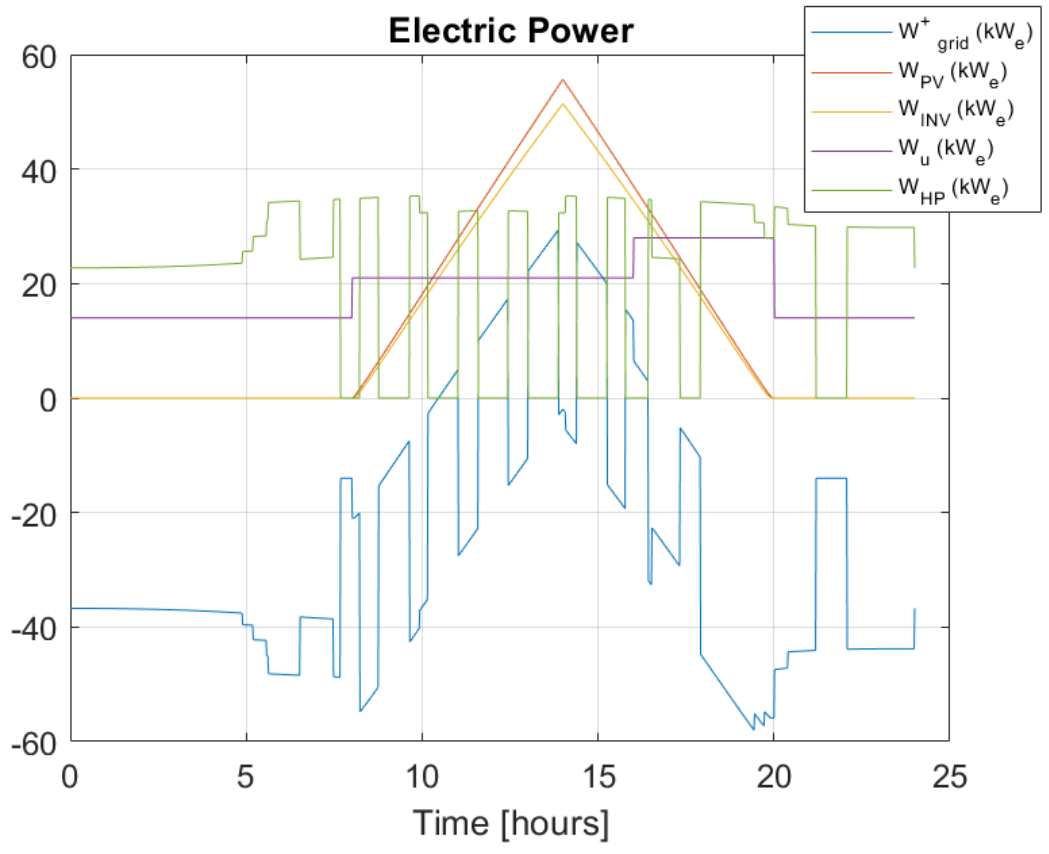*Figure 6.11: Trend of the electric power inside the system for a winter day simulation.*
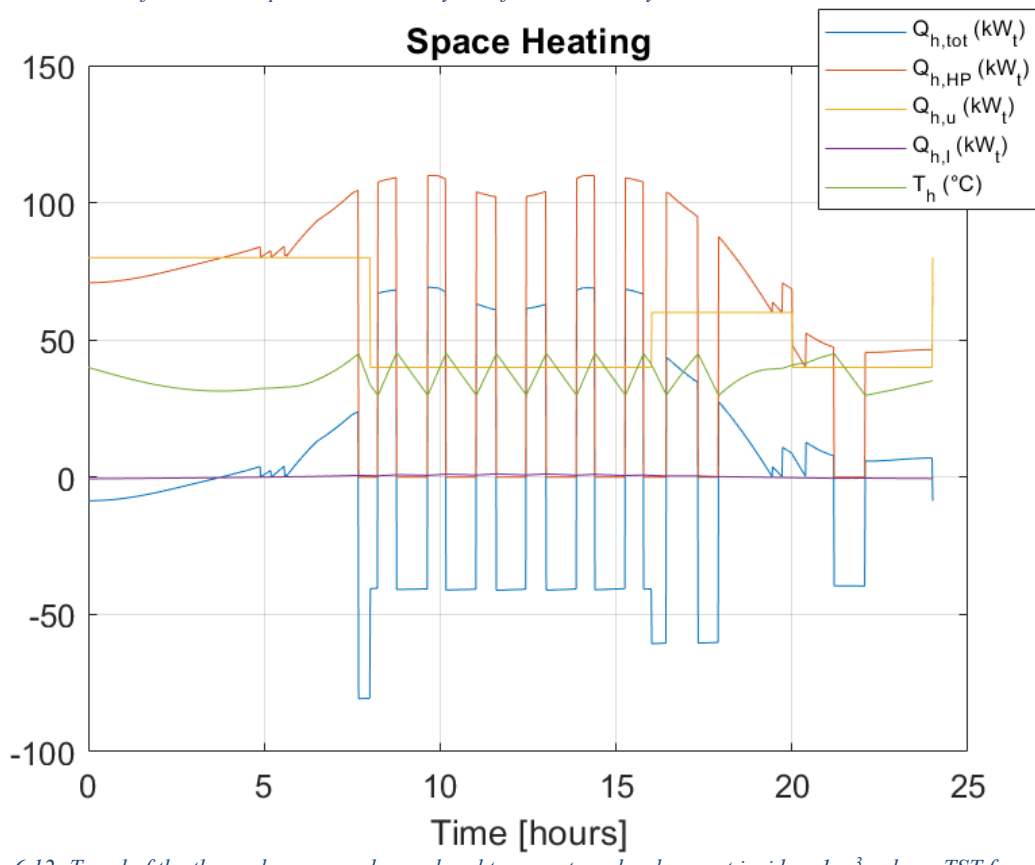

Figure 6.12: Trend of the thermal power exchanged and temperature development inside a 1 m³ volume TST for space conditioning on a winter day simulation.

Even though the temperature inside the TST at the very start of the simulation is in the required range, suddenly the user absorbs thermal power at a high level and for a long time. Moreover, outside temperature is low, so the HP can provide lower heat then when the weather is hotter (i.e. during the daily hours). Thus, HP works more constantly then when the demand is lower, and the external temperature is higher.

The evolution of the heat exchanged for the domestic hot water is shown in Figure 6.13. Temperature T_w lowers even though there is no thermal power required due to thermal losses. T_w gets under the lower boundary of 45 °C, the NGH is switched on to provide the thermal power the solar collector is not able to produce. The most solar thermal energy is collected at solar noon, when the user does not need hot water. In winter case there is not the problem observed in summer, when the temperature reached was too high. This means that the user can fully exploit the fewer amount of thermal power, because T_w is far lower than 75 °C.
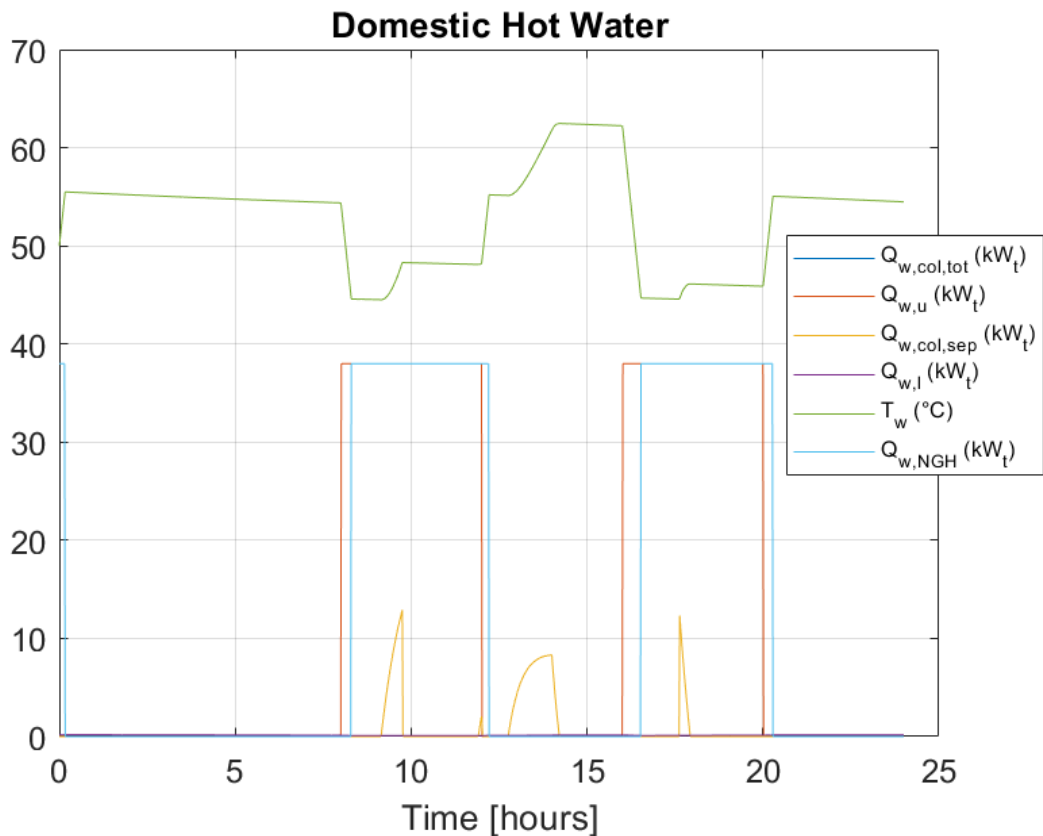

Figure 6.13: Trend of the thermal power exchanged and temperature development inside a 1 m3 volume TST for domestic hot water on a winter day simulation.

6.2   Annual simulation

The annual simulation for both locations was conducted by considering the aspects seen in the base case simulations. The simulation first considered external parameters that do not need to go through optimization, such as external ambient conditions and the energy loads. Then the multi-objective optimization determined the optimal values for the dimensioning of the solar field surface A and the volumes of the TST for the HP V_{HP} and for the DHW V_w.

6.2.1 Configuration parameters & set values

The configuration parameters set are linked to the solver and to the data import/export. In the solver the simulation starts at time $1s$ and stopped at time $3600 * 24 * 365 = 31.536 * 10^6 \, s$, since the simulation has been developed all along the year and the unit value of the time is the second. The solver is the Ordinary Differential Equations 5 (Dormand-Prince), which is a fixed-step type. The fundamental sample time at the beginning is of 60 unit values, i.e. every minute. The periodic sample time is unconstrained, and each discrete rate has been treated as a separate task.

In the data import/export, the values saved outside of Simulink were given as a vector time-dependant, in which one value of the quantity considered at each time step has been taken, i.e. a vector of 1 column and $31536000/60 = 525600$ rows.

As already mentioned, some values have been taken as input data from external spreadsheet. These are the environmental data $T_{amb}(T\_amb), G_{tot}(G\_tot), u_w(u\_w)$ and the loads $\dot{W}_u \, (W\_u), \dot{Q}_{h,u}(Qh\_u), \dot{Q}_{c,u}(Qc\_u), \dot{Q}_{w,u}(Qw\_u)$.

6.2.2 Unconstrained external parameters: Environmental data

The external ambient parameters consider:

- T_{amb} = ambient temperature $(°C)$
- G_{tot}= global solar irradiance (kW/m^2)
- u_w = wind velocity (m/s)

The maximum, minimum and average weather data for both locations are reported in Table 6.4. However, for the implementation in a real system, the global irradiance was adapted to a tilted surface instead of a horizontal one. The tilt angle was determined by implementing the global horizontal solar irradiance at each hour of the year inside the equations from (20) to (24). Then the angle chosen is the one that maximizes the overall energy obtained from the solar irradiance for a surface south-oriented along the whole year. The tilt angles and the respective maximum and average values of solar irradiance for the latitude of each location has been reported in Table 6.5.

The hourly values of the cell temperatures are determined from Eq. (11). The ones reached in Athens and Vicenza are compared with the actual external temperature and are reported in the diagrams of Figure 6.14.

Table 6.4: Maximum, minimum and average values of temperature, global solar irradiance and wind velocity in Athens and Vicenza.

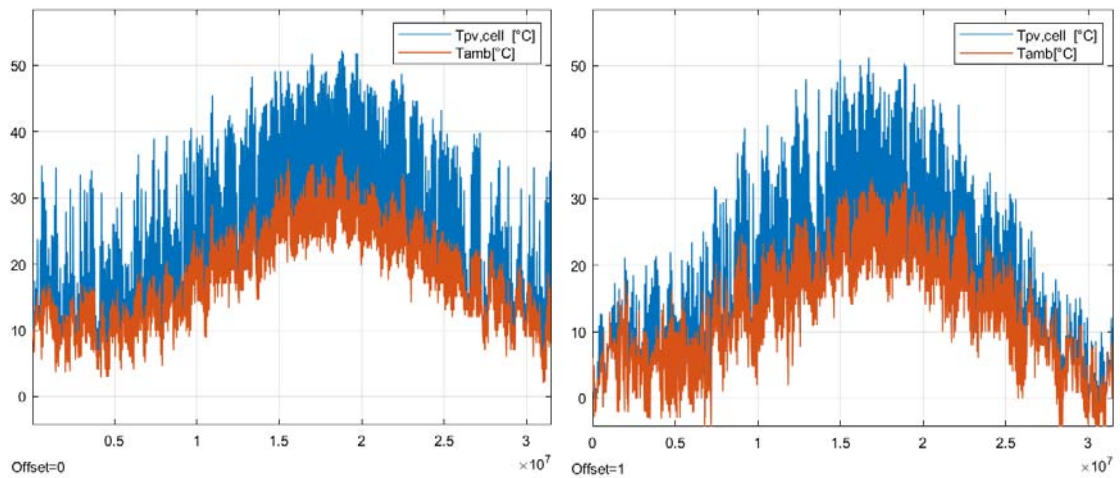| Value	Temperature (°C)		Global Solar Irradiance (W/m²)		Wind Velocity (m/s)	
Location	Athens	Vicenza	Athens	Vicenza	Athens	Vicenza
Maximum	37.2	33.0	997	967	16.4	30.0
Minimum	2.0	-7.1	0	0	0.0	0.0
Average	17.9	12.5	190	126	3.2	0.9

Figure 6.14: Hourly values of cell (blue) and ambient (orange) temperatures for Athens (left) and Vicenza (right) throughout the whole year expressed in °C.

As can be seen, the PV cell temperature is relatively higher than the ambient: in fact, the maximum values of the first are close to 52°C for both locations, while the highest of the second reached are 37.2°C in Athens and 33.0°C in Vicenza as reported in Table 6.4.

By estimating the maximum hourly power output and the values of solar global irradiance for each location, the diagrams in Figure 6.15 result. The hourly power output is measured in (kW/m^2), as at this point the total surface area of the PV/T collectors is not determined. In Table 6.5 it can be noticed how the maximum values of global solar irradiance of a tilted flat surface are higher than a horizontal one, no matter the location.

In Figure 6.14 and Figure 6.15 it can be noticed that the maximum values of both the cell temperature and the power production are observed during summer as the solar irradiance is high and close to standard test conditions.

Table 6.5: Optimal tilt angles and maximum global solar irradiance for each location: $G_{TOT,\beta}$is the maximum tilted surface global solar irradiance, G_{max} is the maximum horizontal surface global solar irradiance

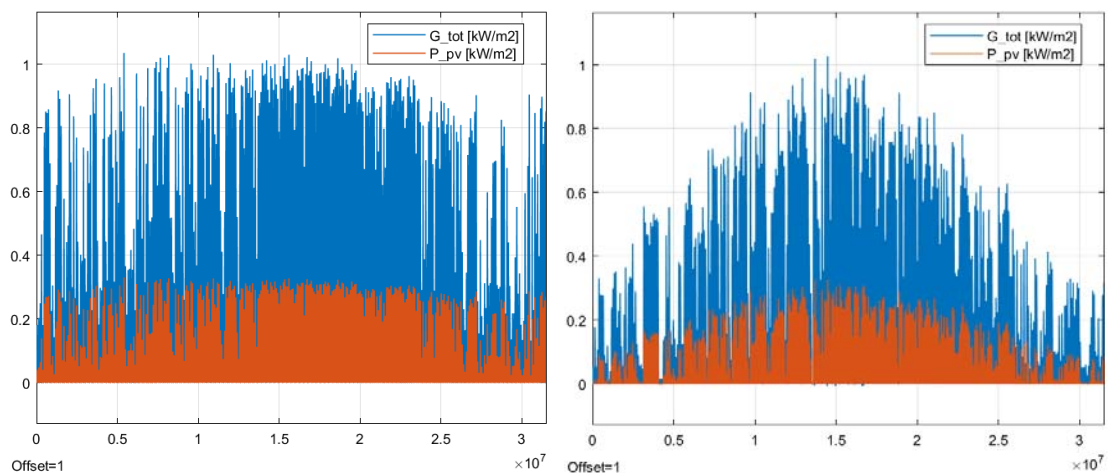|	*Athens*	*Vicenza*
Latitude (°)	37.90	45.55
Tilt Angle (°)	34.92	38.25
$G_{TOT,\beta,max}$ (kW/m²)	1.035	1.027
G_{max} (kW/m²)	0.997	0.967

Figure 6.15: Hourly values of global solar irradiance (blue) and PV power production (orange) in Athens (left) and Vicenza (right) throughout the year, both expressed in kW/m². The values of global solar irradiance are reported on a tilted surface of 34.92° in Athens and 38.25° in Vicenza.

6.2.3 Unconstrained external parameters: Loads

The loads are separated into the demands of:

- $\dot{W}_u$ = electrical power (kW)
- $\dot{Q}_{h,u}$ = space heating (kW)
- $\dot{Q}_{c,u}$ = space cooling (kW)
- $\dot{Q}_{w,u}$ = domestic hot water (kW)

The type of user considered is a district residential one, therefore a set of loads for each location has been evaluated for different types of building:

- Single-family building
- Multi-family building
- Utility building

The residential buildings were split into two categories that had the same temperature demand schedule. The single-family building had a surface of 100 m² on a single floor, while the multi-family one was a 4-storey building with 200 m² surface (50 m² each floor). The heating schedule on weekdays was between 08.00-16.00 at 15 °C and all the other hours (and during weekend) at 20 °C. The cooling schedule on weekdays was between 08.00-16.00 at 27 °C and all the other hours (and during weekend) at 22 °C.

The utility building was a 2-storey building of 200 m² surface (100 m² each floor). The heating schedule on weekdays was between 08-18.00 at 20 °C and all the other hours (and during weekend) at 16 °C. The cooling schedule on weekdays was between 08-18.00 at 22 °C and all the other hours (and during weekend) at 27 °C.

These three types were evaluated for both Athens and Vicenza. The calculations were conducted in the environment of EnergyPlus. To determine the results from the platform, the following parameters were set.

House orientation was set at south. Regarding the adjacent buildings, the choice of neighbouring buildings on both sides at 5 m was selected. For the thermal properties of the walls values from EN ISO 6946 were used, while for the rest inputs choices from the EnergyPlus database were selected. The key properties of the considered materials are listed in Table 6.6.

Material	Thickness (mm)	Thermal Conductivity (W/(m K))	Density (kg/m³)	Specific Heat (J/(kg K))
Walls				
Mortar (Layer 1/5)	20	0.870	1800	1000
Hollow Clay Brick (Layer 2)	90	0.51 (0.45)	1500	1000
Polyurethane foam (Layer 3)	50	0.05 (0.033)	70	1500
Hollow Clay Brick (Layer 4)	60	0.51 (0.45)	1500	1000
Exterior finish				
Stucco	25.4	0.65	1280	488.5
Floor Surface				
Wood (for residential buildings)	15.875	0.115	544.6	1215
Gypsum Concrete (for utility buildings)	50.8	0.685	1601	934

Table 6.6: Thermal properties of building materials based on EN ISO 6946

As roof material was selected light asphalt shingles, from EnergyPlus database, with an absorptivity of 0.8 and an emissivity of 0.91. For the windows, double glazed windows with a thermal break added to the frame were selected (heat transfer coefficient equal to 3.78 W/(m^2 K). The interior shading was selected to be 0.7 for both seasons. This factor decreases the solar gains of the considered buildings based on the set value of the factor. The door surface, for the residential buildings, was selected to be equal to 2.87 m² (30 ft²), made of wood with a heat transfer coefficient of 2.72 W/(m^2 K). For the utility buildings metal doors were used with a heat transfer coefficient of 1.14 W/(m^2 K). The air leakage was set at 8 air changes per hour, while the natural ventilation was set as year-round 3 days/week (from EnergyPlus database).

An overview of the results extracted from EnergyPlus for each type of building and location is presented in Fig. 6.16.

The proportion in numbers of the load is of uttermost importance, therefore a proper ratio between the three types of buildings has been taken from EU Buildings Database of the European Commission. For the system studied, a district of 12 buildings resulted, divided into 4 single-family, 6 multi-family and 2 utility buildings.

The maximum district loads values are taken for sizing purposes; these are presented for both locations in Table 6.7. The hourly annual data are reported in Figure 6.17.
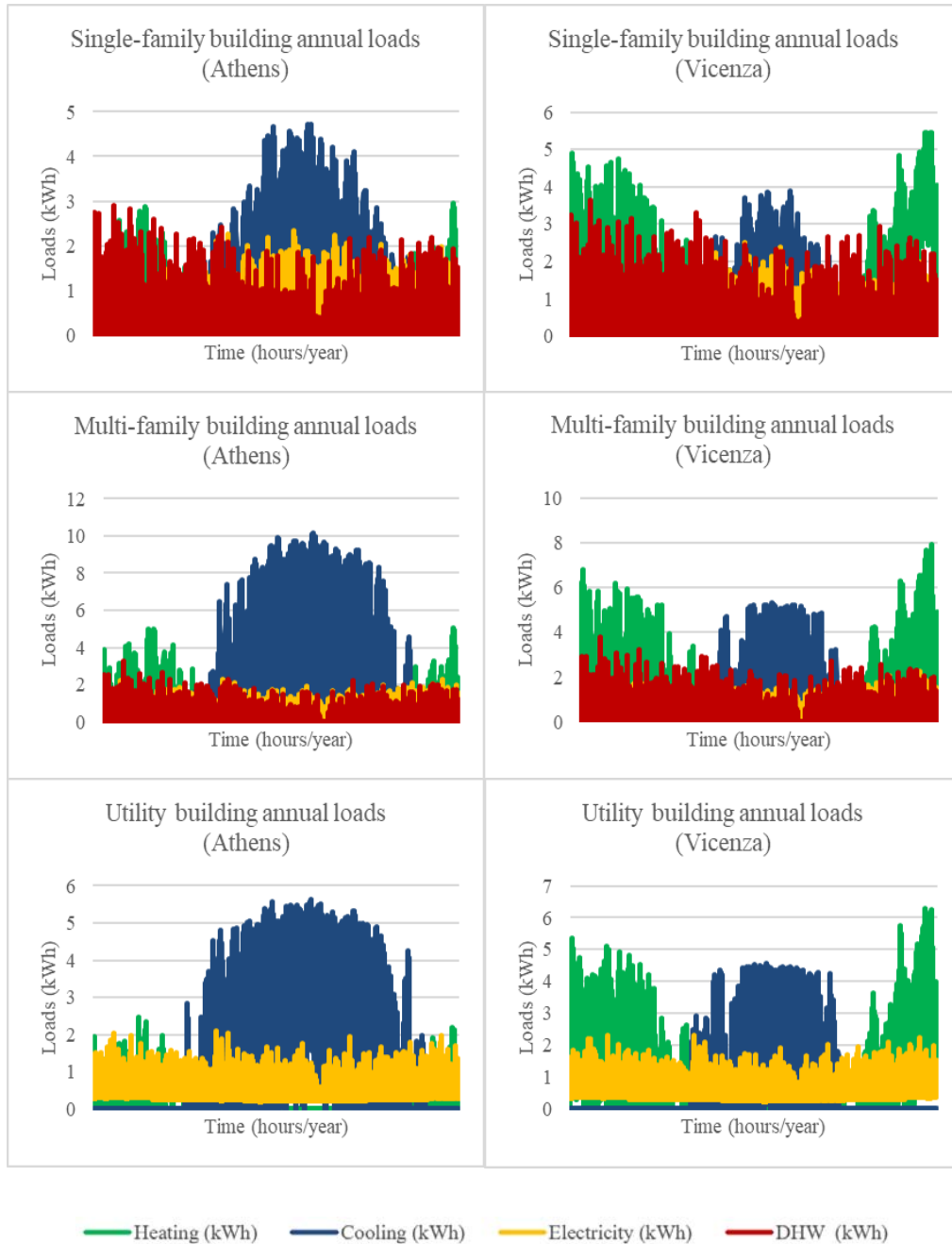
Figure 6.16: Hourly annual loads for each type of building and each location.

Table 6.7: Maximum and overall district loads values for each location

	Maximum power (kW)		Annual demand (MWh)	
	Athens	Vicenza	Athens	Vicenza
Heating	46.12	79.86	25.557	107.810
Cooling	90.42	56.52	121.931	44.461
Electricity	26.46	27.83	75.282	74.014
Hot Water	31.10	37.29	10.690	13.341

Figure 6.17: Hourly annual district loads for each location

6.2.4 Comparison of the annual results

An annual simulation was developed for three different cases. For each type of system, different results came out. The three solutions are reported as follows.

PV/T HYBRID SYSTEM

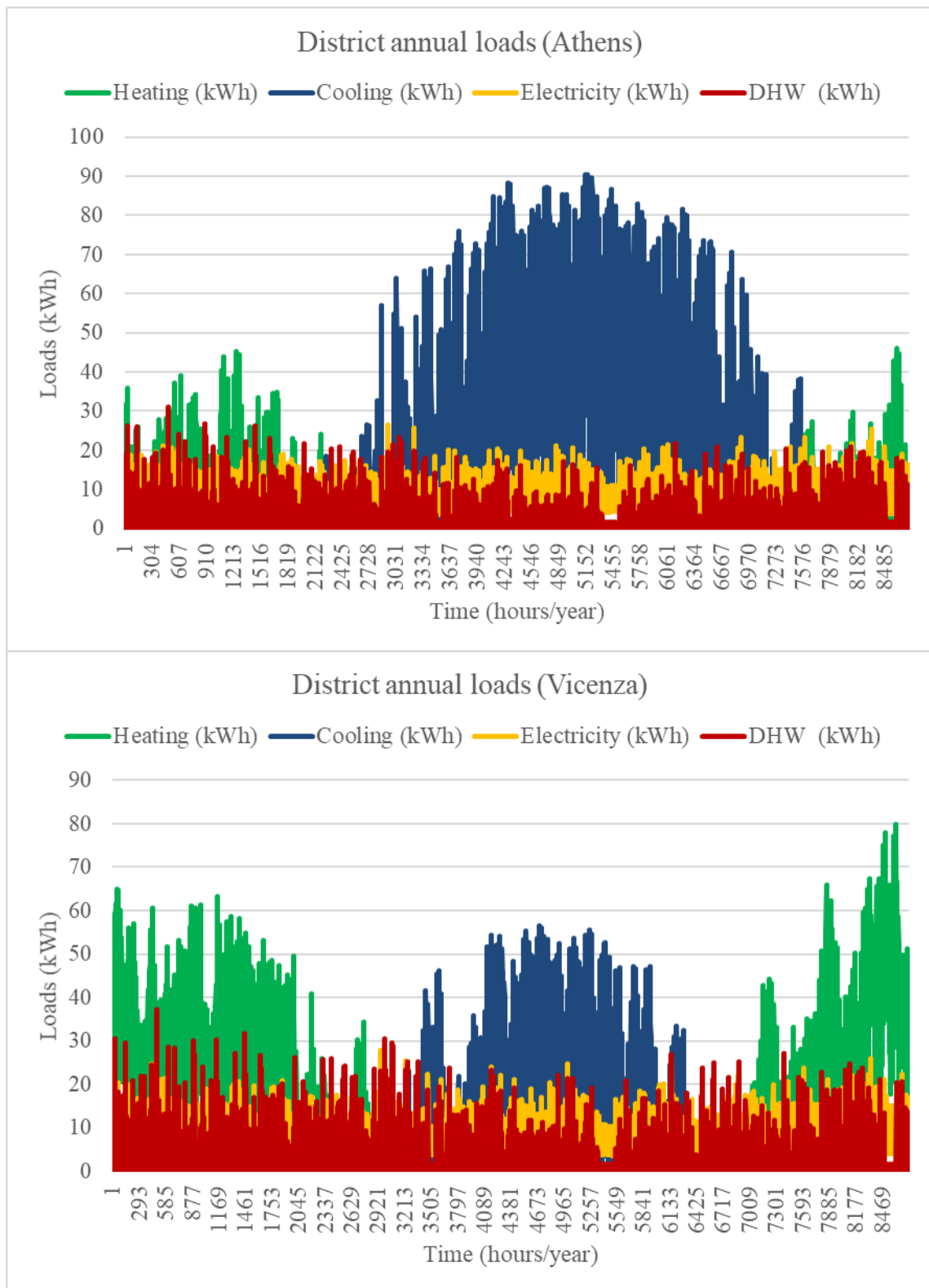The hybrid solution is the main one, in which the PV/T solar hybrid collectors are used to provide both heat and electric power to the user. Compared to the daily simulations seen in Chapter 6.1, in this solution the number of panels was increased from the daily test cases in order to adapt not just to the electricity demand of the user, but also to the power absorbed by the heat pump. Since the maximum electrical power demand of the two locations is roughly comparable, the number of panels has been doubled. Moreover, the two thermal storage tanks are enlarged. The one linked to the heat pump for operational reasons, while the other for the greater amount of thermal energy produced by the solar collector field. The sizing values of each component for both locations are reported in Table 6.8.

Table 6.8: Design variables of the components for an annual simulation of the PV/T hybrid system.

Component size parameter	Number of components	Value of each component	Total amount
A_{PVT}	400	$1.654\ m^2$	$661.6\ m^2$
Vol_{HP}	1	$2\ m^3$	$2\ m^3$
Vol_W	1	$2\ m^3$	$2\ m^3$
$\dot{Q}_{HP,nom}$	3	$40\ kW$	$120\ kW$
$\dot{Q}_{NGH,nom}$	1	$38\ kW$	$38\ kW$
$\dot{W}_{INV,nom}$	10	$11.2\ kW$	$112\ kW$

The annual energy production and consumption are reported in Table 6.9. By comparing the overall energy produced, in Athens both the electric and thermal energy is higher than in Vicenza due to the higher solar irradiance. In the Greek city, not only the energy transferred to the grid is positive, but also the energy absorbed by the heat pump power is lower than in the Italian city due to the milder climate in winter. Nevertheless, relatively in Vicenza the thermal energy available is much more exploited than in Athens. In the

first location, the thermal energy absorbed is 94.92%, while in the second one is just the 57.91%. The values of thermal dissipation are close to the ones found in references (82).

Table 6.9: PV/T hybrid system annual results. Electric and thermal energy exchanged in Vicenza and Athens.

Electric energy (MWh)	W_{hp}	W_{inv}	W_{grid}	$W_{hp} + W_u$
Vicenza	63.03	113.32	-19.03	137.04
Athens	39.85	179.30	+64.17	115.13

Thermal energy (MWh)	$Q_{w,col,tot}$	$Q_{w,col,sep}$	$Q_{w,ngh}$	$Q_{w,d}$
Vicenza	7.46	7.09	8.17	1.96
Athens	11.12	6.44	5.96	1.82

PV+T SEPARATED SOLUTION

The PV+T separated solution is used to compare the performances of the main one with a common solution. The PV panels provide the electric energy, while the solar collectors produce heat. In order to compare the two solutions, the number of panels and collectors is taken to provide the same power at the design conditions as found in Table 6.2. The sizing values of each component for both locations are reported in Table 6.10.

Table 6.10: Design variables of the components for an annual simulation of the PV+T separated system.

Component size parameter	Number of components	Value of each component	Total amount
A_{PV}	336	$1.944 \ m^2$	$653.3 \ m^2$
A_{COL}	108	$2.320 \ m^2$	$250.6 \ m^2$
Vol_{HP}	1	$2 \ m^3$	$2 \ m^3$
Vol_W	1	$2 \ m^3$	$2 \ m^3$
$\dot{Q}_{HP,nom}$	3	$40 \ kW$	$120 \ kW$
$\dot{Q}_{NGH,nom}$	1	$38 \ kW$	$38 \ kW$
$\dot{W}_{INV,nom}$	10	$11.2 \ kW$	$112 \ kW$

The total amount of energy produced is different from the hybrid solution in both locations. As can be seen by comparing Tables 6.9 and 6.11, the electrical production is

slightly higher, while the heat produced is significantly bigger: doubled in Vicenza and more than tripled in Athens. However, the relative thermal energy used is lower than the hybrid solution. Respectively in the Italian and Greek cities are used the 80.29% and the 38.84% of the heat collected from the solar irradiance.

Table 6.11: PV+T separated system annual results. Electric and thermal energy exchanged in Vicenza and Athens.

Electric energy (MWh)	W_{hp}	W_{inv}	W_{grid}	$W_{hp} + W_u$
Vicenza	63.03	118.24	-18.80	137.04
Athens	39.85	184.38	+69.25	115.13

Thermal energy (MWh)	$Q_{w,col,tot}$	$Q_{w,col,sep}$	$Q_{w,ngh}$	$Q_{w,d}$
Vicenza	14.71	11.81	4.47	3.08
Athens	35.35	13.73	0.505	3.91

PV/T + BESS SOLUTION

The introduction of the battery to store the PV power produced is used to see how the presence of an extra storage affects the system. Moreover, a BESS is also required in those remoted areas not reached by the grid or where the connection is too expensive. A stand-alone behaviour is then the target for this system. The choice of the size depended on the power produced during the least sunny days of the year and the energy demanded by the user. Also, the cost of the battery is not negligible. A good compromise resulted to be the installation of 1 kWh for every m² of PV/T collector.

As can be seen in Table 6.12, the annual value of the energy absorbed from the grid by the system is null for both locations. However, it is reasonable to think that the system is more expensive than without the BESS. In order to see how the type of system affects the objective functions, the values of discounted payback time and global utilization factor are reported in Table 6.13.

Table 6.12: PV/T + BESS hybrid system annual results. Electric and thermal energy exchanged in Vicenza and Athens.

Electric energy (MWh)	W_{hp}	W_{inv}	W_{grid}	$W_{hp} + W_u$
Vicenza	63.03	113.32	0	137.04
Athens	39.85	179.30	0	115.13

Thermal energy (MWh)	$Q_{w,col,tot}$	$Q_{w,col,sep}$	$Q_{w,ngh}$	$Q_{w,d}$
Vicenza	7.46	7.09	8.17	1.96
Athens	11.12	6.44	5.96	1.82

By comparing the results, the most convenient solution in economic terms might seem the PV/T hybrid one, both for Athens and Vicenza. Nevertheless, the best option under the energy utilization point of view is the PV/T hybrid solution coupled with a BESS. However, these values refer to specific systems in a determined environment, while many factors affect the resolution of the problem. Inside the system, the surface of the panels and the volumes of the TSTs are design variables that change the results and are studied through the optimization process. Outside the system, the economic parameters affect the discounted payback period.

Table 6.13: Results of discounted payback period (years) and global utilization factor (-) for each system and each location.

Solution		PV/T		PV+T		PV/T+B	
Function		PB	ε	PB	ε	PB	ε
Location	Athens	37.63	0.1752	43.63	0.1762	68.78	0.1978
	Vicenza	46.92	0.2504	54.26	0.2518	49.62	0.3117

6.2.5 Influence of economic parameters

Different simulations are performed in order to see how the economic parameters affect the solution. As base case is used the annual behaviour of a PV/T hybrid system set in Athens. Then different variables varied one by one at every simulation. The economic parameters that are used in the calculation of the *PB* are the price of electricity and gas, the feed-in tariff for the energy sold to the grid and the discount rate. The actual values are the ones reported in Table 5.1. Their variation is set on a possible scenario in which the values might increase or decrease depending on the evolution of the market. The prices of energy and the discount rate are changed in a range from the 50% to the 150%. The only parameters that is likely not to increase at all is the feed-in tariff. Thus, its range of variation is set between 0% to 100% of its actual value.

As can be seen from Figure 6.18, all the parameters have a strong influence on the PB apart from the price of natural gas. In fact, the amount of NG consumed is low because of the high solar thermal production in Athens.
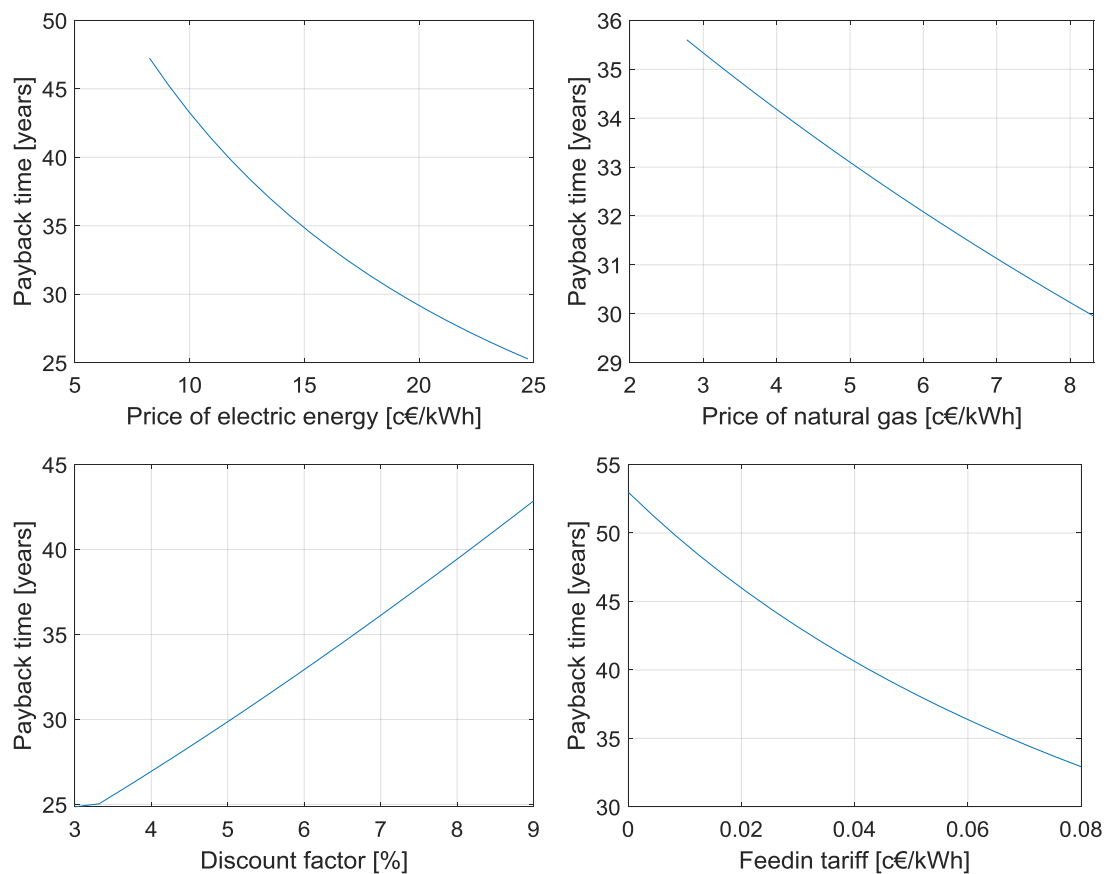

Figure 6.18: Discounted payback period in function of the price of electricity, the price of natural gas, the discount rate and the feed-in tariff.

113

6.3 Optimization results

Before starting the annual simulation, the optimization process started. The multi-objective genetic algorithm took into consideration the upper and lower boundaries expressed in Table 5.2, a population size of 50 individuals, and a number of maximum generations equal to 10. The genealogy, i.e. the number of individuals who generates the offspring at each generation, as well as the other two parameters are shown in Figure 6.19. The results of the optimization process for each case is hereby presented.
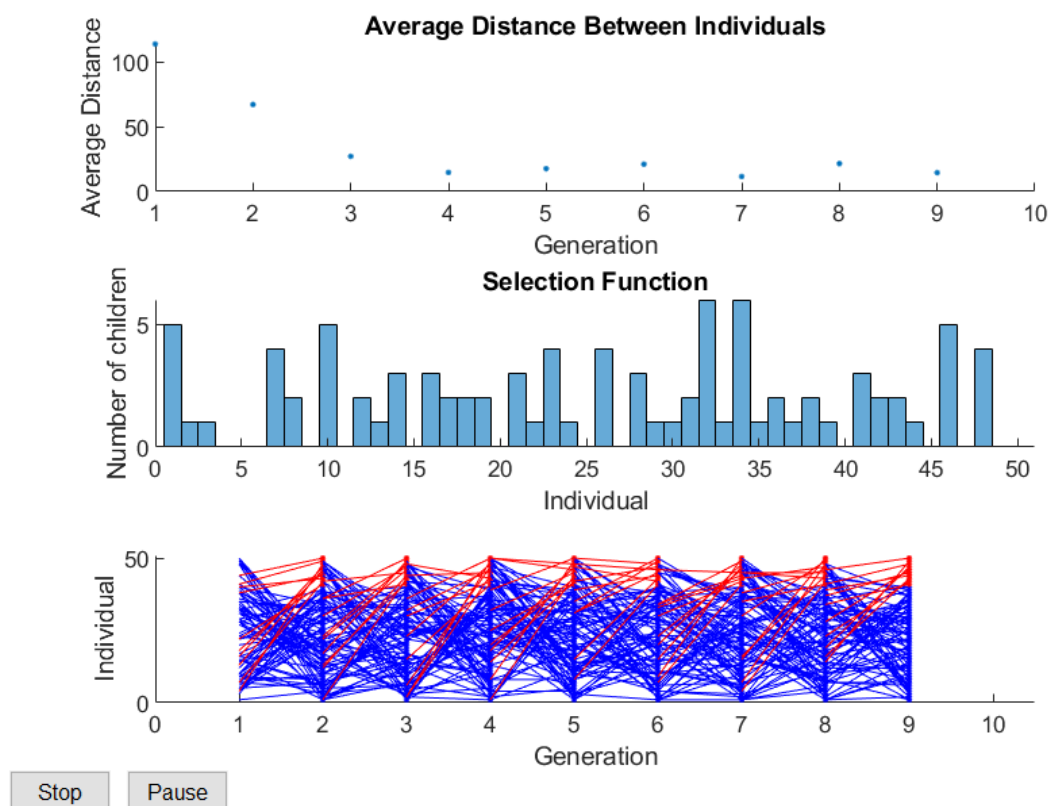

Figure 6.19: Plot of the genetic algorithm parameters: the distance between individuals at each generation, the selection of each generation and the genealogy.

6.3.1 PV/T hybrid system optimization results

The system optimized here is the main one, based on the PV/T hybrid collectors for the energy production. The variables in input of the genetic algorithm are the PV/T panels area A_{PVT}, the volume of the HP storage tank Vol_{HP} and the volume of the DHW storage tank Vol_W. The objective functions are the discounted payback period PB and the global utilization factor ε.

The values of the solutions reached at the 10th generation for Athens and Vicenza are reported in Figure 6.20. Here it is shown how the optimal solutions lay on the Pareto front, i.e. the line in which all the solutions are optimal considering the objective functions chosen. The curves obtained increase PB the bigger ε gets.

In Table 6.14 can be seen the values chosen for both location: these are relative to the point that accomplish better both the choices: lowest PB and highest ε. In Athens the PB is higher than in Vicenza, and the utilization factor is lower. Nevertheless, values in Vicenza of A_{PVT} and Vol$_W$ are close to the lower boundary conditions.
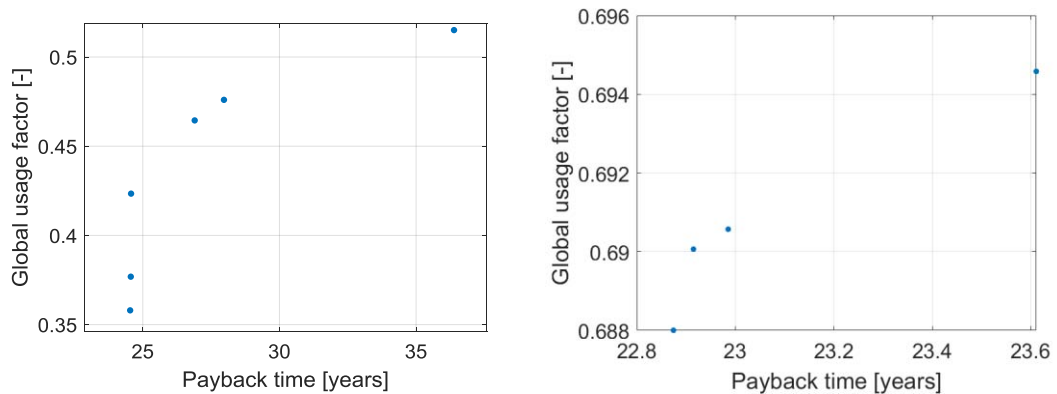

Figure 6.20: PV/T system optimization results of the global utilization factor and the discounted payback period in Athens (left) and Vicenza (right).

Table 6.14: Values of the input variables and objective functions relative to the one of the solutions of the Pareto front in Athens and Vicenza in the PV/T hybrid system.

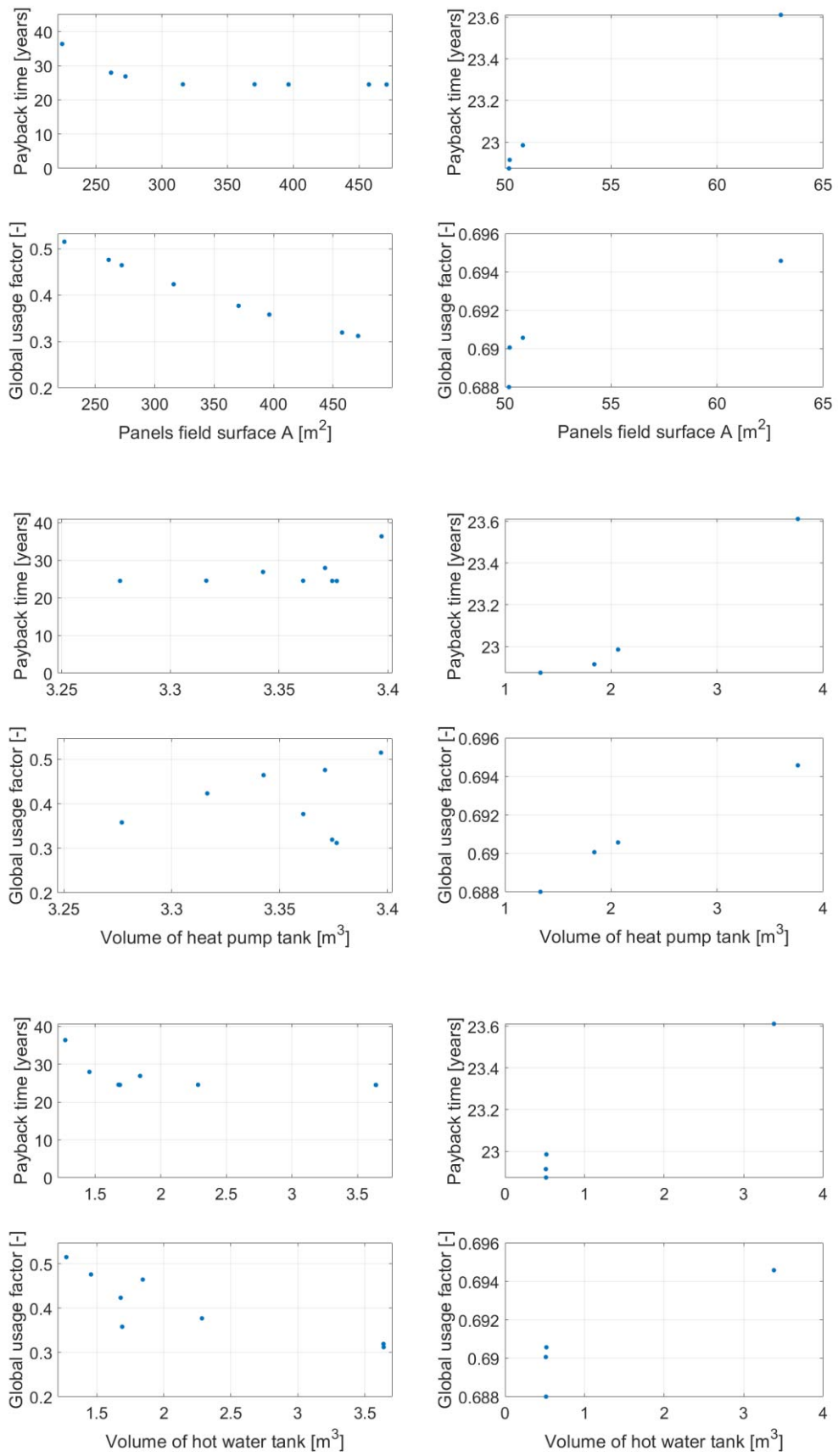|	$A_{PVT}\ (m^2)$	$Vol_{HP}(m^3)$	$Vol_W(m^3)$	$PB(years)$	$\varepsilon\ (-)$
Athens	272.30	3.34	1.84	26.9	0.46
Vicenza	50.22	1.84	0.51	22.9	0.69

115

Figure 6.21: PV/T system optimization results in function of the design variables for Athens (left) and Vicenza (right).

6.3.2 PV/T hybrid system BESS coupled optimization results

The system optimized here is the one based on the PV/T hybrid collectors for the energy production with a battery energy storage system. The variables in input of the genetic algorithm are the PV/T panels area A_{PVT}, the volume of the HP storage tank Vol_{HP} and the volume of the DHW storage tank Vol_w. The objective functions are the discounted payback period PB and the global utilization factor ε.

The values of the solutions reached at the 10th generation for Athens and Vicenza are reported in Figure 6.22. The optimal solutions lay on the Pareto front, i.e. the line in which all the solutions are optimal considering the objective functions chosen. The curves obtained should increase PB the bigger ε gets. Nevertheless, this behaviour is barely visible due to the too high precision of the solver, which selected only the best children.

In Table 6.15 can be seen the values chosen for both location: these are relative to the point that accomplish better both the choices: lowest PB and highest ε. Both locations have almost the same PB and ε. However, this is due to the low value of A_{PVT}, which is strictly connected to the battery size. Nevertheless, values in Vicenza of Vol_W are close to the lower boundary conditions.
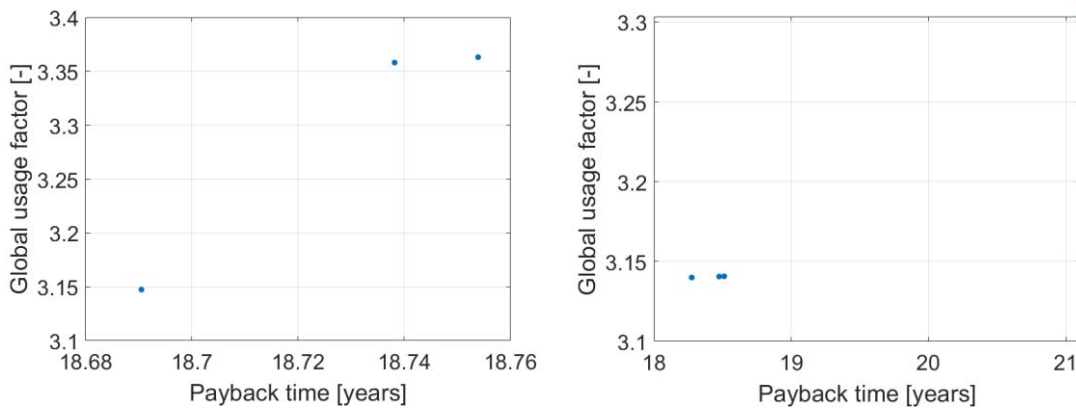

Figure 6.22: PV/T system coupled with BESS optimization results of the global utilization factor and the discounted payback period in Athens (left) and Vicenza (right).

Table 6.15: Values of the input variables and objective functions relative to one of the solutions of the Pareto front in Athens and Vicenza in the PV/T hybrid system coupled with a BESS.

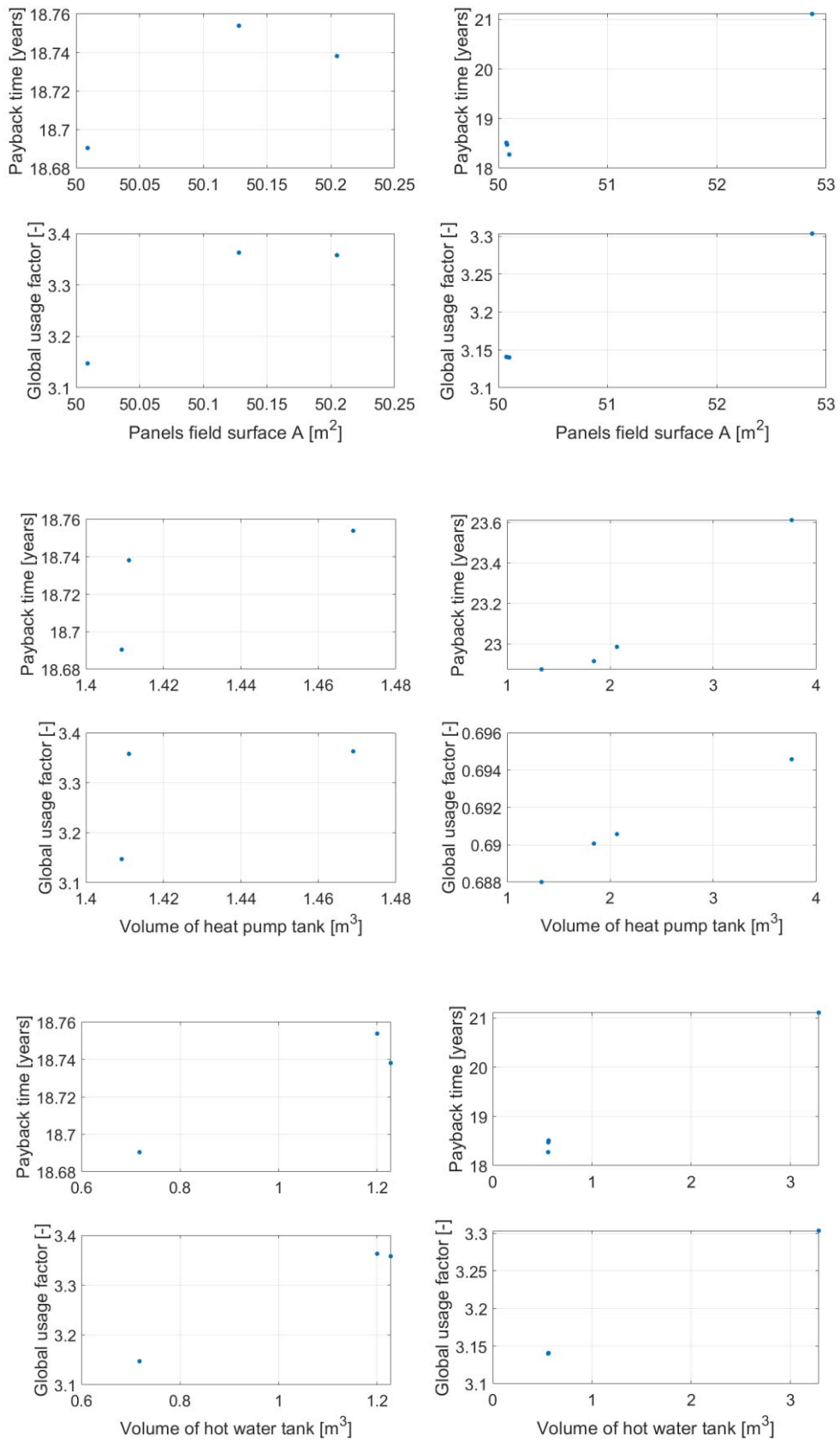|	$A_{PVT}\ (m^2)$	$Vol_{HP}(m^3)$	$Vol_W(m^3)$	$PB(years)$	$\varepsilon\ (-)$
Athens	50.20	1.41	1.23	18.7	3.36
Vicenza	50.07	1.83	0.56	18.5	3.14

Figure 6.23: PV/T system coupled with a BESS optimization results in function of the design variables for Athens (left) and Vicenza (right).

6.3.3 PV+T separated system optimization results

The system optimized here is the separated one. The PV and solar thermal flat collector fields substitute the one based on the PV/T hybrid collectors for the energy production. In order to have a proper comparison, the number of PV panels and solar collectors were chosen in function of the nominal power provided by the corresponding PV/T hybrid collector. The variables in input of the genetic algorithm are the PV panels area A_{PV}, the volume of the HP storage tank Vol_{HP} and the volume of the DHW storage tank Vol_w. The area of the thermal collectors was calculated in function of A_{PV}. The objective functions are the discounted payback period PB and the global utilization factor ε.

The values of the solutions reached at the 10th generation for Athens and Vicenza are reported in Figure 6.24. The global utilization factor increases the higher the payback period gets. The variation is wide close to the initial point, while it is narrow for big variations when PB is doubled. In Table 6.16 can be seen the values chosen for both locations. While in Athens is still convenient to install a wide field of solar panels and collectors, in Vicenza the GA tends to reach the minimum value. However, the volumes of the TST are roughly comparable and are far from the minimum value.
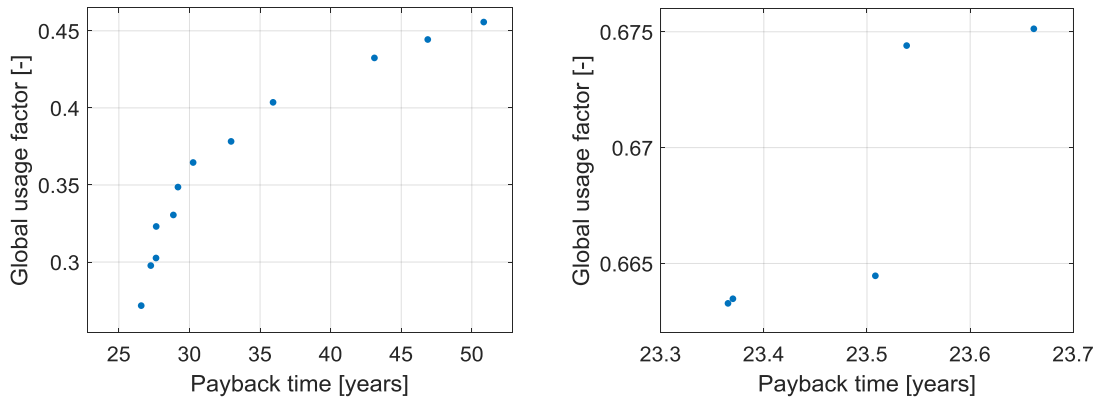

Figure 6.24: Separated PV+T system optimization results of the global utilization factor and the discounted payback period in Athens (left) and Vicenza (right).

Table 6.16: Values of the input variables and objective functions relative to one of the solutions of the Pareto front in Athens and Vicenza in the separated PV+T system.

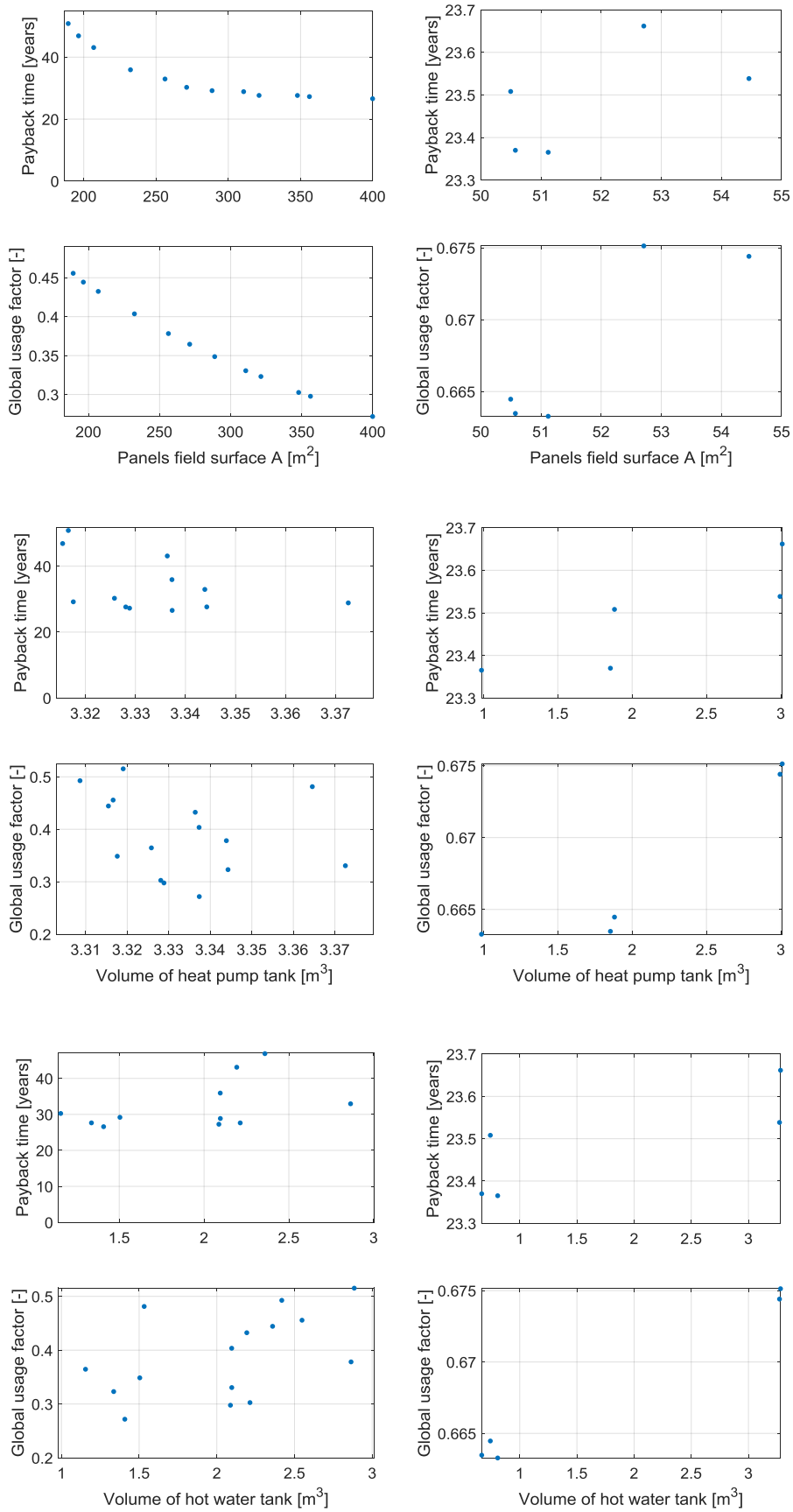|	A_{PV} (m^2)	A_{COL} (m^2)	$Vol_{HP}(m^3)$	$Vol_W(m^3)$	$PB(years)$	ε $(-)$
Athens	232.31	74.67	3.34	2.10	35.9	0.40
Vicenza	54.46	17.51	2.99	3.27	23.5	0.67

Figure 6.25: Separated PV+T system optimization results in function of the design variables for Athens (left) and Vicenza (right).

Conclusions

The results are presented in this chapter. The system based on PV/T hybrid collectors worked in daily and annual simulations for a district of residential and utility buildings in Athens and Vicenza. A comparison with a common separated system and the introduction of an electrochemical storage was introduced. Results showed that the hybrid system is more convenient in economic terms than the common solution.

In addition, the results of the GA operation on the three types of system were shown. The optimized values of the design variables show that the hybrid solution coupled with the battery has the lowest discounted payback periods for both location. The simple hybrid solution is however more convenient than the common separated one. On the other hand, the global utilization factor is strongly higher on the hybrid solution with BESS than on the other two, which are roughly comparable. Nevertheless, ε is higher for the hybrid solution. Results also show that the hybrid solutions have lower PB in Athens but higher ε in Vicenza.

7. CRITICAL REMARKS

The system built in this work is based on PV/T hybrid collector technology for the CCHP demand of a district of residential and utility buildings based in Athens and in Vicenza. The annual simulations show that the system behaves properly: it provides the loads required by the user at all the external conditions set. However, many variables alter the results. The hybrid solution is then compared to a separated one and the introduction of a BESS is evaluated. The results suggest that the PV/T system is economically more convenient than a common one for the same power produced. The dependency of PB on the variation of economical parameters is shown.

Further investigations on this work can be done by implementing one or more of the following aspects.

On the load production side, it might be of interest the possibility to adapt the demand to the production, i.e. to consume energy when the solar irradiance is available.

The hot water produced by hybrid and common solar collectors in Athens is widely dissipated. In order not to waste too much thermal energy, the extra heat could feed the heat pump in winter season.

The electric power absorbed by the HP is high especially in Vicenza, where the space conditioning in winter is higher than the space cooling in Athens. A way to contain the system costs and the consumption of electricity is to reduce the size of the heat pump and in winter season exploit the NGH.

Results in the GA optimization were for some solutions too accurate. A way to decrease the natural selection is to reduce the number of generations.

REFERENCES

(1) Gaye, Amie, *Access to Energy and Human Development*, 2008 - http://hdr.undp.org/en/content/access-energy-and-human-development

(2) IPCC, CLIMATE CHANGE - The IPCC Scientific Assessment, 2018 - https://www.ipcc.ch/site/assets/uploads/2018/03/ipcc_far_wg_I_full_report.pdf

(3) OECD, Green Growth Studies: Energy, 2011 - https://www.oecd.org/greengrowth/greening-energy/49157219.pdf

(4) https://www.iea.org/statistics/

(5) Chapter 2 - *Energy Consumption and Environmental Quality of the Building Sector*, Matthaios Santamouris, Elsevier, 2019, Pages 29-64, ISBN 9780128114179

(6) The European Green Deal, Communication from the European Commission on 11.12.2019

(7) Transforming our world: the 2030 Agenda for Sustainable Development, Resolution adopted by the General Assembly on 25.09.2015

(8) Yokoyama, R., and Ito, K. (December 1, 1995). *Optimal Operational Planning of Cogeneration Systems with Thermal Storage by the Decomposition Method*. ASME. J. Energy Resour. Technol. December 1995; 117(4): 337–342.

(9) A. Toffolo A. Lazzaretto, *Evolutionary algorithms for multi-objective energetic and economic optimization in thermal system design*. Energy, Volume 27, Issue 6, June 2002, pp. 549-567.

(10) A. Lazzaretto, A. Toffolo, *Energy, economy and environment as objectives in multi-criterion optimization of thermal systems design*. Energy, Volume 29, Issue 8, June 2004, pp. 1139-1157.

(11) Wang, L.; Yang, Z.; Sharma, S.; Mian, A.; Lin, T.-E.; Tsatsaronis, G.; Maréchal, F.; Yang, Y. A Review of Evaluation, *Optimization and Synthesis of Energy Systems: Methodology and Application to Thermal Power Plants*. Energies 2019, 12, 73.

(12) Rech, S., *Smart Energy Systems: Guidelines for Modelling and Optimizing a Fleet of Units of Different Configurations*. Energies 2019, 12, 1320.

(13) R. Wolfson. *Energy, Environment, and Climate*, 2nd ed., New York, NY: W.W. Norton & Company, 2012.

(14) A. Fahrenbruch, R. Bube, *Fundamentals of solar cells: photovoltaic solar energy conversion*, Elsevier Science, 2012.

(15) A. Goetzberger, V.U. Hoffmann, *Photovoltaic solar energy generation*, Springer, Berlin Heidelberg, 2005.

(16) PHOTOVOLTAICS REPORT, Fraunhofer Institute for Solar Energy Systems, ISE with support of PSE GmbH Freiburg, 14 November 2019 www.ise.fraunhofer.de

(17) https://us.sunpower.com/products/solar-panels

(18) K. Braimakis, T.C.R., A.D. Leontaritis, S. Karellas, *Comparison of Environmentally Friendly Working Fluids for Organic Rankine Cycles, in Advances in New Heat Transfer Fluids*, A.A. Minea, Editor. 2017. pp. 377-426.

(19) H.L. Zhang, J. Baeyens, J. Degrève, G. Cacères, *Concentrated solar power plants: Review and design methodology*. Renew Sustain Energy Rev, 22 (2013), pp. 466-481

(20) A. B, *Solar power tower design basis document*, Revision 0; 2017.

(21) R. Abbas, M.J. Montes, M. Piera, J.M. Martínez-Val, *Solar radiation concentration features in Linear Fresnel Reflector arrays*, Energy Convers Manage, 54 (2012), pp. 133-144.

(22) D.R. Mills, G.L. Morrison, *Compact linear Fresnel reflector solar thermal powerplants*, Sol Energy, 68 (2000), pp. 263-283.

(23) https://www.seia.org/initiatives/concentrating-solar-power

(24) F.P.G. Márquez, A. Karyotakis, M. Papaelias, *Renewable energies: business outlook 2050*, Springer (2018)

(25)http://solar.fimer.com/sites/default/files/UNO-DM-1.2-2.0-3.0-TL-PLUS_BCD.00684_revA_IT.pdf

(26) Sergio Rech, Andrea Lazzaretto, *Smart rules and thermal, electric and hydro storages for the optimum operation of a renewable energy system*, Energy 147 (2018) pp. 742-756.

(27) A guide to the standard EN 12975 SP – Technical Research Institute of Sweden Peter Kovacs, SP With major contributions from ITW, AIT, ISE, LNEG, TUV, CENER, IZES, ISFH and Demokritos QAiST - IEE/08/593/SI2.529236, Deliverable D2.3, Date of report: 28.05.2012

(28) 5th European Thermal-Sciences Conference, The Netherlands, 2008, *APPLICATIONS OF SOLAR HEAT FOR TEMPERATURES RANGING FROM 50 - 2000°C*, H. Müller-Steinhagen

(29) https://www.iea.org/reports/tracking-buildings/heat-pumps

(30) Cavallini, L. Mattarolo, *Termodinamica applicata*, CLEUP

(31) https://www.energy.gov/energysaver/heat-and-cool/heat-pump-systems

(32) http://www.stats.ehpa.org/hp_sales/story_sales/

(33) https://www.ehpa.org/market-data/

(34) Cengel, Cimbala, *Fluid Mechanics: Fundamentals and Applications*, Ed. 3, McGraw-Hill, 2014.

(35) Vincenzo Bianco, Federico Scarpa, Luca A. Tagliafico, *Estimation of primary energy savings by using heat pumps for heating purposes in the residential sector*, Applied Thermal Engineering, Volume 114, 2017, Pages 938-947, ISSN 1359-4311.

(36) Lamnatou C., C.D., *Photovoltaic/Thermal (PVT) Systems: A Review with Emphasis on Environmental Issues.* Renewable Energy, 2017. **105**(Supplement C): pp. 270-287.

(37) Brahim Taoufik, A.J., *Economical Assessment and Applications of Photovoltaic/Thermal Hybrid Solar Technology: A Review.* Solar Energy, 2017. **153**(Supplement C): p. 540-561.

(38) Zondag, H., *The yield of different combined PV-thermal collector designs.* Solar Energy, 2003. **74**(253-269).

(39) Parida B., I.S., Goic R., *A review of solar photovoltaic technologies.* Renewable and Sustainable Energy Reviews, 2011. **15**(1625-1636).

(40) Michael J., I.S., Goic R., *Flat plate solar photovoltaic-thermal (PV/T) systems: a reference guide.* Renewable and Sustainable Energy Reviews, 2015. **51**: p. 62-88.

(41) Ceylan Ilhan, G.A.E., Ergün Alper, Tabak Abdulsamed, *Performance analysis of a concentrated photovoltaic and thermal system.* Renewable Energy, 2016. **72**: p. 79-87.

(42) Jinshun Wu, X.Z., Jingchun Shen, Yupeng Wu, Karen Connelly, Tong Yang, Llewellyn Tang, Manxuan Xiao, Yixuan Wei, Ke Jiang, Chao Chen, Peng Xu, Hong Wang, *A review of thermal absorbers and their integration methods for the combined solar photovoltaic/ thermal (PV/T) modules.* Renewable and Sustainable Energy Reviews, 2017. **75**: p. 839-854.

(43) Chow TT, H.W., Ji J., *Hybrid photovoltaic-thermosyphon water heating system for residential application.* Solar Energy, 2006. **80**: p. 298-306.

(44) Zhou Jinzhi, Z.X., Ma Xiaoli, et al., *Experimental investigation of a solar driven direct-expansion heat pump system employing the novel PV/micro-channels-evaporator modules.* Applied Energy, 2016. **178**: p. 484-495.

(45) Zhang Xingxing, Z.X., Shen Jingchun, Hu Xi, Liu Xuezhi, Xu Jihuan, *Design, fabrication and experimental study of a solar photovoltaic/loop-heat-pipe based heat pump system.* Solar Energy, 2013. **97**: p. 551-568.

(46) Sopian K., Y.K., Liu HT, Kakaç S., Verizoglu TN, *Performance analysis of photovoltaic thermal air heaters.* Energy Conversion and Management, 1996. **37**(11): p. 1657-1670.

(47) Jin GL., I.A., Chean YK, Daghigh R., Ruslan H., Mat S, et al, *Evaluation of single-pass photovoltaic-thermal air collector with rectangle tunnel absorber.* American Journal of Applied Sciences, 2010. **7**(2): p. 277-282.

(48) Chow TT, P.G., Fong KF, Lin Z., Chan ALS, Ji J., *Energy and exergy analysis of photovoltaic-thermal collector with and without glass cover.* Applied Energy, 2009. **86**: p. 310-316.

(49) Jing D., H.Y., Liu M., Wei J., Guo L., *Preparation of highly dispersed nanofluid and CFD study of its utilization in a concentrating PV/T system.* Solar Energy, 2015. **112**: p. 30-40.

(50) Ghadiri M., S.M., Pasandixleh-fard M., Moghadam A.J., *Experimental investigation of a PVT system performance using nano ferrofluids.* Energy Conversion and Management, 2015. **103**: p. 468-476.

(51) Chow TT, H.W., Ji J., *An experimental study of facade-integrated photovoltaic/water heating system.* Applied Thermal Engineering, 2007. **27**(1): p. 37-45.

(52) Athienitis AK, B.J., O'Neill B., Faille J., *A prototype photovoltaic/thermal system integrated with transpired collector.* Solar Energy, 2011. **85**: p. 139-153.

(53) Tushar M. Sathe, A.S. Dhoble, *A review on recent advancements in photovoltaic thermal techniques*, Renewable and Sustainable Energy Reviews, 2017, **76**: p. 645–672.

(54) Basant Agrawal, G.N. Tiwari, *Life cycle cost assessment of building integrated photovoltaic thermal (BIPVT) systems*, Energy and Buildings, Volume 42, Issue 9, September 2010, Pages 1472-1481

(55) Sleiman Farah, Wasim Saman, and Martin Belusko, *Integrating Solar Heating and PV Cooling into the Building Envelope,* Chapter 79

(56) Chr. Lamnatou, D. Chemisana, *Photovoltaic/thermal (PVT) systems: A review with emphasis on environmental issues,* Renewable Energy, 2017, **105**: p. 270-287

(57) Ayyash, S, and M Sartawi, *Economic Comparison of Solar Absorption and Photovoltaic-Assisted Vapour Compression Cooling Systems*, International Journal of Energy Research, 1983 7 (3): 279–288.

(58) Hartmann, N., C. Glueck, and F. P. Schmidt, *Solar Cooling for Small Office Buildings: Comparison of Solar Thermal and Photovoltaic Options for Two Different European Climates*, Renewable Energy, 2011, 36 (5): 1329–1338.

(59) Beccali M., M. Cellura, P. Finocchiaro, F. Guarino, S. Longo, and B. Nocke. 2014. *Life Cycle Performance Assessment of Small Solar Thermal Cooling Systems and Conventional Plants Assisted with Photovoltaics*, Solar Energy 104 (Supplement C): pp. 93–102.

(60) Calise F., M. Dentice d'Accadia, R. D. Figaj, and L. Vanoli. 2016. *A Novel Solar-Assisted Heat Pump Driven by Photovoltaic/Thermal Collectors: Dynamic Simulation and Thermoeconomic Optimization*. Energy 95 (Supplement C): pp. 346–366.

(61) Bianchini A., A. Guzzini, M. Pellegrini, and C. Saccani. 2017. *Photovoltaic/ Thermal (PV/T) Solar System: Experimental Measurements, Performance Analysis and Economic Assessment*. Renewable Energy 111 (Supplement C): 543–555.

(62) https://ec.europa.eu/energy/eu-buildings-database_en

(63) https://www.ahi-carrier.gr/en/wp-content/uploads/sites/2/2017/06/PSD-30RB_RQ_017_040.pdf

(64) Faiman, D., *Assessing the outdoor operating temperature of photovoltaic modules*. Progress in Photovoltaics: Research and Applications, 2008. 16(4): p. 307-315.

(65) Elena Barykina, A.H., *Modeling of photovoltaic module temperature using Faiman model: Sensitivity analysis for different climates*. Solar Energy, 2017. 146: p. 401-416.

(66) Habbati Bellia, R.Y., Moulay Fatima, *A detailed modeling of photovoltaic module using MATLAB*. NRIAG Journal of Astronomy and Geophysics, 2014. 3: p. 53-61.

(67) Standard Number : UNI EN 12975-2:2006; Title : *Thermal solar systems and components - Solar collectors - Part 2: Test methods*; ICS : (27.160) ; Status :

WITHDRAWN AND REPLACED BY Technical Committees : (CTI - Solar Energy); Start Validity Date : november 9, 2006; End Validity Date : january 23, 2014

(68) DualSun. Available from: https://academy.dualsun.com/wp-content/uploads/DualSun-EN-Datasheet-Spring.pdf.

(69)   Bouraiou A., H.M., Chaker A., Sadok M., Mostefaoui M., Lachtar S., *Modeling and Simulation of Photovoltaic Module and Array Based on One and Two Diode Model Using Matlab/Simulink*. Energy Procedia, 2015. 74: p. 864-877.

(70) H. Laukamp, Wechselrichter in Photovoltaik-Anlagen, *Proceedings of the 4th Symposium on Photovoltaic Energy Conversion*, Staffelstein, 1989.

(71) M. Jantsch, H. Schmidt, J. Schmid, *Results of the concerted action on power conditioning and control, Proceedings of the 11th Photovoltaic Solar Energy Conference*, Montreux, 1992, pp. 15891593.

(72) https://www.austria-email.com/fileadmin/content-en/Products/Buffer_Tanks/Pufferspeicher__240_810_engl.pdf

(73) Stephen R. Turns, *An introduction to combustion*, 2nd edition, McGraw Hill, 2000

(74) Singiresu S. Rao, *Engineering Optimization Theory and Practice*, Fourth Edition, 2009, John Wiley & Sons, Inc, pgg. 693-702 & 761-763

(75) Fonseca CM, Fleming PJ. *Multiobjective optimization*. In: Back T, Fogel DB, Michalewicz Z, editors. Handbook of evolutionary computation. Oxford: Oxford University Press; 1997.

(76) Van Veldhuizen DA, Lamont GB. *Multiobjective evolutionary algorithms: analyzing the state-of-the-art.* Evolutionary computation 2000;8(2):125–47.

(77) A. Kayode Coker, *Cost Estimation and Economic Evaluation*, Ludwig's Applied Process Design for Chemical and Petrochemical Plants (Fourth Edition), Volume 1, 2007

(78) V. Ramanathan, Y. Feng, *Air pollution, greenhouse gases and climate change: global and regional perspectives*, Atmos. Environ., 43 (2009), pp. 37-50

(79) J.G. Speight, *Liquid fuels from natural gas*, S. Lee, J.G. Speight, S.K. Loyalka (Eds.), Handbook of Alternative Fuel Technologies (second ed.), Taylor and Francis Group, LLC, CRC Press (2015), pp. 157-178

(80) Tallmax by Trinasolar. Available from: http://static.trinasolar.com/sites/default/files/PS-M-0328%20E%20Datasheet_Tallmax_US_Feb_2017_A.pdf

(81) Vitosol 100 f by Viessmann. Available from: https://www.viessmann-us.com/content/dam/vi-brands/CA/pdfs/solar/vitosol_100-f_tdm.pdf/_jcr_content/renditions/original.media_file.download_attachment.file/vitosol_100-f_tdm.pdf

(82) Bellos, E., Tzivanidis, C., Symeou, C., and Antonopoulos, K.A., *Energetic, exergetic and financial evaluation of a solar driven absorption chiller – A dynamic approach*. Energy Conversion and Management, 2017. 137: p. 34-48.

(83) Chen H, Cong TN, Yang W, Tan C, Li Y, Ding Y. *Progress in electrical energy storage system: a critical review*. Prog Nat Sci 2009; 19:291-312.

(84) Rodrigues EMG, Godina R, Santos SF, Bizuayehu AW, Contreras J, Catalao JPS. *Energy storage systems supporting increased penetration of renewables in islanded systems*. Energy 2014; 75:265-80.

(85) Luo X, Wang J, Dooner M, Clarke J. *Overview of current development in electrical energy storage technologies and the application potential in power system operation*. Appl. Energy 2015; 137:511-36.